1991

Epitaxy of metal atoms on metal surfaces: deposition and diffusion

David Edward Sanders
Iowa State University

Order Number 9126245

Epitaxy of metal atoms on metal surfaces: Deposition and diffusion

Sanders, David Edward, Ph.D.

Iowa State University, 1991

U·M·I
300 N. Zeeb Rd.
Ann Arbor, MI 48106

Epitaxy of metal atoms on metal surfaces: Deposition and diffusion

by

David Edward Sanders

A Dissertation Submitted to the

Graduate Faculty in Partial Fulfillment of the

Requirements for the Degree of

DOCTOR OF PHILOSPHY

Department: Chemistry
Major: Physical Chemistry

Approved:

Signature was redacted for privacy.

In Charge of Major Work

Signature was redacted for privacy.

For the Major Department

Signature was redacted for privacy.

For the Graduate College

Iowa State University
Ames, Iowa
1991

TABLE OF CONTENTS

FORMAT OF THE DISSERTATION

The detailed dynamics of metal atoms adsorbed on metal surfaces and the theoretical techniques used to examine them are discussed in this dissertation. Two elementary steps in the growth of epitaxial films - single atom deposition and diffusion - are considered in detail. Molecular dynamics (MD) simulations are employed to provide an atomistic view of these processes. Several novel innovations in the modelling the dynamics of clean and adsorbate covered surfaces were made during this work and are also discussed in the dissertation.

This dissertation follows the alternative style format. The study of single atom deposition is contained in Paper I, entitled "*Metal/metal homo-epitaxy on FCC(001) surfaces: Is there transient mobility of adsorbed atoms?*" The work on single atom diffusion is contained in Paper II, entitled "*Predicted hopping rates for adsorbate/substrate combinations of Ni, Cu, Pd, Ag, Pt, and Au.*" A detailed discussion of the MD techniques used in this work appears in Paper III, entitled "*SCT89: a computer code for atomic and molecular scattering from clean and adsorbate covered surfaces.*" The ordering of these papers in the dissertation is not chronological. Paper III was actually written first, but is presented last since it was felt that the applications in Papers I and II would appeal more to a general scientific audience. Papers I and III have been accepted for publication in Surface Science and Computer Physics Communications, respectively. Paper II has been submitted for publication in Surface Science.

GENERAL INTRODUCTION

The deposition of atoms or molecules from a vapor source onto solid substrates is an important method of creating new materials and structures. Epitaxial growth refers to the formation of films where the adlayer crystal structure reflects that of the substrate. The resulting films may have electronic, magnetic, or chemical properties which differ from those of either the pure adsorbate or substrate. For example, a monolayer film of the transition metal Pd on a Nb(110) substrate exhibits electronic and chemical properties characteristic of an inert noble metal [1]. Industrial applications include the printing of circuits on computer chips, the coating of optics for high resolution instruments, and the construction of angstrom scale devices. These technologies require the stringent delineation of layers and thus rely on growth of well-ordered films. Studying the growth of thin films also reveals much about the microscopic details of the adsorbate-substrate interaction. For example, film morphology may be affected by such things as the adsorbate binding site(s) and the presence of surface defects. There is then both a practical and fundamental interest in understanding the details of film growth.

Three distinct modes of film growth have been observed experimentally [2]. The first, termed Frank - Van der Merwe (FV) growth, refers to the case of essentially perfect layer-by-layer film growth. Here, one adsorbate layer fills completely before there is any significant occupancy of the next layer. In the second mode, Volmer - Weber (VW) growth, the deposited atoms form three-dimensional islands and initially do not completely wet the substrate. The third mode, Stranski -

Krastonov (SK) growth, is a combination of FV and VW growth. Initially the film grows in a layer-by-layer, FV, fashion, but after a few monolayers the growth changes to the three-dimensional, VW, mode.

Thermodynamics can be used to rationalize the observed phenomenology in terms of various surface free energies [2]. The system surface free energy, γ, can be written in terms of the free energies for the adlayer-vacuum interface, γ_a, the substrate-vacuum interface, γ_s, and the adlayer-substrate interface, γ_i,

$$\gamma = \sigma_a \gamma_a + \sigma_a \gamma_i + (1 - \sigma_a)\gamma_s \tag{1}$$

where σ_a is the fraction of the substrate wet by the adsorbate. We can minimize the system free energy in this model by optimizing the value of σ_a. The direction of this optimization is determined by examining the variation of γ with respect to σ_a, $\partial\gamma/\partial\sigma_a$,

$$\frac{\partial \gamma}{\partial \sigma_a} \equiv \Delta\gamma = \gamma_a + \gamma_i - \gamma_s \,. \tag{2}$$

This simple model predicts that when $\Delta\gamma < 0$ complete wetting of the substrate occurs and FV growth predominates. If $\Delta\gamma > 0$, the system attempts to minimize the surface area of the adsorbates, thus VW growth results. As $\Delta\gamma$ approaches zero the strong driving force for FV or VW growth vanishes and the combination mode, SK, occurs.

The ability of Eq.(2) to make predictions about real systems is subject to a number of limitations. Not the least of these is obtaining accurate values for the free energies. Experimental values are available but are subject to interpretation [3]. Recently, accurate calculations of surface energies have been performed [4]

and these results could be used in conjunction with calculated entropies [5] to determine values of the surface free energies. Simple models such as these also ignore the role of defects and other microscopic features of the surface structure.

Perhaps a more fundamental limitation is the fact that film growth may be kinetically limited, i.e., true thermodynamic equilibrium may not be reached during the experimental timescale. It was observed experimentally that annealing at 600 K of a Rh film deposited on a Ag(001) surface resulted in a film of Ag forming on top of the Rh layers [6]. Molecular dynamics (MD) calculations were used to study the mechanism of the Rh-Ag exchange [7]. Static energy calculations predict that Rh and Ag layers should form a sandwich structure with Ag constituting the outermost surface layers. Starting from various coverages of Rh on top of Ag substrates, MD simulations were used to follow the formation of these sandwich structures. On the open (100) and (110) faces significant Rh migration subsurface was observed during the 10 picosecond simulations. On both faces migration was found to be thermally activated. No migration was found to occur on perfect close-packed (111) surfaces on this timescale. However, migration was observed on imperfect (111) surfaces which had vacancy defects. These results demonstrate the existence of a structure-dependent kinetic barrier separating the initially deposited Rh overlayer from the thermodynamically favored structure.

We believe that to fully understand film growth an atomistic approach is required. One approach is to use molecular dynamics to directly simulate the growth of thin films [8]. Studies [8a,8b] of Lennard-Jones [9] metals have provided a qualitative view of film growth and reproduce general experimental

trends. Unfortunately, such simple models do not provide a chemically accurate description of real systems. More sophisticated studies have been made of Si epitaxy [8c,8d]. These have made interesting predictions concerning the transition from amorphous to epitaxial growth and the mechanisms of surface reconstruction and unreconstruction. Unfortunately, direct simulation of growth is very computationally intensive. It is desirable to find simpler ways to approach this problem.

Our solution is to examine the elementary steps of film growth which involve the interaction of only one (or a few) adsorbate atom(s) with the substrate. The two simplest processes here are the deposition and diffusion of a single adatom. The dynamics of these processes are not trivial, however, since it involves the many-body interaction of the adatom with the atoms of the substrate.

Recent experiments demonstrate that the adsorbate-substrate dynamics play a critical role in film growth. The onset temperature of experimentally observable single metal atom diffusion on FCC(001) metal surfaces may be generally estimated to be ca. 200 K[1]. It might be expected that films grown below this temperature would be atomically rough because of limited adatom mobility. However, experimental studies of the growth of Cu and Fe films on Cu(001), Ag, Cu, Fe, and Mn films on Ag(001) [10] and Pt and Pd films on Pd(001) [11] provide evidence that such films grow in a smooth, layer-by-layer fashion at temperatures as

---

[1]This is based on an Arrhenius form of the diffusion hopping rate with a prefactor of 10^{13} s^{-1} and an activation energy of 0.6 eV. The threshold of observable diffusion is assumed to be 1 hop/hour.

low as 80 K. Since thermal diffusion is negligible at this temperature, a fundamental new growth mechanism must be operative.

Two novel explanations have been proposed for these results. The first is the idea of ballistic or "transient mobility" of the adsorbing atoms [10]. In this model the large amount of energy (2.5 - 3.5 eV) liberated by the formation of the adatom-surface bond is used by the adatom to overcome the diffusion barrier and skip across the surface until it comes to rest next to a growing island. Transient mobility seems physically reasonable since the diffusion barrier typically represents less than 20 % of the adsorption energy. The adsorbing atom can therefore lose the majority of its energy and still be able to freely move about the surface. There has, however, been no microscopic confirmation of this intriguing proposal.

The second explanation [12,13] involves the idea of "downward funneling" of the impinging adsorbate atom. In this model, the small growing three-dimensional islands cannot adsorb gas phase atoms on their steep sides, and thus the gas atoms "funnel" down to the flat layers below the islands. This model leads to coverages of ca. 85 %, 15 %, and 0 % for the three consecutive top layers [12c]. Thus, the growth is almost layer-by-layer. This "funneling" idea is physically reasonable and is supported by microscopic simulations [12b,12c].

Both explanations of low-temperature epitaxial growth make assumptions about the dynamics of the depositing atoms. The transient mobility model is sensitive to the details of the adatom-surface energy transfer. Downward funneling assumes that the kinetic energy of the impinging adatom is sufficient to overcome

any attraction it has to the sides of three-dimensional crystallites. This demonstrates the need to closely examine the dynamics of the deposition process.

At temperatures above the onset temperature, thermally-activated diffusion of the deposited atom will occur. Field ion microscope (FIM) experiments have revealed that diffusion of metal atoms on metal substrates can be a complicated process [14]. Diffusion rates may vary by orders of magnitude on different crystal faces of the same metal [14a]. Also, experimental observations have changed the simple picture of diffusion as an adatom rolling around on a bumpy surface, often giving way to more complicated mechanisms. For instance, diffusion on the (110) surfaces of the FCC metals Pt, Ir, and Ni has been observed to proceed via an exchange between the adatom and an adjacent substrate atom [14d,14e,14f]. Recent experiments have also indicated an exchange mechanism for the diffusion of Pt on the less open Pt(001) surface [14g]. These results demonstrate that the substrate can play an active role even in simple processes like single atom diffusion.

In this work, the dynamics of the elementary steps of film formation, deposition and diffusion, are examined via computer simulation. In the early stages of film growth, these are the dominant processes, competition between which determines the degree of perfection in the resulting epitaxial layer. By concentrating independently on these elementary steps, we hope to lay the foundation of future efforts to understand epitaxial growth.

Deposition and equilibration typically transpire on a timescale of a few picoseconds. This corresponds to the intrinsic timescale of molecular dynamics calculations, therefore direct simulations of deposition are computationally feasible.

Direct simulations of diffusion are possible only at temperatures where the diffusion rate is greater than one hop per 100 picoseconds. At lower temperatures it may be possible to use kinetic or lattice-gas (LG) models to describe diffusion [15]. These describe atomic motion in terms of activated jumps between points on a lattice. Since they ignore the short-time (i.e., thermal) motion of the atoms, they are much less computationally intensive. The validity of such an approximation is not obvious but molecular dynamics provides a way to evaluate if such models are appropriate in the systems we studied.

A detailed, microscopic examination of transient mobility was the motivation for Paper I. We present the results of detailed molecular dynamics simulations of atom deposition on FCC(001) systems. Special emphasis is placed on Cu atom deposition onto a Cu(001) surface. Results for the Ni, Rh, Pd, Ag, Pt, and Au systems are also presented to determine the generality of the dynamical features. Direct simulation of atom deposition onto a clean surface is used to determine the degree of adatom mobility.

In addition to addressing the question of transient mobility, we explore several fundamental aspects concerning the simulation of processes on surfaces. The first of these is the choice of potential energy surface (PES) from which the interatomic forces are derived. Results were obtained using several potentials, thereby allowing us to separate general dynamical features from fine-points which depended upon the particular choice of PES. Second, a slab of only a few thousand atoms was used to simulate a semi-infinite surface. The effects of finite size were determined by varying the size of the slab model. Finally, in the real system,

energy flows through the solid and is exchanged with the surroundings to maintain thermal equilibrium. Boundary conditions which mimic immersion of the slab in a heat bath were added and their effect on the dynamical results determined [16].

In Paper II, we present results of a study of single metal atom diffusion on FCC(001) metal surfaces. Molecular dynamics simulations were performed of two systems - Ag on Ag(001) and Rh on Rh(001). The Ag system was of interest since experiments have found that Ag atoms have an anomalously low diffusion barrier on metal substrates [17]. In contrast, FIM data [14a] for Rh self-diffusion indicates that a relatively large barrier (ca. 0.9 eV) exists on the (001) face. The detailed dynamics of diffusion in these systems provides a means to test the assumptions of kinetic models.

At temperatures where the diffusion rate is less than 10^{10} s^{-1} direct MD simulation is no longer possible. Therefore, a simple model of surface diffusion, site to site hopping, was considered and rate constants were calculated via transition state theory (TST) for all adsorbate/substrate combinations of the metals Ni, Cu, Rh, Pd, Ag, Pt, and Au. The TST method is expected to be quite accurate [18] and allows us to examine general trends in metal on metal diffusion.

Since molecular dynamics was the primary tool in this work, a discussion of it and how it was implemented here is necessary for completeness. The molecular dynamics method follows the propagation of a system of interacting atoms by solving the equations of motion for each atom. Investigations of surfaces typically involve a slab of 10^3 to 10^4 atoms arranged in the geometry of the crystal face under study.

Due to the large number atoms, usually only the classical motion of the atomic nuclei is considered.

The motion of each atomic coordinate is controlled by the forces exerted on it by the neighboring atoms. Classically, this relationship can be expressed through Newton's equations,

$$m_i \frac{d^2 x_{i,k}}{dt^2} = f_{i,k} \tag{3}$$

where m_i is the mass of atom i, $x_{i,k}$ is its k^{th} coordinate, and $f_{i,k}$ is the k^{th} component of the force on it. In a conservative system the force on an atom is derived from the global potential energy surface (PES),

$$f_{i,k} = -(\nabla_i V)_k \tag{4}$$

where ∇_i is the gradient with respect to the coordinates of atom i and V is the global potential energy surface. The function, V, gives the total potential energy of the system as a function of all the atomic coordinates. Solution of the dynamical problem now depends on the choice of potential energy function used to describe the physical system.

In the past, the potential energy surface has been written as a sum of pairwise interactions such as the Morse [19] and Lennard-Jones (12,6) [9]. These forms describe chemical bonding solely in terms of nuclear coordinates and thus ignore the true source of atomic interaction - the electrons. Recent MD simulations of Si clusters [20] have used a first principles method to relax the electronic structure and calculate the internuclear forces. Unfortunately, at present, these

techniques are restricted to small numbers of atoms (≤ 60). A compromise between simple pairwise forms and *ab initio* methods, which are not yet feasible for large-scale MD calculations, is the effective medium (EM) theory [21e] where the electronic structure is approximated by jellium. The jellium model consists of a homogeneous electron gas with a uniform positive background to provide charge neutrality.

In a number of articles [21], an approach to the calculation of interaction energies based upon direct evaluation of the corrections to the effective medium theory using density functionals has been derived, implemented and applied. This is called the corrected effective medium or CEM theory. Recently, the conceptual and formal simplifications of the CEM theory have been presented which allow it to be used directly in molecular dynamics (MD) and Monte Carlo (MC) simulations of large systems [22], hence the acronym MD/MC-CEM. Within the MD/MC-CEM theory the potential energy for a set of interacting atoms $\{A_i, i = 1, 2, 3, ..., N\}$ is,

$$V(\{A_i\}) = \sum_{i=1}^{N} \Delta F_J(A_i;n_i) + \sum_{i=1}^{N} \sum_{j>i}^{N} \Delta V_c(i,j) \; . \qquad (5)$$

The first term sums the interaction energy, $\Delta F_J(A_i;n_i)$, of embedding each atom A_i in jellium of density n_i. In general these embedding energies are semi-empirical functions, but within the MD/MC-CEM theory their form depends only on the jellium density and the chemical identity of the atom. A more detailed description of their construction will be presented later. The jellium density of atom A_i is evaluated as a weighted average of the atomic electron densities, ρ, of all the other atoms,

$$n_i = \frac{1}{2}\sum_{i\neq j}^{N} \int d\vec{r}\left[\frac{\rho(A_i;\vec{r}-\vec{r}_i)}{Z_i}\right]\rho(A_j;\vec{r}-\vec{r}_j)\ . \qquad (6)$$

In our calculations, spherical Hartree-Fock atomic electron densities are used. The second term in Eq.(5) is the sum of the classical electrostatic atom-atom coulomb energies (i.e., total nuclear-nuclear, nuclear-electron, and electron-electron energies) between atom A_i and all other atoms,

$$\Delta V_c(i,j) = \int d\vec{r}_1 \int d\vec{r}_2 \frac{[\rho(A_i;\vec{r}_1-\vec{r}_i)-Z_i\delta(\vec{r}_1-\vec{r}_i)][\rho(A_j;\vec{r}_2-\vec{r}_j)-Z_j\delta(\vec{r}_2-\vec{r}_j)]}{|\vec{r}_1-\vec{r}_2|}\ . \qquad (7)$$

Note that the coulomb interaction is **completely** determined by specifying the chemical identities of the atoms; there are no adjustable parameters in it.

The embedding energy functions used in this work were determined by requiring that the MD/MC-CEM energy reproduce properties of the homonuclear systems. In particular, the embedding function is chosen so that the MD/MC-CEM energy matches the interaction energy of a bulk atom,

$$\Delta E_{bulk}(A_i;a) = \Delta F_J(A_i;n_i) + \frac{1}{2}\sum_{j\neq i} \Delta V_c(i,j) \qquad (8)$$

where $\Delta E_{bulk}(A_i;a)$ is the interaction energy of an atom in a bulk system with lattice spacing, a. Note that when $a = a_0$, the equilibrium lattice constant, $\Delta E_{bulk}(A_i;a)$ equals the bulk cohesive energy. The embedding function is tabulated by varying the lattice spacing and calculating the jellium density and coulomb energy. The embedding energy is then determined from Eq.(8).

The procedure outlined above depends on being able to accurately describe the variation of the bulk interaction energy with lattice spacing. In the past, a three

parameter Morse function was used to expand the bulk cohesive energy about small changes in the lattice spacing [22]. The bulk energy was written as an explicit function of the lattice constant and parameters were chosen to reproduce experimental values of the equilibrium lattice constant, cohesive energy, and compressibility. This approach was limited due to the inability of the Morse form to describe large expansions or contractions of the lattice spacing. In particular, it was impossible to sufficiently expand the lattice to allow mapping of the low jellium density region. This region is crucial since the jellium density of an atom on the surface is much lower than that of a bulk atom. Consequently, the bulk embedding function had to be supplemented with low density points from a similar treatment of the homonuclear diatomic. Recently, embedding functions have been determined using linear muffin-tin orbital (LMTO) calculations to describe expansions of the bulk system [4]. The LMTO method now provides a consistent description of both the high and low jellium density regions of the embedding function. The LMTO embedding functions were used for all calculations in this work.

Beyond the PES there are a number of other aspects which must be dealt with when performing molecular dynamics simulations of large systems. For example, surface atoms initially placed in their ideal bulk positions tend to relax during the MD calculation as do real surfaces when cut from the bulk. If not dealt with properly, the resulting liberation of energy would interfere with the dynamics of an impinging gas atom. Computational concerns include efficient integration schemes for the equations of motion and optimization of routines to evaluate the potential energy and interatomic forces. Molecular dynamics calculations may

consume hundreds of hours of supercomputer time, it is therefore important that computer codes be written with great care.

In Paper III, we discuss the computer program, SCT89, used to perform the calculations in this work. Considerable time and effort went into the construction of this code which is capable of treating a variety of gas-surface problems. The justification for such an effort is two-fold. First, development of the MD/MC-CEM potential energy surface allows us to efficiently calculate accurate interatomic forces. Second, the development of stochastic molecular dynamics has dramatically lowered the number of atoms necessary to mimic a semi-infinite surface [16]. Together, these provide the ingredients necessary to perform reliable simulations of real systems.

While most of this dissertation discusses the results of SCT89 calculations it is important not to diminish the amount of work which went into construction of the SCT89 program. More than two years effort went into writing, testing, and debugging over 15000 lines of code before production of the results presented here could begin. This is emphasized because writing computer code is an important part in the training of theoreticians. It is analogous to the construction of laboratory instruments by students in experimental research. In both cases the success of the scientific research (i.e., the numbers) is likely to be related to the care that goes into construction of the tools. Also like experimental study, this nuts and bolts work does not happen overnight.

The original version of SCT89 was capable of simulating scattering from clean, low-index surfaces using only pairwise potentials. During its subsequent

development several new capabilities were added. A routine which determines the three-dimensional lattice vectors from the Miller indices and crystal type now allows us to setup any desired crystal face. The ability to place various adsorbate coverages on the surface was also added. A major addition was inclusion of the MD/MC-CEM potential energy function which allows us to consistently treat multi-component systems.

A number of innovative approaches to input/output were utilized to produce a user-friendly tool. For example, it is now a simple matter to specify the system to be studied. The user merely inputs the surface science notation (Miller indices and Wood's notation) which describes the system and the program automatically sets up the atom positions. There is also a special mode in which the program will prompt for all necessary input and create a its own input file. SCT89 also facilitates the visualization of simulation results. One program option periodically writes files containing the current atom positions in a format which can be directly imported into animation software. Such features simplify program use and encourage "experimentation".

It is important to note that SCT89 was not created because of our desire to study deposition and diffusion. Rather, this work was made possible by the fact that SCT89 can treat problems beyond its original intent. SCT89 has also been used in a number of other studies within our research group. It was used to simulate the scattering of Ar from clean and H covered Pd(111). Energy transfer was studied by simulating the collision of high energy Ar atoms with Pt(111). The dynamics of O_2 dissociative chemisorption has been investigated on Pt and Ni surfaces. SCT89 was

also used to examine sandwich compound formation in the Rh-Ag system. The variety of these works demonstrates the wide scope of SCT89's capabilities.

PAPER I.

METAL/METAL HOMO-EPITAXY ON FCC(001) SURFACES: IS THERE TRANSIENT MOBILITY OF ADSORBED ATOMS?

Metal/metal homo-epitaxy on FCC(001) surfaces: Is there transient mobility of adsorbed atoms?

David E. Sanders[a]
and
Andrew E. DePristo

Department of Chemistry
Iowa State University
Ames, Iowa 50011

[a] IBM predoctoral Fellow

ABSTRACT

We have investigated the dynamics of adsorption of a metal atom on a FCC(001) metal substrate of the same atom type. Two points were considered in detail: 1) the extent of ballistic or transient mobility (i.e., ability of the adatom to transform kinetic energy gained by adsorption into motion parallel to the substrate); 2) convergence of results with the number of moving atoms retained in the simulation.

Using the molecular dynamics technique with four different types of potential energy surfaces (PES), we have discovered there is *no* transient mobility for the Cu/Cu(001) system at a surface temperature of 80 K and an incident gas atom kinetic energy of 0.25 eV. We have also discovered an important pitfall in such simulations: use of an insufficient number of active substrate layers leads to incorrect results displaying significant ballistic motion of the adsorbate. Using our most accurate many-body density functional based MD/MC-CEM PES and retaining sufficient number of active layers, we have also found an absence of transient mobility for the Ni/Ni(001), Rh/Rh(001), Pd/Pd(001), Pt/Pt(001), and Au/Au(001) systems. Only the Ag/Ag(001) system, with a very small diffusion barrier, was found to display any mobility.

INTRODUCTION

The growth of thin films on solid substrates has applications including the printing of circuits on computer chips, the coating of optics for high resolution instruments and the construction of miniature angstrom scale devices. These require the growth of well ordered adlayers.

It was thought that significant adatom diffusion (i.e., high substrate temperatures) was necessary to obtain a smooth film morphology. However, recent experiments involving the growth of Cu on Cu(001) [1] and Pt and Pd on Pd(001) [2], have found evidence for smooth layer-by-layer growth at temperatures as low as 80 K where diffusion is negligible on the experimental time-scale. Thus, a fundamental new growth mechanism must be operative.[1]

There have been two novel explanations for these results. The first [1], which has received wide attention [4], is the idea of ballistic or transient mobility of the adsorbing atoms. In this model, to quote from ref.[1], "the deposited atom uses its latent heat of condensation to skip across the surface, preferentially coming to rest at growing island edges." While this idea provides a reasonable and intriguing explanation of the experimental data, there has been no direct microscopic confirmation of it.

The second explanation [5] is the idea of "downward funneling" of the impinging adsorbate atom. In this model, the small growing three-dimensional

---

[1]For completeness, we mention that experimental data on another system, Pt on Pt(111), may also provide evidence for non-diffusive layer by layer growth [3]. However, the very low diffusion barrier on the close packed (111) face makes it more difficult to be rule out significant diffusive motion.

islands cannot adsorb gas phase atoms on their steep sides, and thus the gas atoms "funnel" down to the flat layers below the islands. This model *does not* yield perfect layer-by-layer growth but instead leads to coverages of ≈ 85 %, ≈ 15 % and ≈ 0 % for any three consecutive top layers. Thus, the growth is almost layer-by-layer. This "funneling" idea is also reasonable and is supported by microscopic simulations [5b,5c], but would not be sufficient to explain experimental data that can rule out the ≈ 15 % non-filled first layer.

The purpose of the present paper is to provide a detailed microscopic investigation of the extent of ballistic mobility. The energetics of the adsorption process are illustrated schematically in Figure 1. The energy levels in this diagram are typical of metallic FCC(001) systems at 80 K, as measured relative to the bottom of the adsorption well. The asymptotic energy includes the initial kinetic energy which is approximately calculated at the vaporization temperature of the depositing atoms. The kinetic energy is such a small fraction of the asymptotic energy that its precise value is unimportant.

The three distinct collision outcomes are determined by the final adatom energy relative to the levels in Figure 1. In *trapping*, the adatom loses some fraction of its asymptotic energy (e.g., 10 - 80 %) to fall below the level of the adsorption energy but above the diffusion barrier. In *localization*, the adatom loses a large fraction (e.g., > 80 %) to fall below the diffusion barrier. In *equilibration*, the adatom is thermalized at the 80 K surface temperature; the small thermal energy relative to the diffusion barrier yields a negligible diffusion rate. The transient mobility model assumes that the energy transfer process is inefficient and

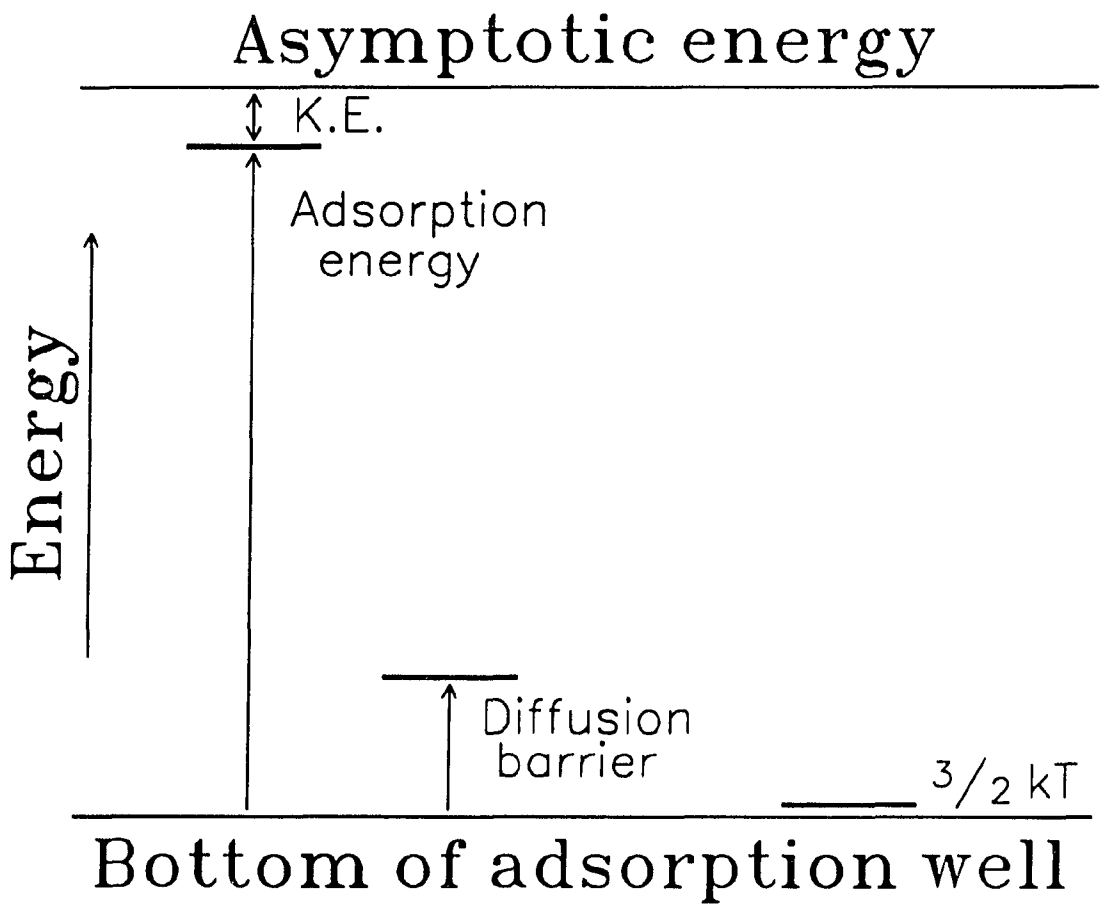

Figure 1. Schematic total (kinetic plus potential) energy diagram for the metal/metal adsorption process on an FCC(001) substrate

Energies are measured relative to the bottom of the adsorption well.

the adatom retains energy in excess of the diffusion barrier for some time after trapping. Since the difference between the adsorption energy and the diffusion barrier is quite large, the transient mobility model appears quite reasonable physically.

We emphasize that the efficiency of energy transfer to the surface controls the extent of transient mobility. It is necessary to determine the energy transfer by direct simulation since this is a difficult quantity to estimate. For example, consider the cube model [6] in which the atom-surface many-body collision problem is replaced by a binary billiard ball collision between the adsorbate and a single massive particle or cube representing several substrate atoms. This yields the following expression for the final energy, E_f, given the initial asymptotic energy, E:

$$E_f = E \frac{(1-u)^2}{(1+u)^2} \tag{1}$$

Here, u is the ratio of the adatom mass to the cube mass and has been assumed to satisfy $0 \leq u \leq 1$ in the derivation. All of the many-body behavior is embodied in the choice of cube mass and the energy transfer efficiency is sensitive to its value. Reasonable choices of $u = 1$, a head on collision with one surface atom, and $u = 0.25$, an equal partitioning among the four nearest neighbor surface atoms, leads to the range $0 \leq E_f \leq 0.36E$. Since this range overlaps the transition from localization to transient mobility at $E_f \approx 0.2E$, it is impossible to make any predictions using the simple cube model.

In this article, we present the results of detailed molecular dynamics (MD) simulations of homo-epitaxy, with particular focus on Cu atom deposition onto a

Cu(001) surface. Results for the Ni, Rh, Pd, Ag, Pt, and Au systems are also presented to determine the generality of the dynamical results. We have taken care in this work to ensure the validity of the MD simulations because we wish to make strong statements about the dynamics of metal on metal deposition and especially answer the question of transient mobility.

Our general approach was to use the MD method to follow the impinging atom from the time it first interacted with the surface until it localized onto an adsorption site. Ideally, the only biases built into MD are the use of classical mechanics and the accuracy of the potential energy function. Other constraints are due to computational limits and/or invalid approximations and should not be allowed to influence the results. We were particularly careful in this work to separate the major dynamical features from any artifacts due to the simulation. This may help establish a better understanding of the requirements for realistic and believable simulations of surfaces. It should at least demonstrate the source of errors in some previous simulations of the adsorption process.

Three major aspects influenced the dynamics of the depositing atoms. First, the motion of all atoms was governed by interatomic forces derived from the global potential energy surface (PES). Since it was difficult to know *a priori* which features of the dynamics were strongly sensitive to the choice of potential energy function, results were obtained using several different PES. By doing this, the general dynamical features were separated from those dependent upon fine points of the PES. Second, a real semi-infinite surface was simulated by a slab of only a few thousand atoms, the simulation cell. The effects of finite size were determined by

varying the size of this simulation cell. Third, in a real system, energy flows through the solid and is exchanged with the surroundings to maintain thermal equilibrium. The total energy in a simulation must remain constant if all forces arise from the PES. In such a system a large number of atoms are needed to realistically model energy dissipation. Boundary conditions which mimic immersion of the moving atoms in a heat bath were added and their effect on the dynamical results was determined.

POTENTIAL ENERGY SURFACE

Although a MD simulation is limited in the description of a real system by the accuracy of the PES, not all processes depend upon the same details of the PES [7]. For example, in high energy atom-surface scattering the depth and shape of the atom-surface attractive potential is unimportant. In addition to direct adsorbate-substrate interactions, the substrate-substrate interactions may also influence the adsorbate dynamics. As an example, the stiffness of the substrate-substrate interactions affects the shape of the adsorbate-surface repulsive wall and therefore the ability of the adsorbate atom to exchange energy with the surface. So, the substrate-substrate interactions control the degree of adiabaticity of the substrate response to the impinging adsorbate.

To judge the sensitivity of the present results to the PES, we use several different forms. The first, and we believe most accurate, is based upon the recently developed version of the corrected effective medium (CEM) theory [8] for molecular dynamics and Monte Carlo simulations (MD/MC-CEM) [9]. The MD/MC-CEM method provides a quantitatively accurate description of bulk cohesive energies and surface energies of transition metal surfaces and is qualitatively correct for surface layer relaxations [9,10]. The latter are unimportant for the present work.

Within MD/MC-CEM the potential energy of an atom, A_i, at position, $\vec{r}_i$, is given by the following expression[2],

$$V(A_i;\vec{r}_i) = \Delta F_J(A_i;n_i) + \frac{1}{2}\sum_{j\neq i} V_c(i,j) \; . \tag{2}$$

The first term is the 'effective' embedding energy of atom A_i into jellium of density n_i, $\Delta F_J(A_i;n_i)$. These 'effective' embedding energies are *empirical* functions that depend on the chemical identity of the atom and the jellium density. They are known for nearly all elements in the periodic table through Xe either from experimental data on homonuclear diatomic and bulk systems [9] or from LMTO calculations on the bulk system [10]. The jellium density of atom A_i is evaluated as a weighted average of the atomic electron densities of all the other atoms,

$$n_i = \frac{1}{2}\sum_{j\neq i} \int d\vec{r} \left[\frac{n(A_i;\vec{r}-\vec{r}_i)}{Z_i}\right] n(A_j;\vec{r}-\vec{r}_j) \; . \tag{3}$$

In our calculations, spherical Hartree-Fock atomic electron densities are used.

The second term is the sum of the classical electrostatic atom-atom coulomb energies (i.e., total nuclear-nuclear, nuclear-electron and electron-electron energies) between atom A_i and all other atoms. It is important to note that the MD/MC-CEM potential energy is determined by specifying the chemical identities of all atoms in the system; there are no adjustable parameters. We are not suggesting, of course,

---

[2]This expression does not conform to the definition in the CEM references which define the total system interaction energy, $\Delta E(\{A_i\})$. The current expression is simply the translation into the interaction potential, and is only valid for the MD/MC-CEM simplification of CEM. In the full CEM theory, one cannot identify potentials for any atom since it contains a complex, non-separable energy functional of the total system electron density.

that the MD/MC-CEM PES will be quantitatively accurate for all systems. For example, calculation of coverage dependent interaction energies for Au on Cu presents great difficulties for the MD/MC-CEM method (which are alleviated in the more accurate but much more computationally expensive CEM theory) [11]. For a more complete description of the MD/MC-CEM theory, the reader is encouraged to consult refs. [8,9,10] and especially the review in ref.[8e].

In addition to the MD/MC-CEM potential, we have used three purely empirical PES based upon addition of pairwise two-body interactions. These PES differ only in the nature of the pair interaction: a Morse and two parametrizations of a Lennard-Jones (12,6). The Morse pairwise function is,

$$V(R) = D\, e^{-\alpha(R-R_0)} \left[e^{-\alpha(R-R_0)} - 2 \right] \qquad (4)$$

with parameters chosen to reproduce three properties of the solid: the cohesive energy, Debye frequency and lattice constant [12]. For Cu, the parameters are D = 0.3429 eV, R_0 = 2.866 Å and α = 1.359 $Å^{-1}$.

The LJ(12,6) pairwise function is,

$$V(R) = D \left(\frac{\sigma}{R}\right)^6 \left[\left(\frac{\sigma}{R}\right)^6 - 2 \right]. \qquad (5)$$

Two parameters cannot reproduce the three properties of the solid. Thus, two different parametrizations were used. The first set, denoted as LJ-C, reproduced the cohesive energy and lattice constant, yielding (D = 0.4093 eV and σ = 2.624 Å) for Cu. The second set, denoted as LJ-D, reproduced the Debye temperature and lattice

constant, yielding (D = 0.05805 eV and σ = 2.624 Å) for Cu. The former set is very near that determined from the heat of vaporization and lattice constant [13].

It is worthwhile to emphasize that the MD/MC-CEM PES duplicates all three properties of the solid. It is intrinsically more flexible and of a different nature than any of the additive two-body PES.

The four different PES can be used to predict several properties of the clean Cu(001) surface and the Cu adsorbate interaction with the Cu(001) surface. In Table 1, the magnitude of the interlayer relaxations are reported in terms of percent expansions (+) and contractions (-) of the ideal bulk interlayer spacings and are compared to experimental data [14]. The MD/MC-CEM results are reasonable, while the others predict expansions of the first layer instead of contractions. This is simply an indication that pairwise additive potentials do not describe well the change in bonding from coordination 12 in the bulk to coordination 8 in the surface. The fact that the Morse results are much worse than the LJ demonstrates that even duplication of more data in one environment (i.e., the bulk system) does not guarantee better accuracy in another (i.e., the surface system), at least for potentials which are not based upon correct physics.

Figures 2 and 3 provide the interaction energy versus the height of the adatom above a four-fold hollow (4fh) adsorption site, where the zero of energy was the relaxed substrate with the adatom separated at infinity. The results in Figure 2 retained these same positions of the surface atoms for every position of the adsorbate (i.e., a rigid surface). By contrast, the results in Figure 3 allowed the surface atoms to move to the lowest energy configuration for each position of the

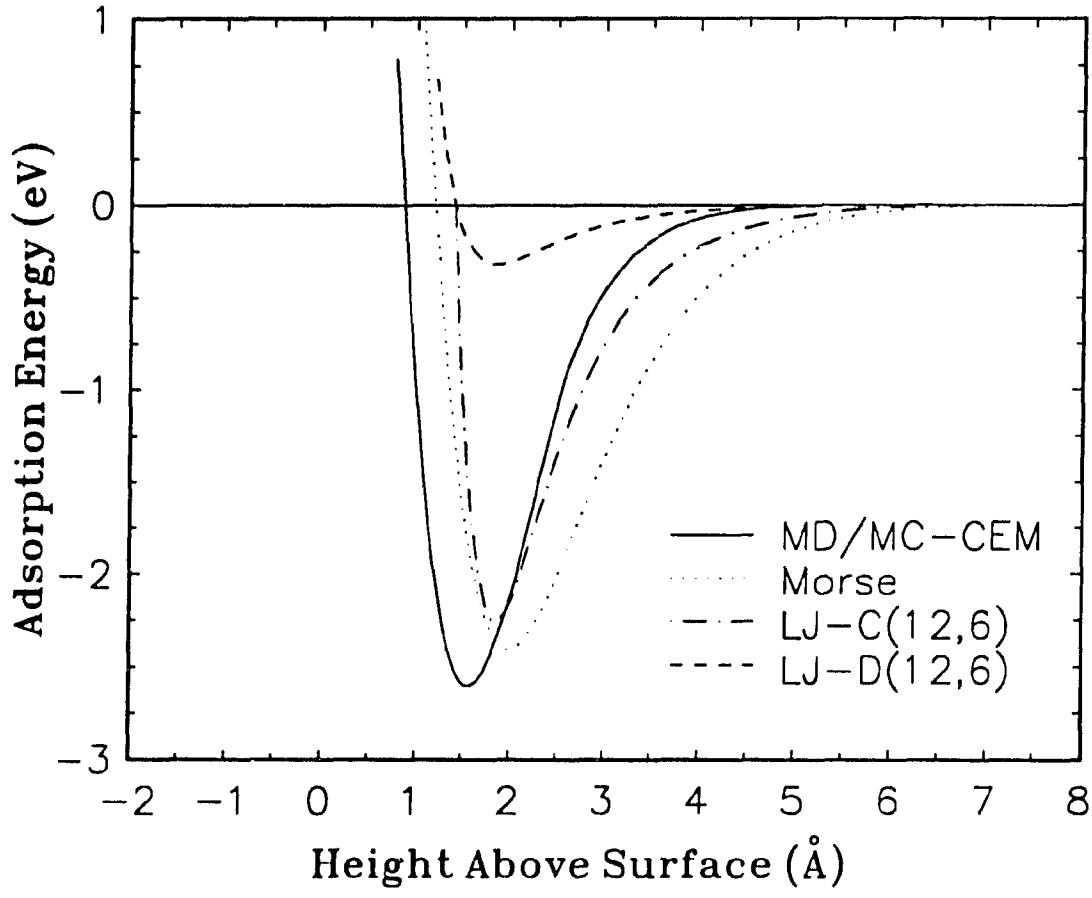

Figure 2. Interaction energy of a Cu atom with a Cu(001) surface as a function of the height of the Cu atom above a four-fold hollow site

Curves are shown for the four different PES defined in the text. The positions of the substrate atoms were held fixed at the clean surface geometry (i.e., rigid substrate).

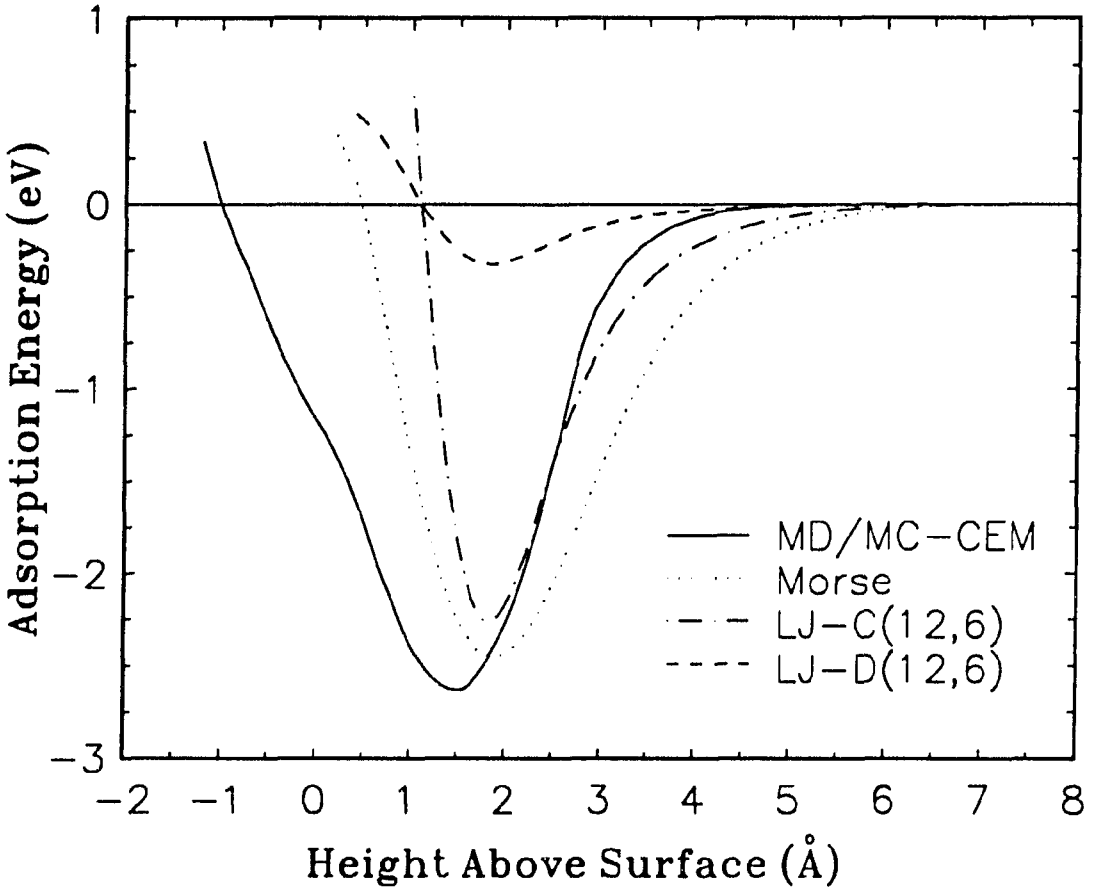

Figure 3. Interaction energy of a Cu atom with a Cu(001) surface as a function of the height of the Cu atom above a four-fold hollow site

Curves are shown for the four different PES defined in the text. The positions of the substrate atoms were moved to minimize the energy (i.e., adiabatic substrate response).

adatom (i.e., an adiabatic surface). The adsorption energies from the adiabatic curves are listed in Table 2.

During a MD trajectory, the interaction is a function of the instantaneous positions of the substrate atoms and therefore depends upon how quickly they can respond to the impinging atom. Neither the adiabatic nor rigid curves correspond to the interaction felt by an atom during any MD trajectory. Figures 2 and 3 do, however, represent the extrema of the interactions and are useful in comparing the different potentials.

Another feature of the PES which is important to Figure 1 is the diffusion barrier. While diffusion samples many parts of the PES, a good estimate of the barrier at low temperatures is the difference between the 4fh site and bridge site adsorption energies. At the very least, this barrier provides a convenient measure of surface corrugation. Values for the various potentials appear in Table 2 along with an experimental estimate [15].

Table 1. Interlayer spacings for Cu(001)

potential energy surface	$\Delta(1,2)$[a]	$\Delta(2,3)$
MD/MC-CEM	-0.9	-0.1
Morse	+9.6	+2.5
LJ(12,6)[b]	+2.4	+0.5
Experiment	-1.1 ± 0.4[c]	+1.7 ± 0.6
	-2.1 ± 1.7[d]	+0.5 ± 1.7

[a] $\Delta(i,j)$ is the percent contraction (-) or expansion (+) of the interlayer distance between layers i and j relative to the ideal bulk spacing (1.81 Å).

[b] The values using the Lennard-Jones form are independent of the strength, D in Eq.(5).

[c] Experimental data from ref.[14a].

[d] Experimental data from ref.[14b].

Table 2. Adsorption energies and diffusion barriers for Cu on Cu(001)

potential energy surface	E_{ads}[a] (eV)	E_{diff}[b] (eV)	diffusion barrier[c] (fraction of kinetic energy)
MD/MC-CEM	-2.63	0.53	0.18
Morse	-2.45	0.22	0.08
LJ-C(12,6)	-2.26	0.63	0.25
LJ-D(12,6)	-0.32	0.09	0.16
Experiment[d]		0.48	

[a]The adsorption energy is for binding in a four-fold hollow site with a fully relaxed substrate.

[b]Diffusion barrier is the binding energy difference between adsorption on fully relaxed 4fh and bridge sites.

[c]This is $E_{diff}/(E_{ads}+0.25\ eV)$ which estimates the diffusion barrier relative to the maximum adatom kinetic energy, assuming 0.25 eV initial kinetic energy.

[d]Experimental data from ref.[15].

The MD/MC-CEM, Morse, and LJ-C potentials all produce similar values for the adsorption energy, but yield very different results for the diffusion barrier and interlayer relaxations. The adsorption energy and diffusion barrier from the LJ-D potential are clearly wrong, but the LJ-D provides an excellent sensitivity test of the dynamical results. Clearly, all properties are predicted more accurately by the MD/MC-CEM PES, as expected. The adiabatic curves provide a measure of the softness of the adatom-surface potential and these show quite a variance in the response to the impinging adatom. The softness of the substrate affects the rate of adatom energy transfer. By using these different potential energy functions, we can identify the dynamical results which are sensitive to the details of the interaction.

ENERGY DISSIPATION

From Figure 1, it is clear that in typical FCC(100) metallic systems the amount of energy that must be lost by an adatom to localize in an adsorption site is ca. 80 % of the adsorption energy. The rate at which the substrate can absorb this energy is limited by the speed at which it can conduct the energy away from the point of impact. This energy propagates into the bulk via collisions between the solid's atoms. In real systems, this energy is eventually dissipated over 10^{23} atoms. A molecular dynamics simulation with only gradient of the potential forces and a (much smaller) finite number of atoms has no such mechanism to dissipate energy; the total energy of the system must be conserved. This leads to an unnatural local heating of the substrate that may induce diffusive motion. In addition with only a finite number of active atoms, the spreading energy must at some time come to an edge where it will be reflected towards the impact point, thereby providing the adsorbate with an unphysical "kick". For a large enough number of atoms, the recurrence time for this "kick" is much longer than any physical process and the amount of energy reflected is negligibly small.

In some previous work on epitaxial growth [16], energy dissipation has been simulated by rescaling the surface atom velocities at arbitrary intervals until the desired temperature was reached. This is a valid method to reach the equilibrium state which is independent of the path. It is not a valid method to determine the dynamics of the equilibration process since arbitrary velocity rescaling does not incorporate the rate of energy exchange. So, there is no physical

temporal or spatial scale built into the energy dissipation mechanism. For example, imagine the impact of a single adsorbate in which the surface atoms closest to the impact will be noticeably perturbed but those at some distance from the impact will undergo negligible perturbation. Velocity rescaling, however, "cools" all the atoms, even those not affected by the collision.

The "brute force" solution is to simply increase the number of atoms in the simulation cell. For processes that transfer large amounts of energy, the number of atoms required to mimic the infinite system could become computationally unfeasible. Alternatively, local frictional and random forces can be added to the atoms on the edge of the simulation cell to mimic energy flow between the active atoms and a heat bath [17]. This is termed the local Langevin equation method. The two added forces are balanced to satisfy the second fluctuation-dissipation theorem and therefore maintain the active atoms at the temperature of the bath [18]. It is important to note that Langevin coupling is used only as a computational convenience; it lowers the number of atoms that must be retained in the simulation but cannot be allowed to alter the dynamical results.

CALCULATIONAL DETAILS

A seven layer slab of a FCC(001) surface was used as the simulation cell. Each layer had a square shape centered on the origin with a side length of eighteen nearest neighbor distances. In layers designated as active, all atoms inside a square shaped zone with a side length of twelve nearest neighbor distances were allowed to move. Boundary atoms were defined as any active atom with at least one fixed nearest neighbor atom [17a]. For each of the four PES, a set of 1000 trajectories were run using one, two, and three active layers. Each of these runs was repeated with and without Langevin coupling applied to the boundary atoms.

The individual trajectories were begun with a single adatom impinging normally towards the simulation cell. The aiming point of the adatom was randomly sampled over the unit cell centered on the origin. The initial kinetic energy of the adatoms was chosen to be 0.25 eV (2900 K) in all trajectories because we assumed that the experimental source of atoms was a hot filament; the asymptotic kinetic energy therefore corresponded roughly to the vaporization temperature. However, this value has very little affect on the trajectories since any reasonable initial energy is small compared to the adsorption energy.

The substrate atoms were initialized to a temperature of 80 K. In runs where Langevin coupling was used, this temperature was maintained with only a slight variation during the initial adatom collision. Without Langevin coupling there was no way to dissipate heat and the temperature therefore increased. In systems with a single active layer, (the fewest number of active atoms), the temperature rose

to ca. 120 K[3] which was still below the onset temperature of thermally activated diffusion.

The atomic motions of the adatom and substrate were propagated for three picoseconds. Preliminary calculations showed this amount of time to be sufficient to ensure adatom trapping in the majority of the trajectories; exceptions to this rule are discussed in the next section.

---

[3]This is a reasonable value based upon dissipation of the initial 3.0 eV kinetic energy, relative to the bottom of the adsorption well, over ca. 140 active atoms which yields a rise of 30 K.

RESULTS AND DISCUSSION

The trajectory results reported are the final (x,y) positions of the adatoms. For each set of trajectories, these points were plotted on a grid representing the substrate lattice as shown in Figure 4. The intersection of two grid lines corresponds to a 4fh adsorption site, while the center of the grid squares corresponds to an atop adsorption site (i.e., the position of a first layer substrate atom). The adatoms were all aimed within the square centered on the origin and marked with an "x".

The first results, using each of the four PES, are shown in Figure 4 for the case in which only a single substrate layer was allowed to move and Langevin coupling was absent on the boundary atoms. The results for the Morse and LJ-D potentials demonstrate that the adatom moves up to six unit cells away from the impact point. In these two cases, the adatoms have not settled into the 4fh adsorption sites and were still moving across the surface at the end of the three picosecond trajectories. For the more corrugated LJ-C and MD/MC-CEM potentials, all adatoms were localized at the end of the trajectory and mobility was reduced to at most four unit cells.

The main dynamical feature of this first set of runs is the non-diffusive movement of the adatoms away from the impact point. As mentioned in the section on energy dissipation, with only a single active layer those substrate atoms first struck by the adatom could ricochet off the fixed atoms below. As a consequence, the adatom would be subject to repeated kicks from the rebounding substrate atoms.

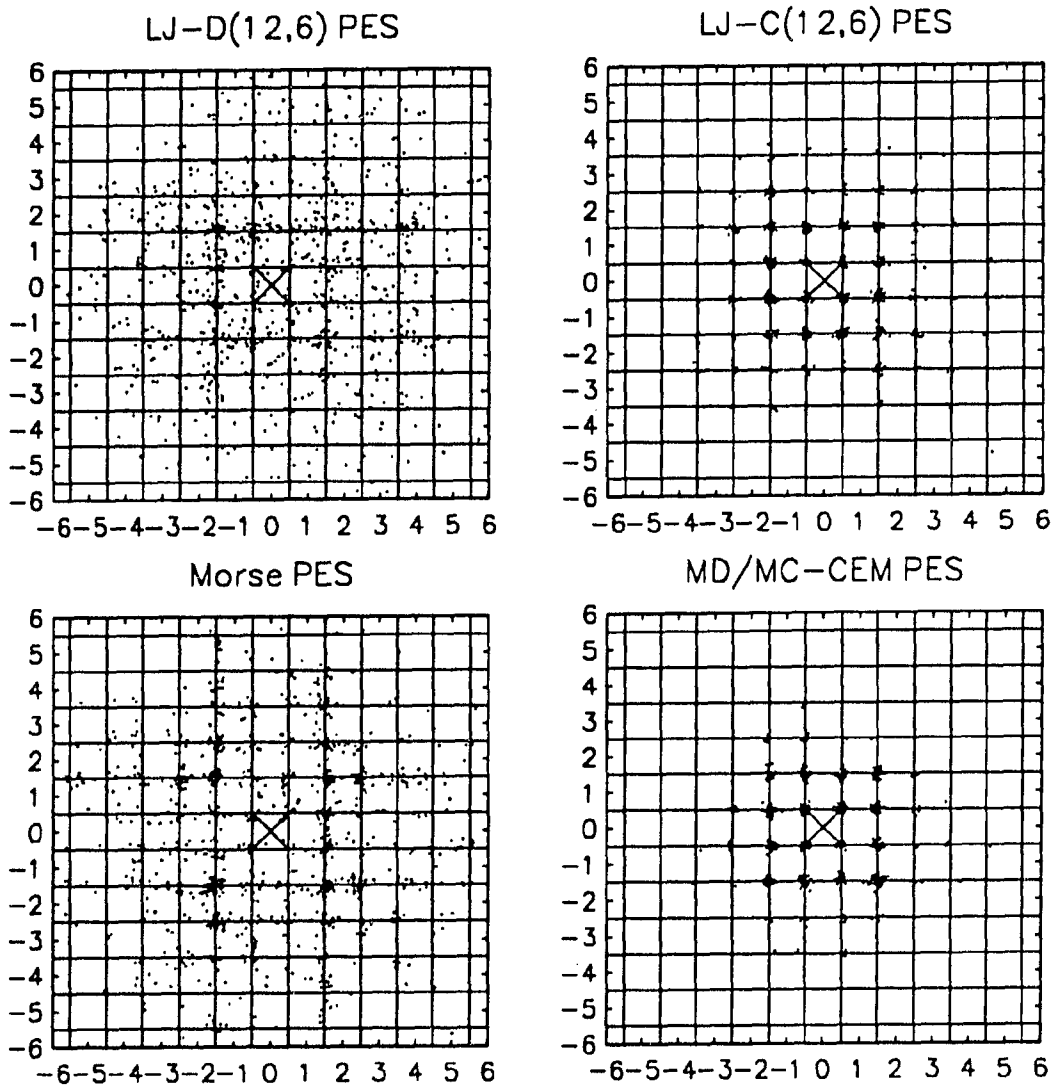

Figure 4. Distribution of the final (x,y) position of the adsorbing atom calculated using various PES

Each dot represents one trajectory value. The trajectories used a random aiming point in the square marked by an "x" and thermally distributed velocities and coordinates of the surface atoms at T=80 K. The axes units are nearest neighbor distance (2.55 Å) while the intersections of the grid lines identify four-fold hollow sites. These runs had one active layer and no local Langevin coupling.

To test for, and eliminate, this possibility identical simulations were performed using two and three active substrate layers.

Results for three active layers appear in Figure 5. Even for the less corrugated LJ-D and Morse surfaces, adatom motion is restricted to at most two unit cells. The results on the LJ-C and MD/MC-CEM surface show no more than one hop of the adatom. In all cases the adatoms were trapped at the end of the trajectories. Comparing Figures 5 and 4 demonstrates that *the enhanced mobility seen in the single active layer results was caused by a non-physical artifact of the simulation.*[4] In the larger simulation, the first layer atoms struck by the adatom transfer the collision energy to the deeper layers; the net result is much less energy reflected at the adatom.

A more quantitative analysis of the convergence of the simulation results with increasing number of active layers for the MD/MC-CEM potential appears in Figure 6. The three sets of histogram bars represent the distribution of final adatom positions for simulations with one, two, and three active substrate layers. With three active layers essentially 100 % of the trajectories stuck in the target unit cell at which they were aimed. Similar convergence of results with the number of active layers was found for the Morse, LJ-C, and LJ-D potentials. Only the (unphysical) LJ-D potential displayed any mobility, but even in this case only 17 % of the trajectories **did not** stick in the target unit cell at which they were aimed.

---

[4]The simulation results in ref.[14] provided some support for the transient mobility concept. Since these used one active layer to start the simulation, the results must be discounted.

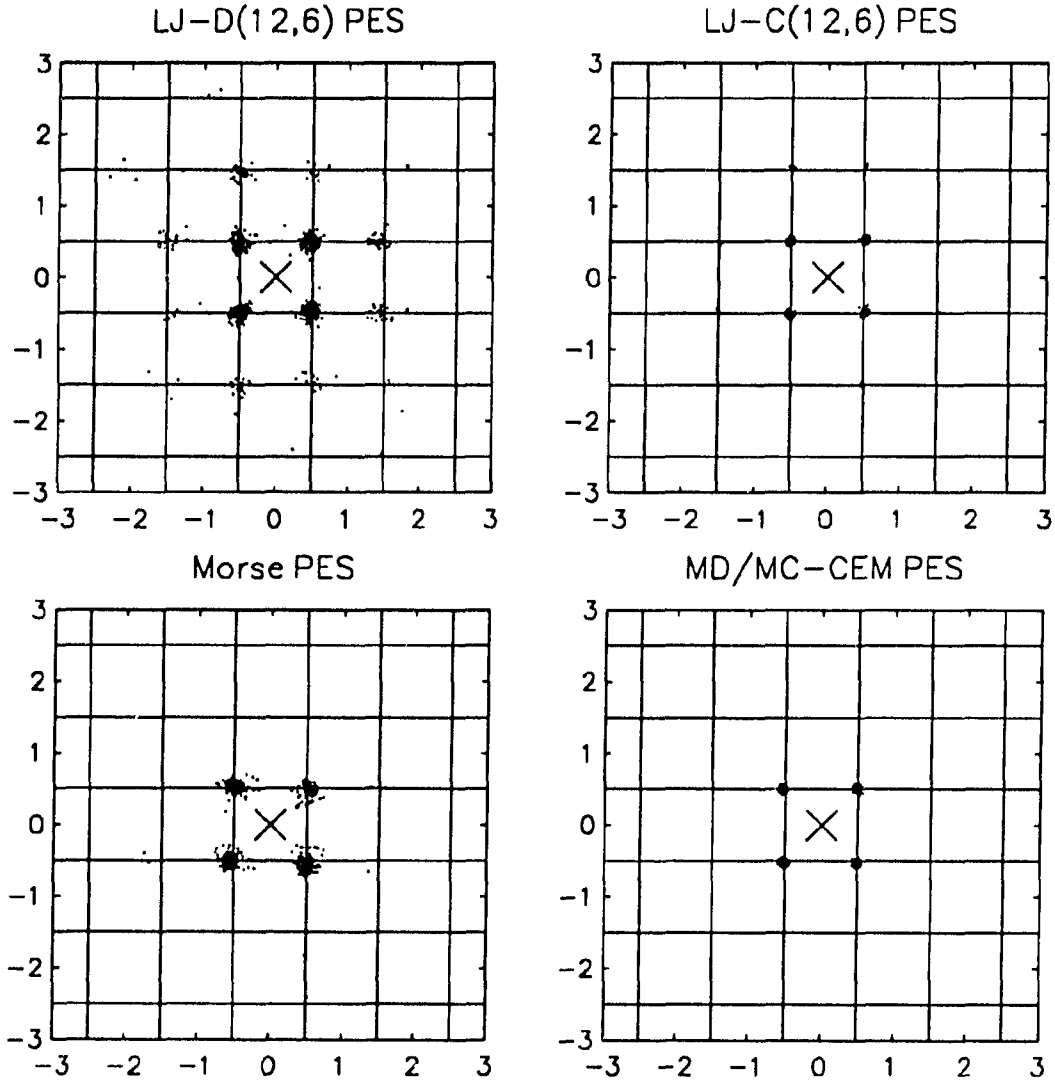

Figure 5. Same as Figure 4 except these runs had three active layers

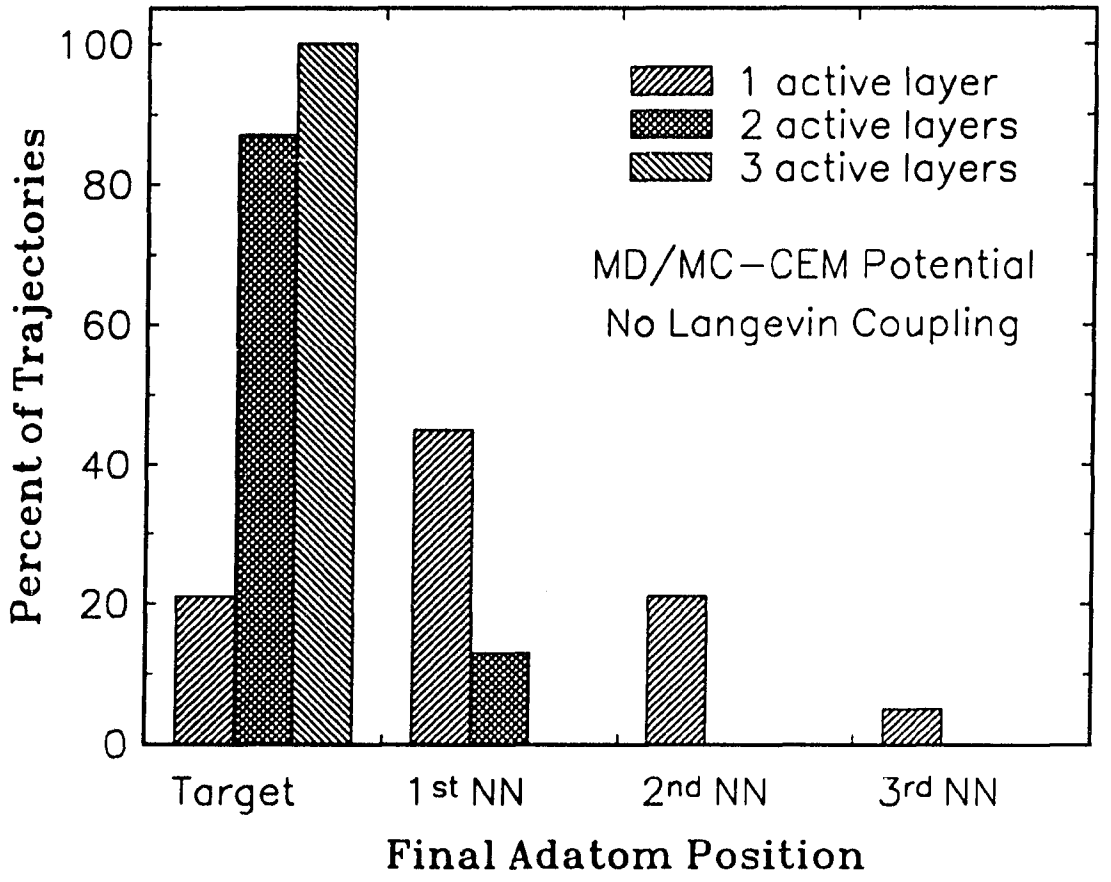

Figure 6. Distribution of the final (x,y) position of the adsorbing atom calculated using the MD/MC-CEM PES and one, two, and three active substrate layers without Langevin coupling

The surface T=80 K. "Target" is defined as any of the four four-fold hollow sites closest to the aiming point. "1^{st} NN" is any of the four first nearest neighbor four-fold hollow sites located 2.55 Å from the "target". "2^{nd} NN" is any of the four second nearest neighbor four-fold sites located $2.55\sqrt{2}$ Å from the "target". "3^{rd} NN" is any of the four third nearest neighbor four-fold sites located 5.10 Å from the "target". The results with 1 active layer do not sum to 100 % because some of these trajectories end up in the eight 4^{th} NN sites at $2.55\sqrt{5}$ Å and the four 5^{th} NN sites at $5.10\sqrt{2}$ Å.

The above results indicate that the majority of adatoms must retain only 10-25 % of their asymptotic energy after the initial collision, since that is the diffusion barrier compared to the maximum kinetic energy in Table 2. This corresponds to 1.9-2.3 eV of kinetic energy being transferred to the substrate. *The ability of the metallic substrate to absorb and quickly dissipate this amount of energy precludes any adatom transient mobility.* This result is generally true even for non-normal incident adsorbates. Simulations of adatoms deposited at 45^0 and even 60^0 from normal still show no transient mobility. The acceleration of the adsorbate due to interaction with the substrate leads to large normal velocities that dominate any small initial velocity parallel to the surface.

Simulations of the deposition process with smaller number of active layers may be feasible with the introduction of frictional forces [17a]. This was investigated using Langevin coupling to simulate the dissipation of energy, with results shown in Figures 7 and 8 using the MD/MC-CEM PES. These are representative of the results obtained using the other potential energy functions as well. Two active substrate layers were used in Figure 7 and three in Figure 8. The results in Figure 7 without Langevin coupling show a significant amount of hopping, while those with Langevin coupling show essentially no mobility. By damping the motion of the boundary atoms, the Langevin coupling reduces the amount of energy artificially reflected off the fixed atoms. The results in Figure 8 generated with and without Langevin coupling are virtually identical.

The addition of a realistic energy dissipation mechanism leads to a faster convergence of these simulation results, essentially requiring only 2 instead of 3

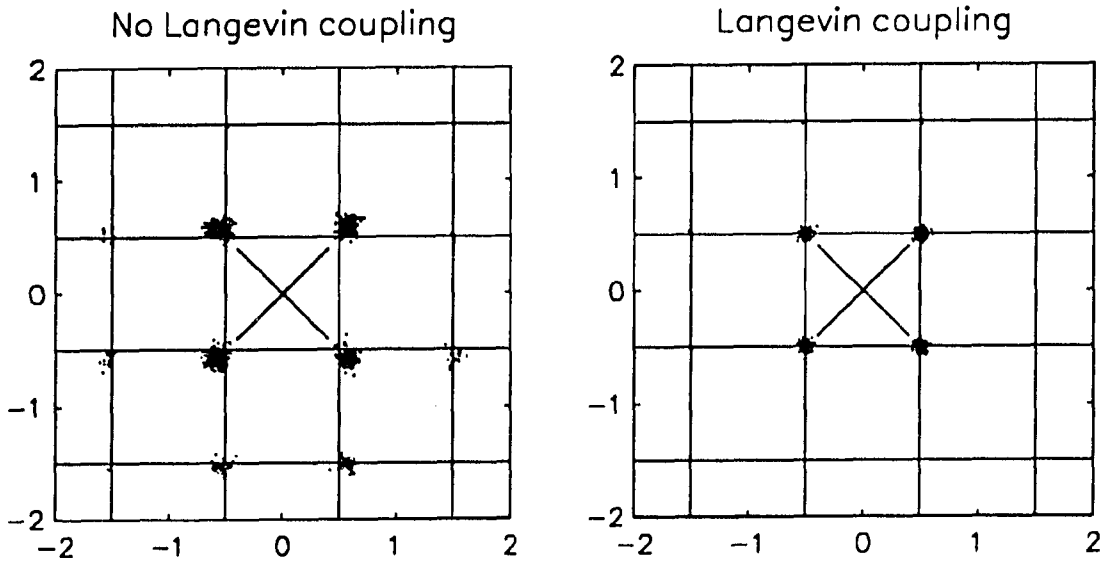

Figure 7. Same as Figure 4 except that only the MD/MC-CEM PES was used and there were two active layers, without and with Langevin coupling as noted

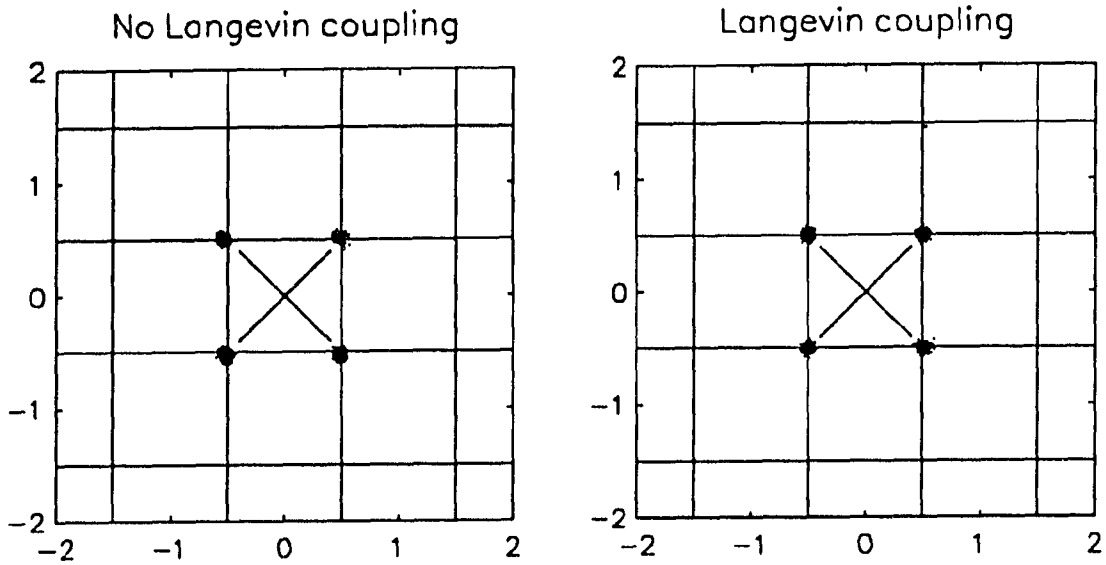

Figure 8. Same as Figure 7 except for three active layers

active layers. Furthermore, the Langevin coupling does not in any detectable way affect the final converged values. This is important since Langevin coupling is a computational convenience and not a physical effect. The fundamental feature remains the lack of any significant amount of transient adatom mobility.

The small differences between results obtained using the different potential energy functions can be ascertained by comparison of the three active layer values in Figure 5. The greater mobility for the Morse and LJ-D PES results from the lower diffusion barriers of these potentials. However, *the most important feature of these results is that the choice of potential makes very little difference in the nearly complete lack of adatom mobility.* Results for other homonuclear transition metal systems were generated using the MD/MC-CEM potential and Langevin coupling. These appear in Figure 9 with the adsorption energies and diffusion barriers appearing in Table 3. The general behavior is identical to that observed for Cu; there is no significant amount of transient mobility for any of these systems. Only Ag on Ag(001) shows any significant amount of mobility and this behavior correlates with the low diffusion barrier.

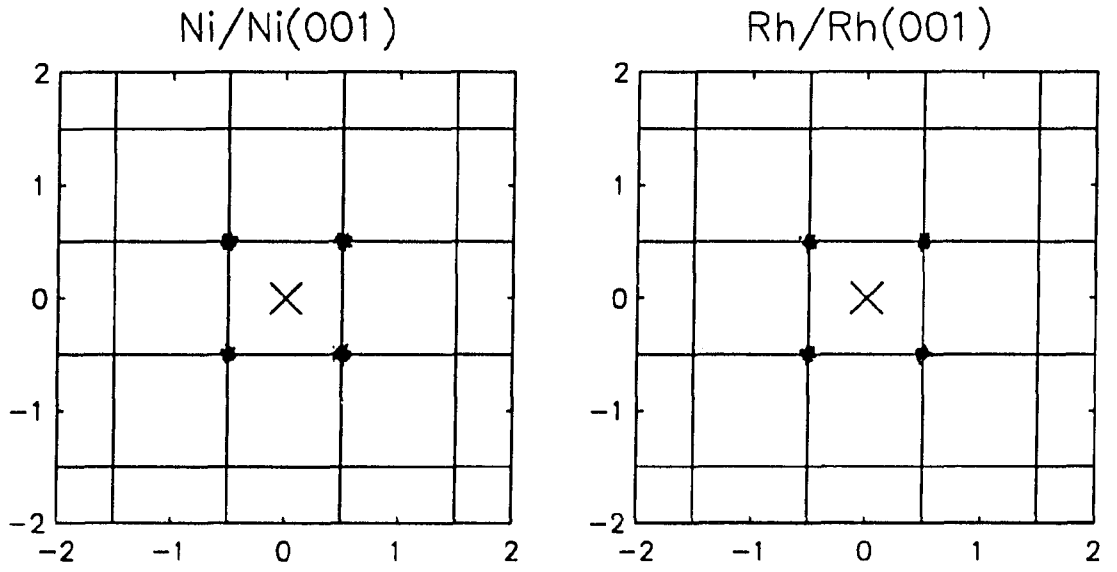

Figure 9. Distribution of the final (x,y) position of the adsorbing atom calculated using the MD/MC-CEM PES for various homonuclear FCC(001) systems

Each dot represents one trajectory value. The trajectories used a random aiming point in the square marked by an "x" and thermally distributed velocities and coordinates of the surface atoms at T = 80 K. The axes units are nearest neighbor distance while the intersections of the grid lines identify four-fold hollow sites. These runs had three active layers and local Langevin coupling, to ensure convergence.

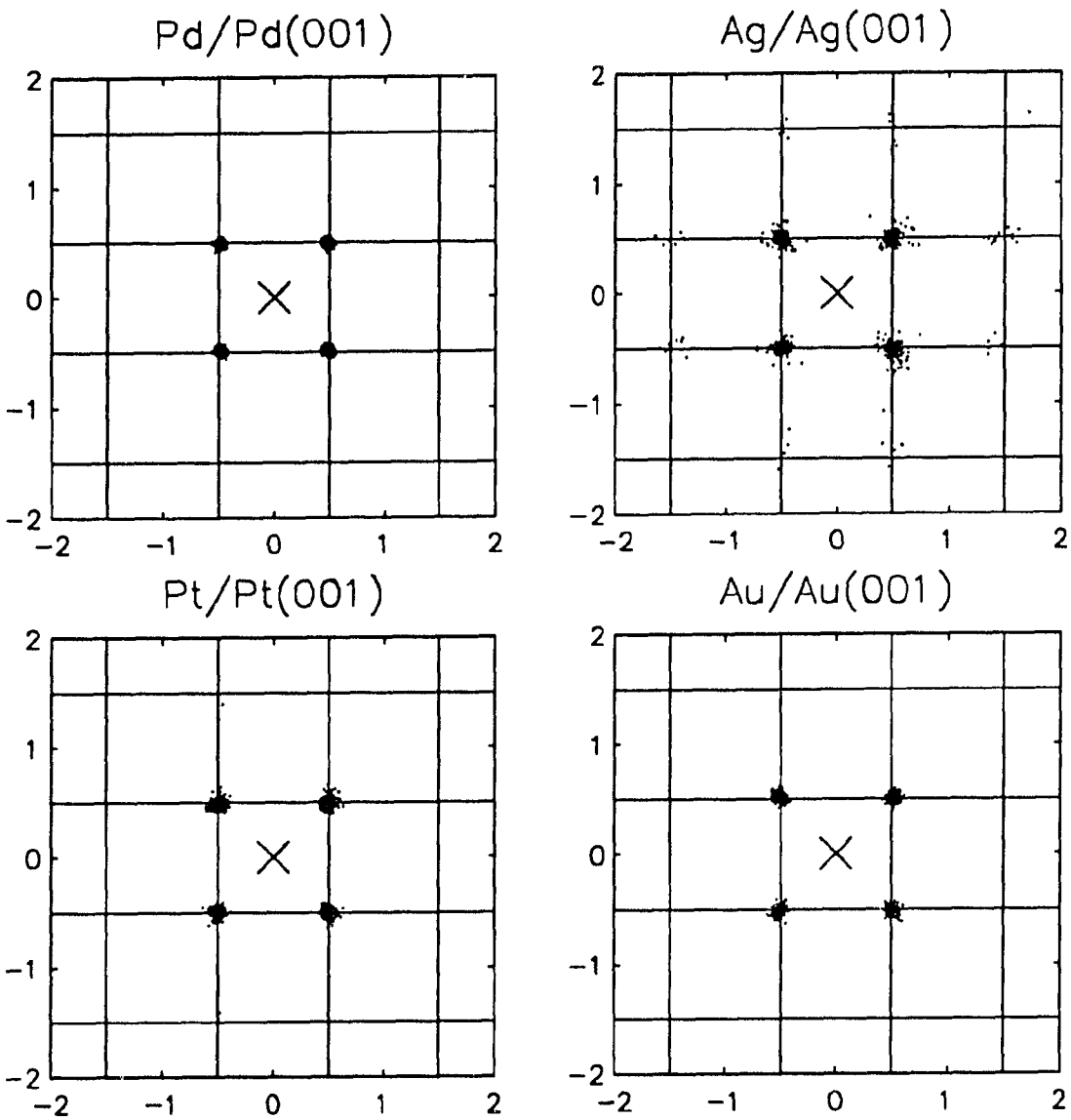

Figure 9. (continued)

Table 3. Adsorption energies and diffusion barriers for various homonuclear systems using the MD/MC-CEM potential energy function

system	E_{ads}[a] (eV)	E_{diff}[b] (eV)	diffusion barrier[c] (fraction of kinetic energy)
Ni/Ni(001)	-3.41	0.61	0.17
Rh/Rh(001)	-4.40	0.80	0.17
Pd/Pd(001)	-2.86	0.61	0.20
Ag/Ag(001)	-2.22	0.24	0.10
Pt/Pt(001)	-4.62	0.72	0.15
Au/Au(001)	-2.94	0.67	0.21

[a]The adsorption energy is for binding in a four-fold hollow site with a fully relaxed substrate.

[b]Diffusion barrier is the binding energy difference between adsorption on fully relaxed 4fh and bridge sites.

[c]This is $E_{diff}/(E_{ads}+0.25\ eV)$ which estimates the diffusion barrier relative to the maximum adatom kinetic energy, assuming 0.25 eV initial kinetic energy.

CONCLUSIONS

We have performed detailed studies of metal on metal deposition to determine the nature of the adatom dynamics. Single atom deposition on a clean (001) surface has been simulated via molecular dynamics for the homonuclear Ni, Cu, Rh, Pd, Ag, Pt, and Au systems. The important common physical point for all of these systems is the lack of any non-diffusive, ballistic motion of the adsorbing atom. To judge from the Cu/Cu(001) system, this behavior is insensitive to the PES used to model the metallic system. The reason for this is the efficient transfer of energy from the adatom to the metallic substrate. The transferred energy is then quickly dissipated.

We have also discovered an important pitfall in such simulations: use of an insufficient number of active substrate layers leads to anomalous results that support the concept of transient or ballistic motion of the adsorbate. The number of layers needed in the simulation can be reduced using Langevin coupling to simulate frictional dissipation.

We emphasize that our calculations neither contradict nor support the experimental evidence supporting layer-by-layer growth at 80 K. Our intent was to more thoroughly study what seemed a physically reasonable explanation for the data. In the end, we must rule out this idea of transient mobility in homonuclear metallic systems. Such a negative result is not as satisfying as providing an explanation for the experimental data. On the other hand, kinetic models have been proposed which can explain much of the experimental data [5]. A continued

important problem for researchers is the origin of these oscillations. Indeed, a definitive answer to the basic question of the extent of layer-by-layer growth in metallic homo-epitaxy is critical to this problem, but is not yet known.

ACKNOWLEDGMENT

Financial support was received from NSF grant CHE-8921099. All calculations were performed on a SiliconGraphics 4D/380S computer, purchased via an NSF instrumentation grant.

REFERENCES

1. W.F. Egelhoff and I. Jacob, *Phys. Rev. Lett.* **62** (1989) 921.

2. D.K. Flynn, J.W. Evans, and P.A. Thiel, *J. Vac. Sci. Technol. A* **7** (1989) 2162.

3. R. Kunkel, B. Poelsema, L.K. Verheij, and G. Comsa, *Phys. Rev. Lett.* **65** (1990) 733.

4.a. S. Clarke, M.R. Wilby, D.D. Vvedenskey, T. Kawamura, and T. Sakamoto, *Appl. Phys. Lett.* **54** (1989) 2417.

b. B. Heinrich, J.F. Cochran, A.S. Arrott, S.T. Purcell, K.B. Urquhart, J.R. Dutcher, and W.F. Egelhoff, *Appl. Phys. A* **49** (1989) 473.

c. S. Clarke, M.R. Wilby, D.D. Vvedenskey, and T. Kawamura, *Phys. Rev. B* **40** (1990) 1369.

d. A. Samsavar, E.S. Hirschorn, F.M. Leibsle, and T.-C. Chiang, *Phys. Rev. Lett.* **63** (1989) 2830.

e. D.D. Chambliss and R.J. Wilson, "Relaxed Diffusion Limited Aggregation of Ag on Au(111) Observed by Scanning Tunneling Microscopy", *J. Vac. Sci. Technol.*, (to appear March/April 1991).

5.a. J.W. Evans, *Vacuum* **41** (1990) 479.

b. J.W. Evans, D.E. Sanders, P.A. Thiel, and A.E. DePristo, *Phys. Rev. B* **41** (1990) 5410.

c. D.E. Sanders and J.W. Evans, "Downward Funneling Model of Low-Temperature Epitaxial Growth: A Hybrid Molecular (MD) - Monte-Carlo (MC) Study", submitted for *Proceedings of the ICSOS-III Conference*, Milwaukee, WI (1990), to appear in The Structure of Surfaces III, Editors: M.A. Van Hove, S.Y. Tong, and X. Xide, Springer Verlag, Berlin.

6. F.O. Goodman and H.Y. Wachman, Dynamics of Gas Surface Scattering, (Academic Press, N.Y., USA, 1976).

7. D.W. Brenner and B.J. Garrison, *Adv. Chem. Phys.* (1989) 281.

8.a. J.D. Kress and A.E. DePristo, *J. Chem. Phys.* **88** (1988) 2596.
b. J.D. Kress, M.S. Stave, and A.E. DePristo, *J. Phys. Chem.* **93** (1989) 1556.
c. T.J. Raeker and A.E. DePristo, *Phys. Rev. B* **39** (1989) 9967.
d. T.J. Raeker and A.E. DePristo, *Surf. Sci.* **235** (1990) 84.
e. T.J. Raeker and A.E. DePristo, *Int. Rev. Phys. Chem.* **10** (1991) 1.

9. M.S. Stave, D.E. Sanders, T.J. Raeker, and A.E. DePristo, *J. Chem. Phys.* 93 (1990) 4413.

10. S.B. Sinnott, T.J. Raeker, M.S. Stave, and A.E. DePristo, (to be submitted).

11. T.J. Raeker and A.E. DePristo, "Theoretical Studies of Dynamical Phenomena in Epitaxial Surface Systems", *Surf. Sci.* (accepted 12/90).

12. L.A. Girifalco and V.G. Weizer, *Phys. Rev.* **114** (1959) 687.

13. T. Halicioglu and G.M. Pound, *Phys. Stat. Solidi A* **30** (1975) 619.

14.a. H.L. Davis and J.R. Noonan, *Surf. Sci.* **126** (1983) 245.
b. R. Mayer, C.-S. Zhang, K.G. Lynn, W.E. Frieze, F. Jona and P.M. Marcus, *Phys. Rev. B* **35** (1987) 3102.

15. J.J. de Miguel, A. Cebollada, J.M. Gallego, J. Ferrón, and S. Ferrer, *J. Cryst. Growth* **88** (1988) 442.

16. M. Schneider, A. Rahman, and I.K. Schuller, *Phys. Rev. Lett.* **55** (1985) 604.

17.a. A.E. DePristo and H. Metiu, *J. Chem. Phys.* **90** (1989) 1229.

b. M. Berkowitz and J.A. McCammon, *Chem. Phys. Lett.* **90** (1982) 215.

c. C.L. Brooks III and M. Karplus, *J. Chem. Phys.* **79** (1983) 6312.

d. R. Lucchese and J.C. Tully, *Surf. Sci.* **137** (1983) 1570.

e. R. Lucchese and J.C. Tully, *J. Chem. Phys.* **80** (1984) 3451.

18.a. S.A. Adelman and J.D. Doll, *Acc. Chem. Res.* **10** (1977) 378.

b. S.A. Adelman, *Adv. Chem. Phys.* **44** (1980) 143 and references therein.

c. J.C. Tully, *J. Chem. Phys.* **73** (1980) 1975.

d. A.E. DePristo, *Surf. Sci.* **141** (1984) 40.

PAPER II.

PREDICTED DIFFUSION RATES ON FCC(001) METAL SURFACES FOR ADSORBATE/SUBSTRATE COMBINATIONS OF NI, CU, RH, PD, AG, PT, AU

Predicted diffusion rates on FCC(001) metal surfaces for adsorbate/substrate combinations of Ni, Cu, Rh, Pd, Ag, Pt, Au

David E. Sanders[a]
and
Andrew E. DePristo

Department of Chemistry
Iowa State University
Ames, Iowa 50011

[a] IBM predoctoral Fellow

ABSTRACT

We investigate the diffusion of a single metal atom on the surface of a FCC(001) metal. Two points concerning the application of kinetic models to diffusion were considered. First, we test the assumption of kinetic models that diffusion occurs via a sequence of uncorrelated jumps. Second, when kinetic models are applicable we predict reasonable values of the kinetic rate constants.

Direct molecular dynamics (MD) simulations were performed for Ag on Ag(001) and Rh on Rh(001) systems. Diffusion was found to obey an Arrhenius-type dependence on temperature in both systems. The barriers and prefactors extracted from the MD results agree with estimates made from transition state theory (TST) and the experimental values for the Rh system. We conclude that kinetic models are applicable to diffusion on FCC(001) surfaces.

Transition state theory was then used to estimate diffusion parameters for all other adsorbate/substrate combinations of the metals Ni, Cu, Rh, Pd, Ag, Pt, and Au. These results indicate that the characteristics of diffusion are primarily a property of the adsorbate. We also predict Ag atoms to have an anomalously low diffusion barrier on all of the substrates in this study. We use the accurate many-body density functional based MD/MC-CEM potential energy surface which allows us to consistently treat these multi-component systems.

INTRODUCTION

Diffusion of atoms and molecules on the surface of a metal substrate is an intriguing and technologically important phenomena. Diffusion is the primary mechanism for the transport of matter across surfaces. It therefore plays a key role in many problems of interest to the chemist and material scientist, e.g., the growth of thin films and the formation of epitaxial layers. Catalytic behavior is also dependent upon the mobility of the reactive species.

Diffusion is interesting fundamentally since it reveals much about the microscopic features of the metal surface. It is sensitive to fine details of the strength and corrugation of the adsorbate-surface interaction.

In recent years, atomistic views of metal atom diffusion on metal substrates have been provided by the field ion microscope (FIM) [1]. These experiments have revealed that diffusion can be a very complex process. Diffusion rates may vary by orders of magnitude on different crystal faces of the same metal [2]. The diffusion mechanism can even vary from face to face. For example, simple hopping between adjacent sites often gives way to such exotic phenomena as adatom-substrate exchange. Diffusion on the (110) faces of the FCC metals Pt [3], Ir [4], and Ni [5] has been observed to proceed via an exchange between the adatom and an adjacent substrate atom. In addition, both experiment [6,7] and theory [8,9] have reported an exchange mechanism for diffusion on the (001) surfaces of Pt, Ir, and Al. Such rich detail provides motivation for the theoretical study of surface diffusion.

The simultaneous development of accurate potential energy surfaces and affordable computing power has stimulated interest in the theoretical modelling of diffusion. The primary techniques are molecular dynamics (MD) [10] and kinetic Monte Carlo or lattice-gas (LG) simulations [11]. The MD approach involves numerical solution of the classical equations of motion for the atomic positions, based on the interatomic forces. When performed correctly, its provides an accurate solution of the diffusion process limited only by the intrinsic accuracy of the potential energy surface (PES), assuming that all quantal effects are negligible of course. However, since MD follows atomic motion, with its characteristic time scale of 10^{-14} second, it is it is impractical computationally for studying processes that take longer than about a nanosecond. Diffusion at temperatures much lower than the activation barrier can easily be shown to involve isolated atomic hopping on a time scale of seconds [1].

Lattice-gas models ignore the short-time atomic motion and instead describe diffusion in terms of activated hops between sites on a lattice. This simplification is much less computationally demanding since it utilizes kinetic equations with rates on the appropriate time-scales. However, all relevant physical processes must be explicitly included in the model, and all these processes must be parameterized with characteristic rate constants.

In a recent article, Voter [12] demonstrated the use of LG models to simulate the diffusion of Rh clusters on a Rh(001) surface. Here transition state theory was used to extract hopping rate constants for individual cluster atoms using a Lennard-Jones (LJ) (12,6) potential.

In this article we present results from a study of the diffusion of single metal atoms on FCC(001) metal surfaces. There are three goals. The first is to test the adequacy of transition state theory in conjunction with the corrected effective medium (CEM) theory description for interaction potential and forces [13,14] as a method for the prediction of diffusion constants. The second is to test the accuracy of the kinetic description of diffusion. And the third is to test the accuracy of the diffusion constants in comparison to experimental data.

A simple model of surface diffusion, site to site hopping, is considered and rate constants are calculated via transition state theory (TST).[1] The PESs and forces are computed directly from the corrected effective medium (CEM) theory in its recent semi-empirical MD/MC-CEM form [14]. This method utilizes the Hartree-Fock electron density distribution of the metal atoms along with a semi-empirical embedding energy term to define the interactions. The PES and forces are computed at each configuration of the dynamics without fitting or representation of the PES in simple forms. A brief description of the MD/MC-CEM method is provided in the following section, but further details can be found in refs.[13,14].

Since the semi-empirical MD/MC-CEM embedding term depends *only* on the properties of the bulk, homonuclear system for each element [13b,15], we can *predict* diffusion parameters for all 49 adsorbate/substrate combinations of the metals Ni, Cu, Rh, Pd, Ag, Pt, and Au. Our diffusion constants do not result from

---

[1]In ref.[12], this is referred to as simple transition state theory (STST). We have deleted the additional modifier for compatibility with essentially all other applications of TST. It is corrections to the original formula such as variational determination of the transition state that generally are referred to by additional modifiers and thus new acronyms.

fitting to reproduce experimental values. These values represent the beginning of the database necessary to implement realistic kinetic models of surface processes.

The TST diffusion rates are compared to available experimental values as well as to the results of MD simulations performed with the same MD/MC-CEM PES and forces. Comparison of TST and MD values provides a consistency check and also tests the underlying assumptions of transition state theory.

POTENTIAL ENERGY SURFACE

The topology of the PES is defined by the variation of the adatom's binding energy over the unit cell. Of particular importance are the minima, corresponding to stable four-fold hollow (4fh) binding sites on all the systems studied here, and the higher energy saddle points, corresponding to bridge sites on most of these systems. The difference in these energies, referred to as the diffusion barrier for now, typically ranges from 0.4 to 0.9 eV. Accurately determining such barriers is a test for a model potential energy function, but this is necessary since the diffusion rate depends exponentially on the barrier height.

More complications arise since the adsorbate binding energies are sensitive to the degree of adsorbate induced substrate relaxation; the surface cannot be treated as a static object. Even in the simplest model of hopping between adjacent sites there is a great deal of substrate activity. The presence of the adatom in a four-fold hollow (4fh) site causes the neighboring substrate atoms to relax. This relaxation lowers the calculated binding energy by as much as 3 % in the systems studied here. The effect of substrate relaxation on bridge site bonding is even greater, reduction by up to 6 %. The net result is a major change between the diffusion barriers for relaxed and unrelaxed surfaces of up to 18 %. Clearly, any potential energy function used to model diffusion must realistically describe both the adatom-substrate and substrate-substrate interactions.

Simple pairwise additive potentials such as the Lennard-Jones (LJ) 12,6 have been used in simulations of surface diffusion [10]. The agreement between these

results and the available experimental data suggest that the LJ form is capable of reproducing some of the dynamical properties of surface diffusion. However, the LJ and other simple pairwise forms do not accurately predict properties of the surface such as interlayer relaxations and are not capable of simultaneously reproducing such basic properties of the bulk solid as the lattice constant, heat of formation, and Debye frequency [15,16]. It is not surprising that these simple models fail to accurately describe metal systems. The dominant characteristic of metallic systems is their delocalized electronic distribution. Models which consider only the nuclear coordinates thus ignore much of the relevant physics and therefore lack predictive ability.

Various forms are available to describe bonding on the surface of a metal which go beyond the level of pair potentials [13e]. In the present work we use a potential energy surface based upon the recently developed version of the corrected effective medium (CEM) theory [13,14] for molecular dynamics and Monte Carlo simulations (MD/MC-CEM) [14]. The MD/MC-CEM method provides a quantitatively accurate description of bulk cohesive energies and surface energies of transition metal surfaces and is qualitatively correct for surface layer relaxations [14,15].

For completeness, we provide a very brief description of the MD/MC-CEM theory, referring the inquisitive reader to refs.[14,15] for details. The potential energy of an atom, A_i, at position, $\mathbf{r}_i$, is given by the following expression,

$$V(A_i;\vec{r}_i) = \Delta F_J(A_i;n_i) + \frac{1}{2}\sum_{j\neq i} V_c(i,j) \ . \qquad (1)$$

The first term is the 'effective' embedding energy of atom A_i into jellium of density n_i, $\Delta F_J(A_i;n_i)$. These 'effective' embedding energies are *empirical* functions that depend on the chemical identity of the atom and the jellium density. They are known for nearly all elements in the periodic table through Xe either from experimental data on homonuclear diatomic and bulk systems [13] or from LMTO calculations on the bulk system [15]. The jellium density for embedding atom A_i is evaluated as a weighted average of the atomic electron densities of all the other atoms,

$$n_i = \frac{1}{2}\sum_{j\neq i} \int d\vec{r} \left[\frac{n(A_i;\vec{r}-\vec{r}_i)}{Z_i}\right] n(A_j;\vec{r}-\vec{r}_j) \ . \qquad (2)$$

For the systems studied here, spherical Hartree-Fock atomic electron densities are used.

The second term is the sum of the classical electrostatic atom-atom coulomb energies (i.e., total nuclear-nuclear, nuclear-electron and electron-electron energies) between atom A_i and all other atoms. These are computed by standard methods for each type of pair A_i and A_j and then placed on a grid in $|\vec{r}_i-\vec{r}_j|^{-2}$, as detailed in ref.[14].

It is important to note that the MD/MC-CEM potential energy is determined by specifying the chemical identities of all atoms in the system; there are no adjustable parameters. We are not suggesting, of course, that the MD/MC-CEM PES will be quantitatively accurate for all systems. For example, calculation of

coverage dependent interaction energies for Au on Cu presents great difficulties for the MD/MC-CEM method (which are alleviated in the more accurate but much more computationally expensive CEM theory) [17].

Before leaving this section it is worthwhile to note that Eq.(1) does not conform to the definition in the CEM references, which discuss the rigorously definable total system interaction energy, $\Delta E(\{A_i\})$. In the full CEM theory, one cannot identify a potential for any atom since there is an additional term in the system interaction energy containing a non-separable energy functional of the total system electron density. In the MD/MC-CEM simplification of CEM, this term is incorporated into the 'effective' embedding energy which enables the translation of $\Delta E(\{A_i\})$ into the interaction potential expression in Eq.(1). We have used Eq.(1) to help connect the MD/MC-CEM formula to simpler potential energy functions using only nuclear coordinates. However, even for the MD/MC-CEM expresssion, one should note that one of the variables, n_i, is determined directly from electron densities.

TRANSITION STATE THEORY DIFFUSION RATES

Diffusion fundamentally involves analysis of the long time square displacement, $\langle R(t)^2 \rangle$, for an adatom moving on a substrate. When this square displacement is linear in time, t, the coefficient can be defined as the diffusion coefficient, taking into account certain dimensionality factors.

TST is a method for calculating reaction rates from reactants to products. There is no inherent reason to expect TST, or any chemical reaction rate methodology for that matter, to be applicable to diffusion. Thus, it is important to state first the fundamental dynamical assumption about diffusion that allows application of such reaction rate approaches. Basically, one assumes that diffusion consists of numerous uncorrelated activated chemical reactions, each involving an isolated hop of an an adatom from one equilibrium binding site to a different binding site. The two binding sites do not have to be either equivalent or adjacent. Under this physical assumption, we are then left to choose a method for calculation of the 'hopping' rates between binding sites. TST is perhaps the simplest such method and has been applied already to surface diffusion [12,18,19,20,21,22],[2] as have more sophisticated quantal flux-flux correlation methods [23].

Focus on the transition of an adatom from one stable binding site (A) to another (B), proceeding over some barrier. Based on equilibrium statistical mechanics, TST makes two assumptions about the reaction dynamics. First, once

---

[2]For a general review of TST and its newer developments, the reader should consult ref.[22]. Here, we only focus on the application to surface diffusion.

the barrier separating state A from state B is crossed the reaction will always proceed irreversible on to B. Second, equilibrium exists between the initial and transition states. One can symbolize these two assumptions in the chemical equation, $A \rightleftharpoons (TS) \rightarrow B$.

TST replaces the difficult determination of reaction rate with the much simpler calculation of an equilibrium constant between reactants and transition state. The TST rate constant is given by the following relation,

$$k_{TST} = \frac{1}{\beta h}\frac{Q^{\ddagger}}{Q} e^{-\beta E^{\ddagger}} \tag{3}$$

where the activation energy, $E^{\ddagger}$, is the difference between the initial and transition state energies and $\beta = (k_B T)^{-1}$. The canonical partition functions of the transition and reactant state are denoted as $Q^{\ddagger}$ and Q, respectively. The former does not include motion along the direction from A→B at the TS and has one less degree of freedom than the latter.

In systems where the equilibrium condition is not satisfied (e.g., at high temperatures in surface diffusion), TST becomes inaccurate. The high thermal energy of the adatom may allow it to recross the transition state back into the reactant state or to cross yet another barrier without equilibrating in the supposed product state. The former violates the first fundamental assumption of TST, with corrections evaluated by starting particles in the transition state and following the short-time dynamics [12]. The latter violates the assumption that diffusion can be modelled as a kinetic rate process, and thus we have not evaluated dynamical corrections to TST as part of this work. Instead, we have performed full MD

simulations to determine $\langle R(t)^2 \rangle$ vs. t, and determined when TST hopping rates accurately describe diffusion.

It is worthwhile to mention a few mathematical points about transition states. For any potential V, first find all minima, defined as the points in (mass weighted coordinate) configuration space where $\nabla V=0$ and all eigenvalues of $\nabla\nabla V$ are non-negative. Then, find all saddle points, defined as the points in configuration space where $\nabla V=0$ and all eigenvalues of $\nabla\nabla V$ are non-negative except one. The (minimum energy) reaction path connects reactants and products by following the direction of the gradient from any particular saddle point. The point is simply that one can define a TS for even very complex processes. The literature should be consulted for further descriptions of reaction paths [21,22,24] and more complex PES features [25].

The numerical problem in implementing TST is defining the reaction (diffusion) pathway and identifying the transition state. Even for the case of single atom diffusion considered in this article we must consider not only the adatom but also the behavior of the neighboring substrate atoms. It is the configuration of all atomic positions which defines the equilibrium and transition states, not just the position of the adatom. For more complicated systems (e.g., cluster diffusion or diffusion on rough or partly covered surfaces) identification of the pathway and transition state is not trivial. However, established techniques are available [21,26] which can help find the transition state even in these complicated cases.

To help understand the particular problem for surface diffusion, we show the minimum energy contours of an **adiabatic** potential energy surface for a single Rh

atom on a Rh(001) surface in Figure 1. This surface, which is representative of the other systems studied, shows the saddle point to occur for an adatom located above a bridge site and the minimum energy diffusion pathway to be the direct line between two adjacent 4fh sites. The simplest model of diffusion is then single hops between adjacent 4fh sites. This mechanism has been observed experimentally for Rh/Rh(001) [2] and Pd/Pt(001) [6].

Recent experiments by Kellogg have observed an alternate mechanism for the diffusion of Pt on Pt(001) [6]. Here the adatom moves diagonally (in the <010> direction) by displacing an adjacent substrate atom. This displacement mechanism was predicted by SCF-LD calculations for Al on Al(001) [8]. Subsequent calculations using the embedded atom method (EAM) have found that the barrier to displacement is lower than that of bridge site hopping for Pt on Pt(001) [9]. Within a TST formalism, one would find rates for both processes and thus diffusion would proceed via both mechanisms. However, the displacement mechanism will dominate at low temperatures since the rates depend exponentially on the energy barrier. The experiments do not observe hopping diffusion for Pt but these are all conducted at temperatures below 210 K. It is still worthwhile to discuss hopping diffusion for Pt on Pt(001) and other systems which may also exhibit this novel displacement mechanism.

It remains to evaluate the canonical partition functions for the equilibrium and transition states in Eq.(3). These will affect only the pre-exponential term in k_{TST}, which is much less important than the activation barrier, $E^{\ddagger}$, since the latter occurs in an exponential. Thus, we have made two approximations to allow for

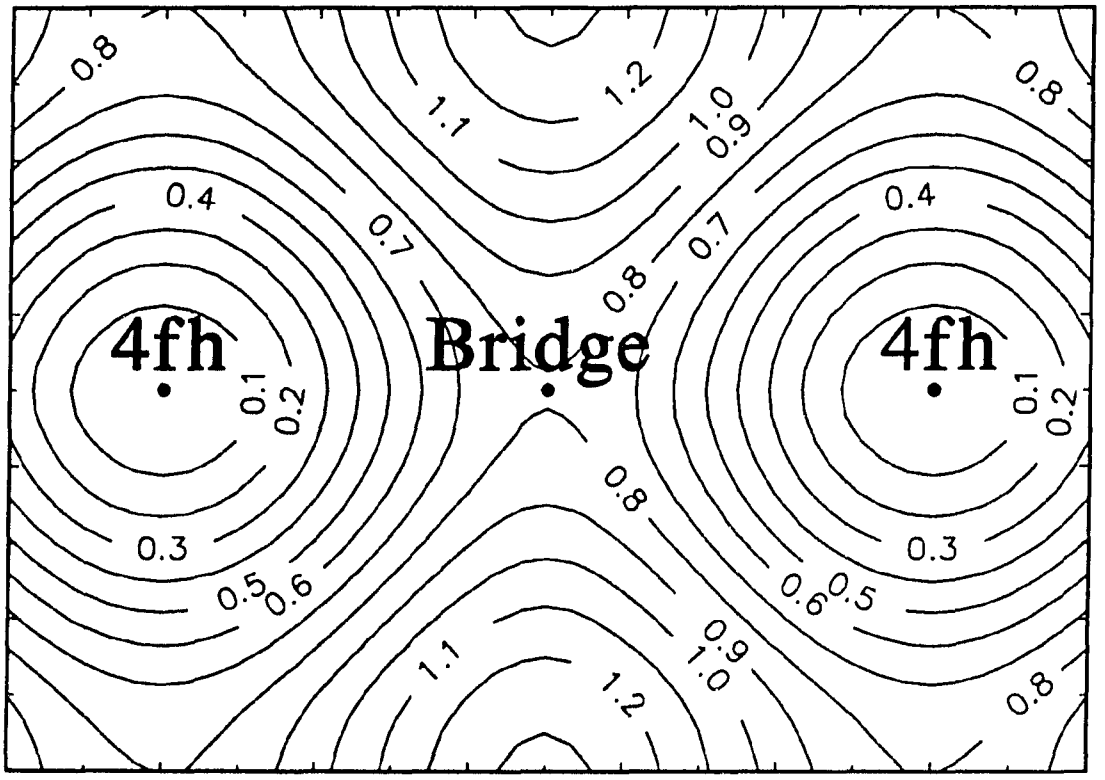

Figure 1. Minimum energy contours of an adiabatic potential energy surface for a Rh atom on a Rh(001) substrate calculated with the MD/MC-CEM method

The contour levels (eV) are relative to the bottom of the four-fold hollow adsorption well. Points on the surface were generated by holding the adatom fixed in (x,y) and allowing all other atomic positions to relax.

simple numerical evaluation of the ratio $Q^{\ddagger}/Q$: 1) all vibrational motion is harmonic; and, 2) the substrate responds adiabatically to adatom motion.

To see the effects of these approximations, consider just the first and let there be N_s substrate atoms. Both Q and $Q^{\ddagger}$ involve only vibrations, the former for $3N_s$-3 and the latter for $3N_s$-4 degrees of freedom. Denoting the normal mode frequencies by $\{\nu_m, m=1,...,3N_s-3\}$ and $\{\nu_k^{\ddagger}, k=1,...,3N_s-4\}$, we can write,

$$\frac{Q^{\ddagger}}{Q} = \frac{\prod q(\nu_k^{\ddagger})}{\prod q(\nu_m)} \tag{4}$$

where $q(\nu)$ is the harmonic oscillator partition function for frequency ν. This expression is difficult to evaluate because of the large number of substrate atoms. It is best to change the summation to an integral over the vibrational density of states and this is under development in our lab.

The second approximation is thus to assume that the ratio in Eq.(4) is mainly effected by changes in normal modes which are predominantly of adatom character. In this case the ratio $Q^{\ddagger}/Q$ is greatly simplified to,

$$\frac{Q^{\ddagger}}{Q} = \frac{q(\nu_1^{\ddagger})\, q(\nu_2^{\ddagger})}{q(\nu_1)\, q(\nu_2)\, q(\nu_3)} . \tag{5}$$

Here $\{\nu_1,\nu_2,\nu_3\}$ are the vibrational frequencies of the adatom in the equilibrium state, and $\{\nu_1^{\ddagger},\nu_2^{\ddagger}\}$ are the vibrational frequencies for the adatom in the TS for the two degrees of freedom orthogonal to the reaction path. Some recent work including clusters of active surface atoms to evaluate Eq.(4) vs. Eq.(5) indicate that Eq.(5) is quite adequate [20].

The normal mode partition functions, q(ν), can be formulated using either classical or quantum mechanics. The former has the following form,

$$q(\nu) = \frac{e^{-\frac{1}{2}\beta h \nu}}{1 - e^{-\beta h \nu}} . \tag{6}$$

The TST rate constant for a quantum mechanical oscillator is therefore,

$$k_{TST}^{QM} = \frac{1}{\beta h} \prod_{i=1}^{3} \left(1 - e^{-\beta h \nu_i} \right) \prod_{j=1}^{2} \left(1 - e^{-\beta h \nu_j^{\ddagger}} \right)^{-1} e^{-\beta E_a} . \tag{7}$$

The effective activation energy, E_a, is related to the potential barrier via,

$$E_a = E^{\ddagger} + \frac{h}{2} \sum_{j=1}^{2} \nu_j^{\ddagger} - \frac{h}{2} \sum_{i=1}^{3} \nu_i . \tag{8}$$

In most cases then the inclusion of zero-point vibration is expected to lower the effective diffusion barrier since the sum of two frequencies in the TS will not be larger than the sum of three reactant frequencies.

The partition function of a classical harmonic oscillator is simply the high temperature limit of Eq.(6),

$$q(\nu) = \frac{1}{\beta h \nu} . \tag{9}$$

This leads to a much simpler form for the TST rate constant for the classical oscillator,

$$k_{TST}^{CM} = \nu_0 \, e^{-\beta E^{\ddagger}} \, . \tag{10}$$

The prefactor, ν_0, is defined by the following,

$$\nu_0 = \frac{\nu_1 \, \nu_2 \, \nu_3}{\nu_1^{\ddagger} \, \nu_2^{\ddagger}} \, . \tag{11}$$

The reason for defining ν_0 in Eq.(11) is to write Eq.(10) in the familiar Arrhenius form.

We reiterate that Eqs.(7) and (10) utilize the approximation of invariant substrate partition functions as the adatom moves between the equilibrium and transition state. This is certainly a crude approximation for the substrate atoms in the vicinity of the diffusing atom. It would be possible to include directly those substrate atoms which most strongly interact with the diffusing atom. The only constraints here are determining which atoms to include and the computational problem of finding the 3N vibrational frequencies. In the the classical limit, only the prefactor would be affected by including substrate changes, while both the prefactor and the more sensitive exponential term are influenced in the quantum formulation.

At high temperatures ($\beta h\nu << 1$) the classical and quantum rate constants coincide. Since the pre-exponential is less critical than the barrier, we expect that any difference between quantum and classical rates will be reflected in the zero-point energy difference of Eq.(8). Of course, for metallic systems where $\nu \approx 10^{12}$ s^{-1}, the zero-point lowering will likely be a small effect.

TRANSITION STATE THEORY RESULTS

First, the clean surface is relaxed to determine the zero of energy. Second, the adatom-surface system is relaxed with the adatom in the 4fh site to determine the adsorbate binding energies. The 3x3 force constant matrix is determined numerically and then diagonalized to yield (ν_1,ν_2,ν_3). The 4fh site binding energies for the various systems are reported in Table 1. It is apparent that the binding energy varies substantially more with changing the adatom than the substrate. However, neither variation yields negligible changes.

While it is obvious that 4fh site adsorption should use fully relaxed adatom and substrate positions, the situation for bridge site adsorption is less certain. Diffusion is characterized as an activated process with long residence times in the stable binding sites. This ensures that the adatom has sufficient time to reach equilibrium. The residence time in the transition state is expected to be much smaller and therefore a question exists as to whether the substrate atoms have time to respond. The fully relaxed transition state has used in this work because it is consistent with the underlying assumptions of simple transition state theory (i.e., that the initial and transition states exist in equilibrium with each other). As before, the 3x3 force constant matrix is determined numerically and then diagonalized. In the transition state one of the resulting modes will have a negative force constant (i.e., an imaginary frequency); this corresponds to motion along the reaction path. The two real frequencies of the transition state are identified as $\nu_1^{\ddagger}$ and $\nu_2^{\ddagger}$.

Table 1. Adsorption energy (eV) in a four-fold hollow site on fully relaxed FCC(001) substrates as calculated with the MD/MC-CEM potential energy function

		Substrate						
		Ni	Cu	Rh	Pd	Ag	Pt	Au
Adatom	Ni	-3.41	-3.12	-3.68	-3.31	-2.84	-3.50	-2.79
	Cu	-2.90	-2.66	-3.16	-2.84	-2.40	-2.74	-2.50
	Rh	-4.19	-3.81	-4.40	-3.93	-3.29	-3.56	-3.19
	Pd	-3.11	-2.80	-3.26	-2.86	-2.32	-2.63	-2.31
	Ag	-2.89	-2.64	-2.98	-2.66	-2.22	-2.52	-2.27
	Pt	-3.87	-3.71	-3.98	-3.70	-3.18	-4.62	-4.30
	Au	-2.59	-2.57	-2.62	-2.39	-1.95	-3.21	-2.94

Third, and in accord with the above argument, the adatom-surface system in relaxed with the adatom in the bridge site. This is a saddle point on the PES, and to ensure numerical stability, the adatom motion is constrained parallel to the surface (i.e., it cannot move in x and y) but is free to move perpendicular to it (in z). This is necessary to prevent the adatom from falling back into the 4fh site during the relaxation. The potential barrier, $E^{\ddagger}$, is calculated as the difference between the 4fh and bridge adsorption energies, and is shown in in Table 2.

The most striking feature of these results is the relatively small barrier predicted for Ag on all of the substrates studied. This seems to correlate with the large lattice constant (4.1 Å) and small cohesive energy (3.0 eV) of the bulk Ag system.

Other trends in the calculated binding energies and diffusion barriers are difficult to discern. It is apparent that there is no correlation between the diffusion barrier and the adsorption energy that is at all quantitative. The diffusion barrier does seem to correlate with the identity of the adatom not the identity of the substrate, with the notable exception of the Ag adatom where the variation with substrate is quite significant. For the majority of the substrates, the barrier height increases with adatom identity in the following order, Ag < Au < Pd ≤ Pt < Ni < Cu < Rh. However for Pt and Au substrates the order becomes Ag < Pd < Ni < Rh < Au ≤ Cu < Pt. A ranking based on the ratio of cohesive energy to lattice constant predicts barriers increasing in the order Ag < Au ≤ Cu ≤ Pd < Ni < Pt ≤ Rh. This simple rule thus correlates some but not all of the observed trends.

Table 2. Classical Diffusion barriers[a] (eV) as calculated with the MD/MC-CEM potential energy function

		Substrate						
		Ni	Cu	Rh	Pd	Ag	Pt	Au
Adatom	Ni	0.61	0.64	0.76	0.71	0.71	0.57	0.61
	Cu	0.62	0.66	0.74	0.72	0.73	0.61	0.66
	Rh	0.67	0.71	0.80	0.75	0.74	0.57	0.62
	Pd	0.55	0.58	0.66	0.61	0.58	0.49	0.53
	Ag	0.42	0.36	0.50	0.42	0.24	0.41	0.32
	Pt	0.55	0.61	0.66	0.64	0.59	0.72	0.82
	Au	0.48	0.56	0.55	0.54	0.54	0.58	0.67

[a]The classical diffusion barrier is the binding energy difference between adsorption on fully relaxed bridge and four-fold hollow sites.

The three frequencies (ν_1, ν_2, ν_3) of the adsorbate in the equilibrium binding site and the two frequencies ($\nu^{\ddagger}_1$, $\nu^{\ddagger}_2$) of the adsorbate in the transition site are required to evaluate either formulation of the TST rate constant. Since these quantities are determined by diagonalizing the 3x3 force constant matrix of the adatom to yield the normal modes in each site, such a procedure is independent of coordinate system and would work equally well with non-square substrate faces.

An Arrhenius plot of the quantum mechanical and classical rate constants for the Ag on Ni(001) system appears in Figure 2 and illustrates the worst agreement between the classical and quantum formulation for all of the systems studied. As expected the quantum and classical rate constants diverge at lower temperatures. However, at temperatures where the divergence becomes significant the rate constant is usually negligibly small. We define the onset temperature as the point at which the classical diffusion rate exceeds 1 hop/hour. We believe this rate represents the lower limit of experimentally observable diffusion. For Ag on Ni(001) the ratio of quantal to classical hopping rate is ca. 1.3 at the onset temperature of 128 K. For the majority of the systems studied there is much smaller differences between the two formulations, at least at temperatures above the onset temperature. Furthermore, values of the zero-point energy term in Eq.(8) typically are $\leq$ 0.010 eV and represent only 1-2 % of the potential barrier. Such values are less than the estimated uncertainty of the MD/MC-CEM potential energy. For these reasons, the effect of zero-point energy can be neglected.

Since the classical and quantum formulations are essentially the same, the five adatom frequencies necessary to evaluate Eqs.(7) and (8) are not reported.

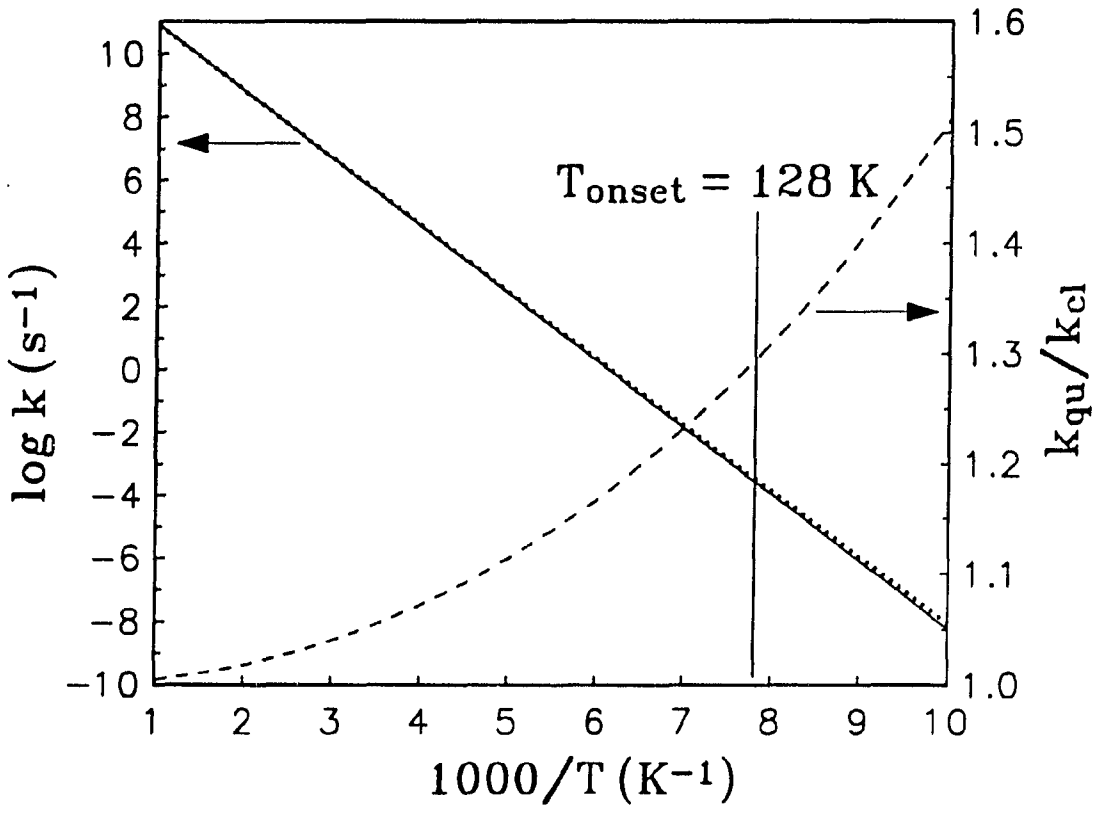

Figure 2. Arrhenius plot of the transition state hopping rate constant for the Ag on Ni(001) system

The classical and quantum mechanical rate constants are shown as solid and dotted lines, respectively. The ratio of the quantum mechanical to classical rate constant is shown with a dashed line.

Instead, values of the classical prefactor calculated with Eq.(11) appear in Table 3. The variation with substrate is even less than for the diffusion barrier, again with the notable exception of the Ag adatom which displays an unusual variation of an order of magnitude in ν_0. This certainly points out that Ag is a very unusual adatom as appears to be indicated by recent experimental work [27].

Table 3. Classical prefactors, ν_0 (10^{12} s^{-1}), from Eq.(11) for FCC(001) systems calculated with the MD/MC-CEM potential energy function

		Substrate						
		Ni	Cu	Rh	Pd	Ag	Pt	Au
	Ni	5.2	5.2	5.5	5.2	5.0	4.5	4.6
	Cu	5.2	5.5	5.4	5.3	5.6	4.5	5.0
A	Rh	4.5	4.6	4.4	4.3	4.5	3.3	3.6
d	Pd	4.2	4.6	4.1	4.2	5.0	3.2	3.7
a	Ag	10.	6.9	4.9	8.0	1.0	9.3	5.8
t	Pt	3.7	4.1	3.7	4.0	3.7	2.5	2.5
o m	Au	2.9	3.1	2.7	2.8	3.2	2.1	2.2

COMPARISON TO EXPERIMENT

Diffusion of a single adatom on a clean surface is characterized by a linear dependence of the mean square displacement on time. The proportionality or diffusion constant, D, is defined by the following,

$$D = \lim_{t\to\infty} \frac{\langle R^2(t) \rangle}{2dt} \tag{12}$$

where d is the dimensionality of the motion. The limit in Eq.(12) reflects the fact that at short times, the adatom's linear displacement is proportional to time. Note that R^2 $(= (x - x_0)^2 + (y - y_0)^2)$ on a FCC(001) surface is the two-dimensional displacement of the atom and thus d = 2 here. The position of the adatom at t = 0 is denoted by (x_0,y_0).

It is the diffusion constant, D, rather than the rate constant which is observed experimentally. Experimental diffusion data are often characterized by a phenomenological equation of the Arrhenius form,

$$D = D_0 \, e^{-\beta E^{\ddagger}} . \tag{13}$$

This is very similar to the form of the classical rate constant. The relationship between D_0 and the prefactor, ν_0, is defined as follows [28],

$$D_0 = \frac{z}{2d} \langle \ell^2 \rangle \nu_0 \tag{14}$$

where z is the number of nearest-neighbor sites (z = 4 for diffusion on FCC(001) surfaces). Only nearest-neighbor hops are considered in the present work, therefore

the jump length, ℓ, is equal to the nearest-neighbor distance, $a/\sqrt{2}$, where a is the bulk lattice constant.

The limited amount of experimental data available for direct comparison with the present TST results is listed in Table 4. Much of the early experimental work on surface diffusion was done on poorly characterized, polycrystalline surfaces [29]. More recent work on single crystals has shown that diffusion is very sensitive to the choice of substrate face [1]. For this reason Table 4 includes only those results obtained on single crystal samples [2,5,29,30]. There is generally quite good agreement between the TST results and the experimental data for both ν_0 and $E^{\ddagger}$. Perhaps the only significant disagreement occurs for Rh/Rh(001) in which ν_0 is three times larger than experiment.

The values in Tables 1-3 represent the beginnings of a database for the modelling of diffusion and film growth. The ability of the MD/MC-CEM theory to accurately predict properties of metal surfaces is of central importance here. Since its predictions are independent of experimental results, processes whose rates cannot be measured in the laboratory can be studied with the computer.

Table 4. Arrhenius parameters for surface diffusion

system	$E^{\ddagger}$ (eV)	D_o (cm^2/sec)	Reference
Ag/Cu(001)	0.43	2.5×10^{-4}	29
	0.36	4.5×10^{-3}	TST[a]
Cu/Cu(001)	0.48	2.3×10^{-3}	30
	0.66	3.6×10^{-3}	TST[a]
Ni/Ni(001)	0.63	--	5
	0.61	3.2×10^{-3}	TST[a]
Rh/Rh(001)	0.77 ± 0.06	$(5 \pm 3) \times 10^{-3}$	MD[b]
	0.80	3×10^{-3}	TST[a]
	0.88 ± 0.07	1×10^{-3}	2
Ag/Ag(001)	0.25 ± 0.02	$(15 \pm 3) \times 10^{-4}$	MD[b]
	0.24	8.4×10^{-4}	TST[a]

[a]Result of transition state theory using the MD/MC-CEM potential energy function.

[b]Result of direct molecular dynamics simulation using the MD/MC-CEM potential energy function.

DIRECT SIMULATIONS

Direct simulations of surface diffusion were performed for the Ag on Ag(001) and Rh on Rh(001) systems using the MD technique. The advantage of MD is that it does not build in any explicit bias towards a diffusion mechanism and provides a direct link between the PES and experimental observations. Unfortunately, MD simulations of diffusion are computationally expensive and it was not feasible to perform calculations on all of the systems previously studied with TST. Two systems, Rh on Rh(001) and Ag and Ag(001), were chosen for the MD study. The Rh system was chosen because well known experimental results exist [2], and the TST prediction differs somewhat from these, as shown in Table 4. The Ag system was chosen because it has the smallest barrier in Table 2 and thus is most likely to provide a severe test of the independent isolated hop assumption. In other words, the high mobility provides a good test of TST since it is not clear whether highly mobile adatoms maintain equilibrium with the substrate.

The molecular dynamics calculation is used to evaluate the square displacement of the adatom as a function of time t, $R^2(t)$. The calculation is performed by placing a single adatom at the center of a large slab of moving substrate atoms. These moving or active atoms are surrounded on the sides and bottom by a set of fixed atoms. The fixed atoms serve to smooth out evaluation of the potential and act as a structural template for the surface. Local frictional and random forces are added to the atoms on the edge of the simulation cell to mimic energy flow between the active atoms and a constant temperature heat bath [31].

This is termed the local Langevin equation method. The two added forces are balanced to satisfy the second fluctuation-dissipation theorem and therefore maintain the active atoms at the temperature of the bath [32]. The positions of the adsorbate and substrate atoms are propagated for 10 ps with a standard Verlet integrator [33].

Many such simulation runs, or trajectories, are necessary to determine the mean value of the square displacement. The uncertainty in the mean value is expected to decrease like (number of trajectories)$^{-1/2}$, therefore a large number of trajectories may be necessary. However, it is possible to extract a great deal of information from each trajectory. The raw data of the simulation consist of the position vector of the adatom printed out at 0.1 ps time intervals. The single 10 ps trajectory is broken up into a number of shorter overlapping trajectories. With the 0.1 ps increment a single 10 ps simulation thus yields thirty 7 ps trajectories. Key to this procedure is the fact that only the relative displacement of the adatom from an arbitrary zero position matters in diffusion. We assume that each of the first thirty printed positions represent the beginning of an independent trajectory. Even if this assumption is not completely valid there will be no anomalous biasing of the results. In the worst case that all thirty of these quasi-trajectories yielded identical information the resulting averages would be **identically** the same as those produced without this overlapping scheme.

The simulation must be run long enough to ensure that the square of the displacement exhibits a linear dependence on time, in other words that the diffusive

limit is reached. Utilizing the definition in Eq.(12), we define the function $\Delta(t)$ as follows,

$$\Delta(t) = \frac{\langle R^2(t) \rangle}{2dt} . \tag{15}$$

A plot of $\Delta(t)$ versus t is used to determine the time, t_D, when the adatom motion reaches the diffusive limit. Such plots for the Ag system appear in Figure 3 while those for the Rh system are shown in Figure 4. From these, it is apparent that the diffusive limit for both systems is typically reached at t_D = 6 ps. The final value of $\Delta(t)$ at t = 7 ps is reported as the diffusion constant for each temperature. An Arrhenius plot of the diffusion constants for the Ag system appears in Figure 5 and for the Rh system in Figure 6.

Diffusion in the Ag system appears to obey an Arrhenius type dependence on temperature. The extracted barrier and prefactor appear in Table 4 with the former in excellent agreement with the TST values. The latter is about twice the size of the TST result indicating that the assumption of isolated hops is slightly in error.

For the Rh system at temperatures > 1600 K, $\Delta(t)$ does not reach a clear limit even if the trajectories are plotted to their full 10 ps extent. The high temperature points, though not converged, show clear deviation from Arrhenius behavior, especially when one realizes that the asymptotic values, (i.e., the converged diffusion rates) would be smaller than plotted in Figure 6. For this reason only the points corresponding to $T \leq 1600$ K are included in the analysis of the temperature dependence in Figure 6. These results are reported in Table 4 and agree with the TST values for both ν_0 and $E^{\ddagger}$. Thus, the slight disagreement between experiment

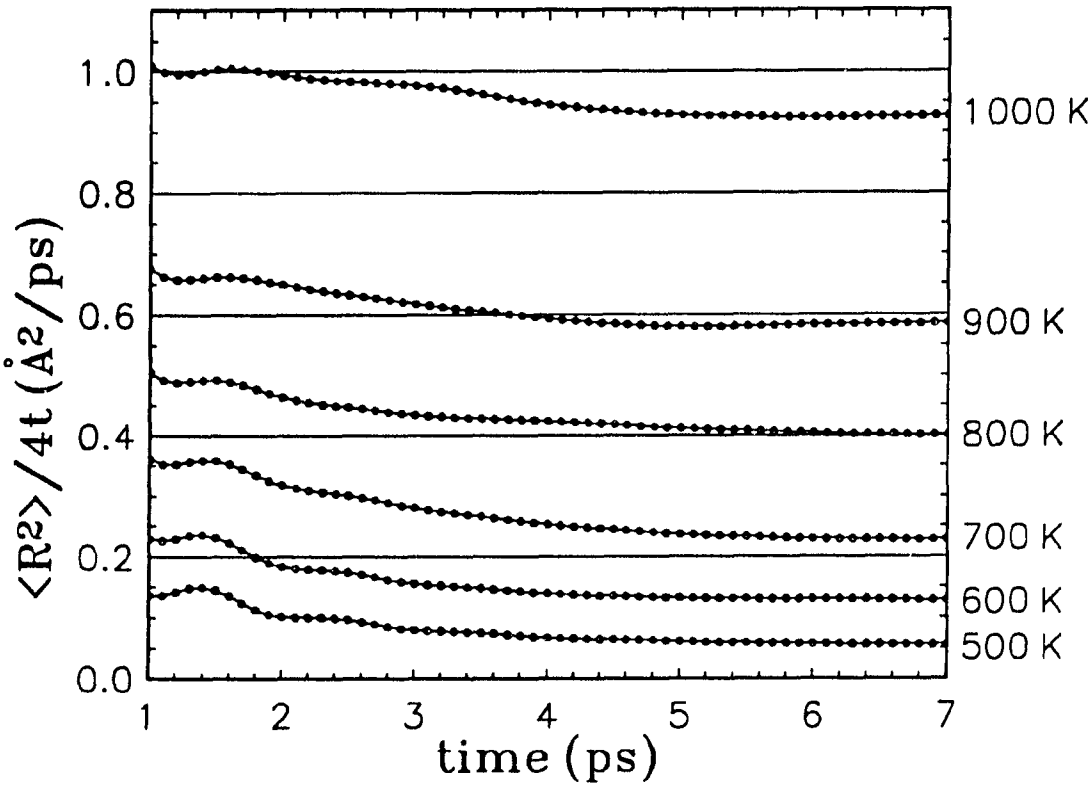

Figure 3. Time evolution of $\Delta(t)$ from Eq.(15) in the Ag on Ag(001) system for several substrate temperatures.

The long-time asymptotic limit, when it exists, is the diffusion constant.

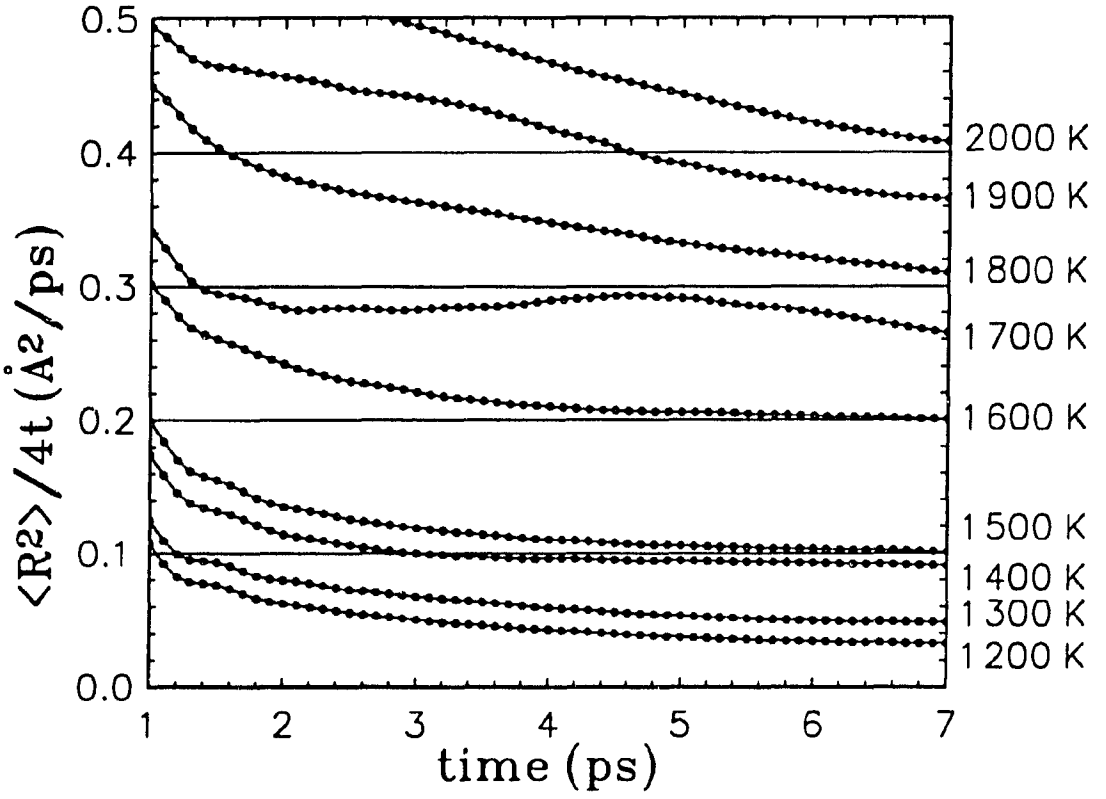

Figure 4. Same as Figure 3 but for the Rh on Rh(001) system

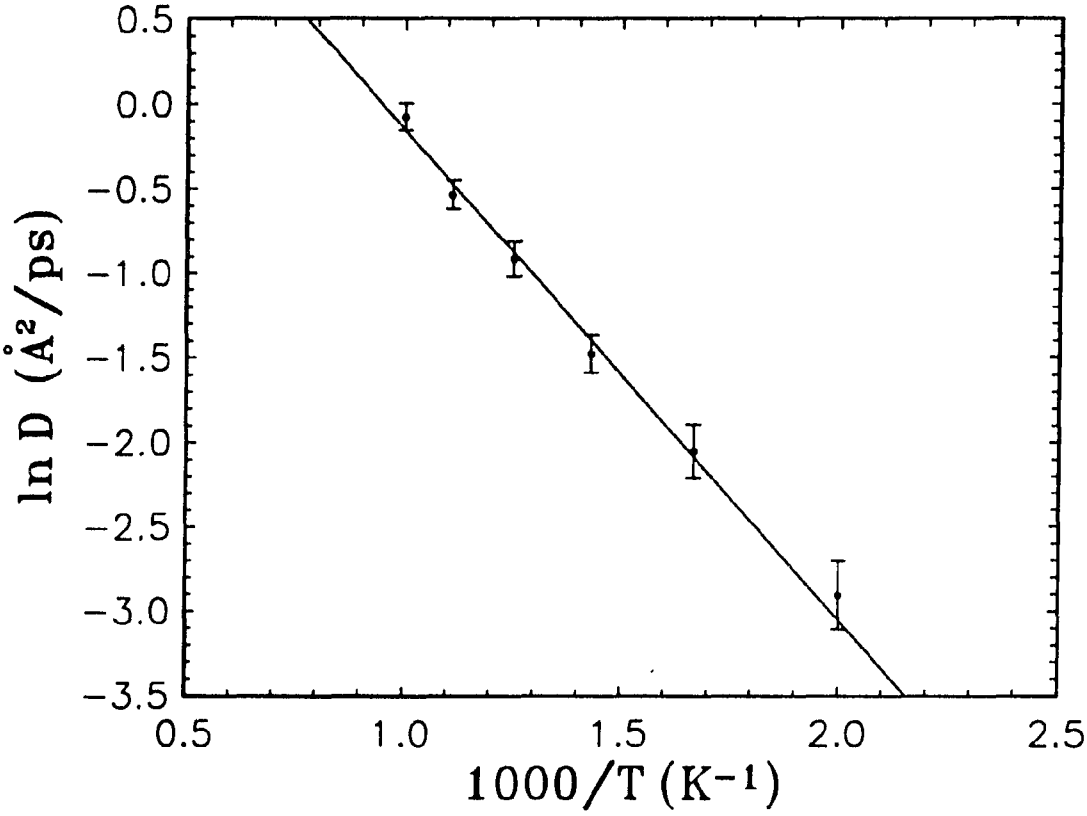

Figure 5. Arrhenius plot of the diffusion constant for the Ag on Ag(001) system extracted from direct molecular dynamics simulations.

The best fit line was determined by weighted least-squares. The resulting prefactor and activation barrier are reported in Table 4.

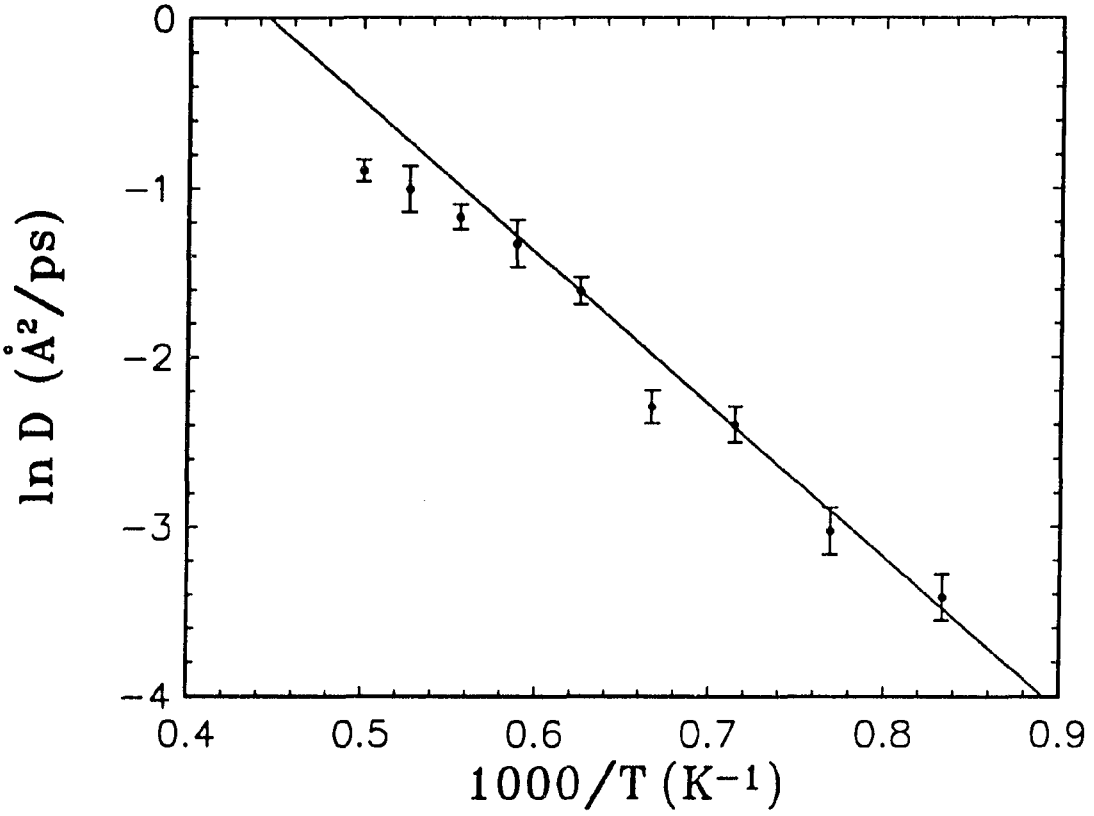

Figure 6. Arrhenius plot of the diffusion constant for the Rh on Rh(001) system extracted from direct molecular dynamics simulation

The best fit line was determined by weighted least-squares using only the points for T ≤ 1600K. The resulting prefactor and activation barrier are reported in Table 4.

and theory for ν_0 in this system is not due to either the isolated hop or TST approximations.

CONCLUSIONS

We have used the combination of TST and the MD/MC-CEM PES to predict diffusion rate constants for all 49 adsorbate/substrate combinations of the metals Ni, Cu, Rh, Pd, Ag, Pt, and Au. Comparisons to the limited experimental data indicated that the results were of good accuracy without adjustable parameters. Even for the atomically smooth Ag on Ag(001) system with a small barrier, TST was found to be accurate by comparison to full MD simulations of diffusion. Thus, our results represent the beginning of a reliable database for the modelling of diffusion. Future work will be directed to other surface faces, more complex diffusion mechanisms, diffusion of small clusters, and eventually to chemical diffusion.

ACKNOWLEDGEMENT

Financial support was received from NSF grant CHE-8921099. All calculations were performed on a SiliconGraphics 4D/380S computer, purchased via an NSF instrumentation grant.

REFERENCES

1.a. G. Ehrlich and K. Stolt, *Ann. Rev. Phys. Chem.* **31** (1980) 603 and references therein.

b. A. Kapoor, R.T. Yang, and C. Wong, *Catal. Rev. - Sci. Eng.* **31** (1989) 129 and references therein.

c. G. Ehrlich, *CRC Crit. Rev. Solid State Mater. Sci* **10** (1982) 391.

2. G. Ayrault and G. Ehrlich, *J. Chem. Phys.* **60** (1974) 281.

3. D.W. Bassett and P.R. Webber, *Surf. Sci.* **70** (1978) 520.

4. J.D. Wrigley and G. Ehrlich, *Phys. Rev. Lett.* **44** (1980) 661.

5. R.T. Tung and W.R. Graham, *Surf. Sci.* **97** (1980) 73.

6. G.L. Kellogg and P.J. Feibelman, *Phys. Rev. Lett.* **64** (1990) 3143.

7. C. Chen and T.T. Tsong, *Phys. Rev. Lett.* **64** (1990) 3147.

8. P.J. Feibelman, *Phys. Rev. Lett.* **65** (1990) 729.

9. M.S. Daw, A.F. Wright and C.Y. Fong, "Embedded atom method calculations concerning the exchange mechanism for diffusion of Pt and Pd adatoms on the Pt (001) surface", Program of the 37th Annual Symposium of the American Vacuum Society, (1990) 198.

10.a. M.R. Mruzik and G.M. Pound, *J. Phys. F* **11** (1981) 1403.
b. G. De Lorenzi, G. Jacucci, and V. Pontikis, *Surf. Sci.* **116** (1982) 391.
c. J.D. Doll and H.K. McDowell, *J. Chem. Phys.* **77** (1982) 479.
d. J.D. Doll and H.K. McDowell, *Surf. Sci.* **123** (1982) 99.
e. H.K. McDowell and J.D. Doll, *Surf. Sci.* **121** (1982) L537.
f. H.K. McDowell and J.D. Doll, *J. Chem. Phys.* **78** (1982) 3219.

11.a. K. Binder and D.P. Landau, *Adv. Chem. Phys.* (1989) 91.
b. W.H. Weinberg, *Ann. Rev. Phys. Chem.* **34** (1983) 217.

12. A.F. Voter, *Phys. Rev. B* **34** (1986) 6819.

13.a. J.D. Kress and A.E. DePristo, *J. Chem. Phys.* **88** (1988) 2596.
b. J.D. Kress, M.S. Stave, and A.E. DePristo, *J. Phys. Chem.* **93** (1989) 1556.
c. T.J. Raeker and A.E. DePristo, *Phys. Rev. B* **39** (1989) 9967.
d. T.J. Raeker and A.E. DePristo, *Surf. Sci.* **235** (1990) 84.
e. T.J. Raeker and A.E. DePristo, *Int. Rev. Phys. Chem.* **10** (1991) 1.

14. M.S. Stave, D.E. Sanders, T.J. Raeker, and A.E. DePristo, *J. Chem. Phys.* **93** (1990) 4413.

15. S.B. Sinnott, T.J. Raeker, M.S. Stave, and A.E. DePristo, (to be submitted).

16. D.E. Sanders and A.E. DePristo, "Metal/metal Homo-epitaxy on FCC(001) Surfaces: Is there Transient Mobility of Adsorbed Atoms?", *Surf. Sci.* (accepted 2/91).

17. T.J. Raeker and A.E. DePristo, "Theoretical Studies of Dynamical Phenomena in Epitaxial Surface Systems", *Surf. Sci.* (accepted 12/90).

18. J.D. Doll and A.F. Voter, *Ann. Rev. Phys. Chem.* **38** (1987) 413.

19. T. N. Truong and D. G. Truhlar, *J. Chem. Phys.* **93** (1990) 2125 and references therein.

20. B. M. Rice, B. C. Garrett, M. L. Koszykowski, S. M. Foiles and M. S. Daw, *J. Chem. Phys.* **92** (1990) 775.

21.a. L.M. Raff, I. NoorBatcha, and D.L. Thompson, *J. Chem. Phys.* **85** (1986) 3081.
b. B.M. Rice, L.M. Raff, and D.L. Thompson, *Surf. Sci.* **198** (1987) 360.
c. B.M. Rice, L.M. Raff, and D.L. Thompson, *J. Chem. Phys.* **88** (1988) 7221.
d. P.M. Agrawal, D.L. Thompson, and L.M. Raff, *J. Chem. Phys.* **91** (1989) 6463.

22. D. G. Truhlar, A. D. Isaacson and B. C. Garrett, in Theory of Chemical Reaction Dynamics, ed. M. Baer (CRC, Boca Raton, FL, 1985) Vol. IV, p65.

23.a. G. Wahnström and H. Metiu, *J. Phys. Chem.* **92** (1988) 3240.
b. G. Wahnström, in: Interaction of Atoms and Molecules with Solid Surfaces, Eds. V. Bortolani, N.H. March, and M.P. Tosi (Plenum Press, New York, 1990) ch. 16.

24. W. H. Miller, N. C. Handy and J. E. Adams, *J. Chem. Phys.* **72** (1980) 99.

25.a. K. Ruedenberg and P. Valtazanos, *Theor. Chim. Acta* **68** (1986) 281.
b. W. A. Kraus and A. E. DePristo, *Theor. Chim. Acta* **69** (1986) 309.

26. See, for example, C. Gonzalez and H. B. Schlegel, *J. Chem. Phys.* **90** (1989) 2154.

27. D.D. Chambliss and R.J. Wilson, "Relaxed Diffusion Limited Aggregation of Ag on Au(111) Observed by Scanning Tunneling Microscopy", *J. Vac. Sci. Technol.* (to appear March/April 1991).

28. V.P. Zhdanov, *Surf. Sci.* **214** (1989) 289.

29. H.P. Bonzel, in: Surface Physics of Materials, Vol. II, Ed. J.M. Blakely (Academic Press, New York, 1975) ch. 6.

30. J.J. de Miguel, A. Cebollada, J.M. Gallego, J. Ferrón, and S. Ferrer, *J. Cryst. Growth* **88** (1988) 442.

31.a. A.E. DePristo and H. Metiu, *J. Chem. Phys.* **90** (1989) 1229.
b. M. Berkowitz and J.A. McCammon, *Chem. Phys. Lett.* **90** (1982) 215.
c. C.L. Brooks III and M. Karplus, *J. Chem. Phys.* **79** (1983) 6312.
d. R. Lucchese and J.C. Tully, *Surf. Sci.* **137** (1983) 1570.
e. R. Lucchese and J.C. Tully, *J. Chem. Phys.* **80** (1984) 3451.

32.a. S.A. Adelman and J.D. Doll, *Acc. Chem. Res.* **10** (1977) 378.
b. S.A. Adelman, *Adv. Chem. Phys.* **44** (1980) 143 and references therein.
c. J.C. Tully, *J. Chem. Phys.* **73** (1980) 1975.
d. A.E. DePristo, *Surf. Sci.* **141** (1984) 40.

33. L. Verlet, *Phys. Rev.* **159** (1967) 98.

PAPER III.

SCT89: A COMPUTER CODE FOR ATOMIC AND MOLECULAR SCATTERING FROM CLEAN AND ADSORBATE COVERED SURFACES

SCT89: A Computer Code for Atomic and Molecular Scattering from Clean and Adsorbate Covered Surfaces

David E. Sanders[a]
Mark S. Stave
and
Andrew E. DePristo

Department of Chemistry
and
Ames Laboratory USDOE*
Iowa State University
Ames, Iowa 50011

[a] IBM predoctoral Fellow

*Ames Laboratory is operated for the U.S. Department of Energy by Iowa State University under contract No. W-7405-Eng-82.

ABSTRACT

We present the first version of SCT89, a general user-friendly program for performing molecular dynamics simulations of processes on metal surfaces. Incorporation of the recently developed MD/MC-CEM potential energy surface allows us to consistently treat systems containing up to four chemically distinct types of atoms. Techniques to efficiently calculate the interatomic forces from this complicated potential function are discussed in detail. Features such as interactively prompting for input parameters and creating its own input files provide a simplified user interface. The scope of problems which can be treated with SCT89 include the scattering of atoms and diatomic molecules from clean and adsorbate covered surfaces, diatomic adsorption/dissociation dynamics, and adsorbate overlayer dynamics. SCT89 provides performance in the 50 to 60 MFLOPS range on a Cray Y-MP and also performs well on the new generation of mini-supercomputers.

INTRODUCTION

Collisions of atoms and molecules with solid surfaces lead to energy transfer and chemical reactions of importance in a number of technological areas. These include the processing of automobile exhaust fumes in catalytic converters, the refining of petroleum, the fabrication of microelectronic devices, and the synthesis of ammonia. Cosmological problems such as the formation of organic molecules on interstellar dust grains also depend upon these collisions. In general, these systems contain many types of atoms and a number of surfaces of different geometry, making any description complex.

The dynamical process involves the strong interaction among a small number of atoms (e.g., a gas molecule and perhaps a hundred properly chosen adsorbate and solid atoms) which in turn interact less strongly with a vast number of atoms (e.g., the remainder of the adsorbate/solid system). Brute force simulations of these processes can involve molecular dynamics calculations on many thousands of atoms. However, recently devised stochastic molecular dynamics methods have lowered this number via replacement of the weakly interacting atoms by a suitably chosen heat bath [1,2,3,4]. This is important since measurables generally involve some sort of average over initial conditions of the system, requiring many trajectories each of which must be reasonably fast to calculate. Solution of this dynamical bottleneck has provided considerable impetus for development of the present computer program: the capability to treat complex processes made it reasonable to invest considerable effort in the design and construction of an efficient,

general, user-friendly piece of software to simulate the important processes mentioned above.

The description of the scattering problem also requires the potential energy surface (PES) and forces. The common procedure used to obtain these is empirical: one assumes a convenient functional form with adjustable parameters that are fitted to some (arbitrary) combination of calculated and experimental quantities. The simplest forms rarely describe well many properties of a real system. A good example is the use of the Lennard-Jones (12,6) form for the binding energy of monatomic metals [5]: the two parameters in the potential can be fixed by specification of the lattice constant and cohesive energy or the lattice constant and the Debye frequency. The former choice leads to an overestimate of the Debye frequency by a factor of about three while the latter leads to an underestimate of the cohesive energy by about a factor of five [6]. Any process in which both numbers are important such as surface diffusion will then be described inaccurately. Replacement of the LJ(12,6) by a three parameter Morse potential, which can duplicate all three pieces of experimental data [7], leads to unphysically large expansions of the surface layers [6]. The use of such arbitrary potentials provides insight into the behavior of model systems, which nevertheless may be rather irrelevant for real experimental systems.

One is thus led quite quickly to complex forms with many parameters. The construction is tedious and must be redone for each system. This limits the predictive ability of the theory since one must almost "know" that a particular system is interesting in order to justify the large effort to construct a PES to explain

the interesting fact. This approach leads to theoretical interpretations of already available experimental data. It can provide insight into the meaning of experimental measurements but cannot let theory predict the interesting data and systems beforehand. Thus, in both cases, there is an uncoupling of theory and experiment.

For systems up to ten or twenty atoms, recent work of Car and Parrinello [8] have demonstrated the feasibility of performing self-consistent electronic structure calculations fast enough to evaluate the forces directly, at least within a SCF-LD framework. Approximate molecular structure techniques can also be used in an analogous manner [9].

For still larger systems, such direct calculations are not feasible. Progress has been made for metallic systems, however. The recently developed embedded atom method (EAM) [10], and the related Finnis-Sinclair [11] and "GLUE" model [12] approaches, provide a theoretically based form for metal-metal bonding with a limited number of parameters. These have been applied successfully to a number of simulations in which many thousands of atoms evolve dynamically [12,13]. The effective medium (EM) method [14], predating the EAM and related methods, has also been applied to large systems [15].

In a number of recent articles [16,17,18,19,20,21], we have derived, implemented and applied an approach to the calculation of interaction energies based upon direct evaluation of the corrections to the EM theory using density functionals (i.e., the corrected EM, CEM theory). The fundamental theoretical development occurs in refs.[17] and [18] with refinements and symmetry inclusions

in refs.[18,19,20]. A detailed review of EAM, EM and CEM methods is available in ref.[21].

The calculation of the interaction energy for any number (N) and type of atoms $\{A_i, i=1,...,N\}$ is provided by CEM-N. The basic idea of this theory is to replace each atom A_i interacting with all other atoms $\{A_j, j=1,...,N, j\neq i\}$ by atom A_i embedded in a spin-unpolarized jellium of density n_i. The SCF-LD interaction or embedding energy for nearly all atoms through Cu is known as a function of the jellium density [22]. For chemical accuracy, semi-empirical embedding functions can also be constructed from experimental data or from LMTO calculations on the bulk system. The differences between the real and atom-jellium systems due to inhomogeneities of the electron density and the point charge of the nuclei are determined non-self-consistently and involve both coulombic and kinetic-exchange-correlation energies. Further details can be found in the original papers [17,18,19,20] and the upcoming review [21].

Recently, we have presented the conceptual and formal simplifications of the CEM theory that allow the theory to be used directly in MD and MC simulations of large systems [23], hence the acronym MD/MC-CEM. The essential idea involves adjustment of the CEM embedding functions to include approximately the original explicit correction for kinetic-exchange-correlation energy differences between the real system and the many atom-jellium systems used as the zeroth order model. Examples of this construction were provided for the Ni, Pd, Ar and H/Pd(111) systems [23] and the Rh and Ag systems [24].

The MD/MC-CEM PES requires these semi-empirical embedding functions along with the atomic electron densities. The former are universal functions of the atom's identity and the jellium density while the latter can be found simply from tabulated ab-initio results [25]. Thus, all of this information is now available for nearly all elements in the periodic table lighter than Xe. This has provided the remaining impetus for the development of the present program.

In this article, we present a first version of a general, user-friendly computer program for the simulation of atomic and molecular scattering from solid surfaces, adsorbate dynamics on solid surfaces, and the generation and mapping of multi-dimensional PES in such systems. A number of properties have been incorporated into this code to allow for generality. For example, it is a simple problem to treat scattering from adsorbate covered surfaces in arbitrary ordered and disordered coverages. More examples and details are provided in this article. We emphasize that SCT89 is only capable of simulation via classical mechanics. It is left to the user to decide whether quantum mechanical effects play a significant role in any problem of interest.

BRIEF OVERVIEW OF THE THEORY

We start by defining the notation. Denote the positions of the N_s solid atoms by $\underset{\sim}{Y}=\{\vec{Y}_1, \vec{Y}_2,...\}$ and the masses by M_{Yi}; similarly, the N_a adsorbates by $\underset{\sim}{Z}$ and M_{Zi}; and the N_g gas atoms by $\underset{\sim}{X}$ and M_{Xi}. All gas atoms follow classical dynamics with,

$$M_{Xi}\, d^2\vec{X}_i/dt^2 = -\partial V(\underset{\sim}{X},\underset{\sim}{Y},\underset{\sim}{Z})/\partial \vec{X}_i \qquad \text{(gas atoms)} \qquad (1)$$

where $V(\underset{\sim}{X},\underset{\sim}{Y},\underset{\sim}{Z})$ is the full PES for the system. (The symbol $\partial/\partial \vec{X}_i$ symbolizes the gradient with respect to the coordinates of $\vec{X}_i$.)

The adsorbate atoms are divided into two classes: active and fixed. The active adsorbate atoms follow classical dynamics with

$$M_{Zi}\, d^2\vec{Z}_i/dt^2 = -\partial V(\underset{\sim}{X},\underset{\sim}{Y},\underset{\sim}{Z})/\partial \vec{Z}_i \qquad \text{(active adsorbates).} \qquad (2)$$

The fixed adsorbates do not move.

The solid's atoms are divided into three classes: inner active, edge active and fixed. The inner active atoms follow classical dynamics with,

$$M_{Yi}\, d^2\vec{Y}_i/dt^2 = -\partial V(\underset{\sim}{X},\underset{\sim}{Y},\underset{\sim}{Z})/\partial \vec{Y}_i \qquad \text{(inner active solid).} \qquad (3)$$

The edge atoms follow either classical dynamics as described above or Langevin dynamics in which local (isotropic) frictional and gaussian white noise random forces are added to the potential forces,

$$M_{Yi}\, d^2\vec{Y}_i/dt^2 = -\partial V(\underset{\sim}{X},\underset{\sim}{Y},\underset{\sim}{Z})/\partial \vec{Y}_i - M_{Yi}\gamma d\vec{Y}_i/dt + \vec{f}_{Yi}(t) \qquad (4a)$$

$$\gamma = \pi\omega_D/6 \qquad \text{(edge active solid)} \qquad (4b)$$

$$\vec{f}_{Yi}(t) = (2\gamma kTM_{Yi}/h)^{1/2}\, \vec{\xi}_{Yi}\,. \qquad (4c)$$

Here, ω_D is the Debye frequency; Eq.(4b) ensures that long time energy transfer into the bulk system is given correctly [1,4,26]. The time step in the integration is "h" and $\vec{\xi}_{Yi}$ is a vector of gaussian random numbers. Eq.(4c) ensures that the frictional and random forces obey the second fluctuation-dissipation theorem [26],

$$<\vec{f}_{Yi}(t)\vec{f}_{Yi}(0)^T> = \delta(t)\, 2\gamma M_{Yi}kT\, \underset{=}{1} \qquad (5)$$

at least over the time step of the numerical integration. This allows the surface and adsorbate system to be kept at any desired temperature. The fixed atoms surround the active atoms and are not allowed to move. They provide a structural template for the surface and smooth out the potential energy of the active atoms.

The potential for the entire system can be chosen in a number of ways. The first and most complete involves use of the MD/MC-CEM formulation. This

allows a consistent description of all the atoms. Since all atoms are considered on equal footing, we denote all of them by $\{A_i, i=1, ..., N\}$ where $N=N_s+N_a+N_g$. Each A_i can be essentially any atom in the entire periodic table. The nuclei are located at $\{\vec{R}\}=(\vec{R}_1, \vec{R}_2, ..., \vec{R}_N)$.

The MD/MC-CEM expression for the interaction energy $\Delta E(\{A_i\})$, which is identical to the full PES, is given by the expression,

$$\Delta E(\{A_i\}) = \Sigma\, \Delta F_J(A_i;n_i) + 1/2\, \Sigma_i\, \Sigma_{j\neq i}\, V_c(i,j)\,. \qquad (6)$$

The first term is the sum of the effective embedding energies for each atom A_i into jellium of density n_i, $\Delta F_J(A_i;n_i)$. Each such function can be constructed by two different methods: 1) from experimental data on homonuclear diatomic and bulk systems [21,23a]; 2) from LMTO calculations on the bulk system [23b]. The latter procedure provides the most reliable embedding functions for metals and are the **only functions included in the first release of the SCT89 program.** The second term is the sum of atom-atom coulomb energies (i.e., total nuclear-nuclear, nuclear-electron and electron-electron energies for each pair of atoms).

Evaluation of the coulomb energy and determination of the jellium density for each atom, n_i, requires specification of the atomic densities. In MD/MC-CEM theory, the approximation of superposition of atomic Hartree-Fock (HF) electron densities is utilized which makes evaluation of these quantities non-empirical and straightforward. The jellium densities are given by,

$$n_i = (2Z_i)^{-1} \Sigma_{j \neq i} S(i,j) \tag{7a}$$

where the density overlap is defined by,

$$S(i,j) = \int n(A_i;\vec{r}-\vec{R}_i)\, n(A_j;\vec{r}-\vec{R}_j)\ d\vec{r}\,. \tag{7b}$$

The coulomb integral is,

$$V_c(i,j) = \int [n(A_i;\vec{r}-\vec{R}_i) - Z_i\, \delta(\vec{r}-\vec{R}_i)]\, |\vec{r}-\vec{r}'|^{-1} [n(A_j;\vec{r}'-\vec{R}_j) - Z_j\, \delta(\vec{r}'-\vec{R}_j)]\, d\vec{r}\, d\vec{r}'\,. \tag{7c}$$

The atomic HF density [25] of atom A_i is $n(A_i;\vec{r}-\vec{R}_i)$ and Z_i is the atomic number. These HF densities are provided in terms of a number of Slater-type basis functions; the densities are then fit in an even-tempered Gaussian basis [27] to facilitate the integral evaluations [28]. We must evaluate all these integrals for the MD/MC-CEM PES. Through use of Chebyshev smoothing techniques, equally spaced grids in inverse square distance and cubic polynomial interpolation, we have developed techniques to perform this complicated evaluation at speeds approaching that of simple pair potentials of the LJ(12,6) form. This is detailed in the next section.

There are other potentials which can be used in the SCT89 program but these are not general for the entire system. They are included mainly for the convenience of the user in generating results for comparison to previous literature

values. In these cases, the PES is assumed separable in solid-solid, solid-adsorbate and solid-gas interactions. Thus we have,

$$V(\underset{\sim}{X},\underset{\sim}{Y},\underset{\sim}{Z}) = V_{SS}(\underset{\sim}{Y}) + V_{SA}(\underset{\sim}{Y},\underset{\sim}{Z}) + V_{SG}(\underset{\sim}{Y},\underset{\sim}{X}) + V_{AA}(\underset{\sim}{Z}) + V_{AG}(\underset{\sim}{Z},\underset{\sim}{X}) \qquad (8)$$

in obvious notation. For V_{SS}, V_{SA} and V_{AA}, it is possible to use summed pairwise potentials of either the LJ(12,6) or Morse form. For V_{SA}, a different empirical form, developed originally for V_{SG} [29], can also be used,

$$V_{SA}(\underset{\sim}{Y},\underset{\sim}{Z}) = \Sigma_{i=1,Na}\, \Delta E_P(\rho_i) + \Sigma_{i=1,Ns}\, \Sigma_{j=1,Na}\, v_2(|\vec{Y}_i - \vec{Z}_j|)\,. \qquad (9)$$

Here the embedding energy is taken directly from the SCF-LD results of Puska et al. [22] but arbitrary two body interactions, specified by the user, are added. The density, ρ_i, is just the surface atom density at the position of the adsorbate nucleus, $\vec{Z}_i$. An identical construction is available for the gas atom(s).

If there are two gas atoms, the modified 4-body LEPS form [29] can be used which consists of:

(a) a Morse potential between the two gas atoms;

(b) an empirical two body plus embedding energy for each gas-surface interaction (as in Eq.(11) for V_{SG});

(c) a combination of the above interactions using the LEPS form with adjustable Sato parameters.

This LEPS form is useful in the description of dissociative chemisorption reactions where the prediction of accurate activation barriers for reaction are beyond the capabilities of the MD/MC-CEM theory (as well as any other methods at present.) Current research by the authors and others [14d,30] is devoted to solution of this problem, but at present the limitation exists.

NUMERICAL IMPLEMENTATION

The computational details of the MD/MC-CEM approach are discussed here. The reader solely interested in the capabilities of the program may skip to the next section. We focus on evaluation of the expressions in Eqs.(6) and (7). The discussion will be limited to the case when the electron density around each atom is spherical and unpolarized, $n(A_i;\vec{r}) = n(A_i;r)$.

First, a straightforward evaluation of Eqs.(6) and (7) will be described, then all modifications necessary for computational speed and numerical accuracy in the determination of the energy and forces will be presented. ***The goal is to evaluate energies and forces based upon Eqs.(6) and (7) at speeds comparable to the use of pairwise additive two body potentials of the Lennard-Jones (12,6) form.*** This requirement forces the use of special techniques.

Both $V_c(i,j)$ and $S(i,j)$ involve two-dimensional integrals over the atomic densities: the former in r and r′ and the latter in r and $\vec{r}\cdot\hat{Z}$ where $\hat{Z}$ is the internuclear axis. Even placing the atomic densities on a large radial grid, equally spaced in r^2 with evaluation by linear interpolation, is much too slow by factors of 10^4-10^6 due to the large number of quadrature points.

As an alternative, which can also be used for non-spherical densities, we have constructed an even-tempered Gaussian basis [27] to represent the atomic densities that are generated from Slater-type atomic Hartree-Fock densities [25]. Use of gaussians allows for efficient, analytic evaluation [28] of $V_c(i,j)$ and $S(i,j)$. The density due to p-orbitals had to be fit separately from the remaining density.

The number of gaussian basis functions was typically greater than 25 for the spherical density part and also greater than 25 for the p-density part, at least for atoms with $Z_i > 10$. The number of integrals is considerably smaller than the number of integration points necessary for the direct quadrature scheme mentioned previously. Thus, this approach is considerably more efficient. However, since each analytic integral is considerably more time consuming than evaluation of a LJ(12,6) potential, even this approach is much too slow (by a factor of 10^3-10^4).

The reader may wonder why one does not simply fit some arbitrary function to the $V_c(i,j)$ and $S(i,j)$. First, this would not be a very general solution. Second, unless one was lucky in providing an accurate fit with a very simple function, the evaluation would be much more time-consuming than computation of the LJ(12,6) form. For the accuracy desired here ($\pm 10^{-4}$ eV in $V_c(i,j)$ and $\pm 10^{-7}$ bohr^{-3} in $S(i,j)$), such a simple form would be extremely fortuitous. (This accuracy is more than adequate for chemical energies.)

Our approach developed below is purely numerical and thus is not tied to any properties of the particular functions appearing in the present article. It is illustrated for $V_c(i,j;R)$ where $R=|\vec{R}_i-\vec{R}_j|$. Assume that V_c must be known on $[R_{min}, R_{max}]$. First, the function is approximated by a Chebyshev polynomial expansion [31] in $x=R^{-2}$ on the range $[x_<,x_>]$ where $x_<=R_{max}^{-2}$ and $x_>=R_{min}^{-2}$,

$$V_c(i,j;R) = \Sigma_{k\geq 0}\, V_T(i,j;k)\, T_k(t) \qquad (10a)$$

where T_k is the Chebyshev polynomial of k^{th} order and,

$$t = [\ x-1/2(x_> + x_<)\ ]/[\ 1/2(x_> - x_<)\ ]. \qquad (10b)$$

The expansion coefficients, $V_T(i,j;k)$, are determined by numerical integration using Gauss-Chebyshev quadrature. The number of quadrature points, and hence the maximum number of terms in the series, was fixed at 31 since less than 25 terms always represented $V_c(i,j;R)$ to better than $\pm 10^{-4}$ eV and $S(i,j;R)$ to better than $\pm 10^{-7}$ bohr^{-3}. Expanding in R^{-2} eliminates any square root evaluations and effectively samples the function more in the small R region, where the function varies more rapidly, than in the large R region. It would be very slightly more efficient to expand in R^2 but this effectively samples the function more at large R, where the function varies more slowly. This leads to much larger storage requirements for the same accuracy.

As an example both $V_c(i,j;R)$ and its derivative with respect to R^{-2} are shown in Figure 1 vs. R^{-2} for two Ni atoms. This fitting procedure provides an accurate representation of $V_c(i,j;R)$ along with continuous higher derivatives (well past any order of importance in the dynamics, force constant evaluation, anharmonicity constant calculation, etc.). The expansion is too slow to be evaluated directly in the dynamics; further, only smooth first derivatives are required for the forces.

Instead, as the second step, the Chebyshev series representation is used to generate a set of function and first derivative values, $\{x_k, f_k, f_k'; k=1, \ldots, K\}$, where f_k' is the derivative with respect to the variable "x". These are evaluated at points equally spaced in x with spacing δx in the interval $[x_<, x_>]$. Interpolation of these

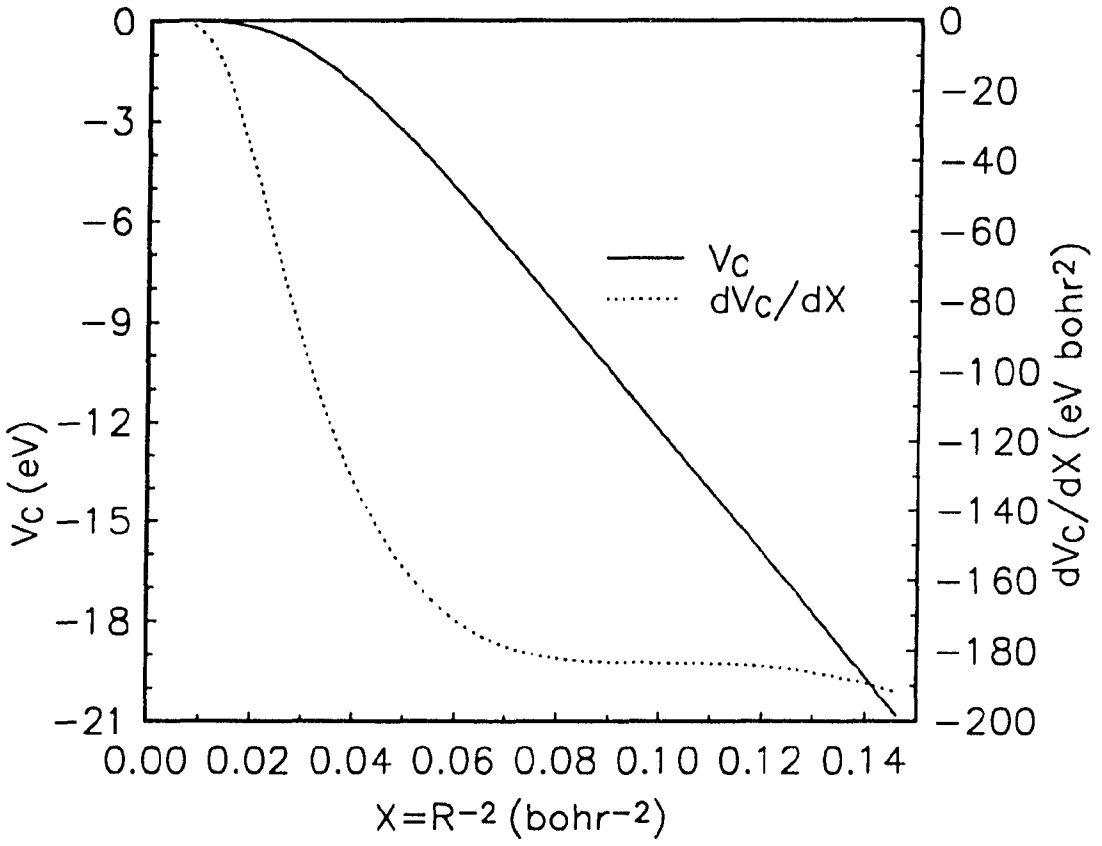

Figure 1. The Chebyshev series representation for the coulomb interaction (solid curve) and its derivative (dashed curve) between two Ni atoms as a function of R^{-2}

points is then implemented by passing a piecewise cubic polynomial through the set. Thus, for $x_\alpha \le x < x_{\alpha+1}$,

$$V_c(i,j;R) = V_c(i,j;R_\alpha) + d\,\{\, C_1(i,j;\alpha) + d\,[\, C_2(i,j;\alpha) + d\, C_3(i,j;\alpha)\,]\,\} \qquad (11a)$$

$$\partial V_c(i,j;R)/\partial R = \{\, C_1(i,j;\alpha) + d\,[\, 2\, C_2(i,j;\alpha) + d\, 3\, C_3(i,j;\alpha)\,]\,\}\,(-2/R^3) \qquad (11b)$$

where α is the interval in which x lies, C_k is the coefficient of the k^{th} power term, and,

$$d = x - x_\alpha\,. \qquad (11c)$$

Since the grid is evenly spaced in x, the interval is found directly as,

$$\alpha = 1 + \text{Integer}[(x-x_<)/\delta x] \qquad (11d)$$

where Integer(Z) extracts the integer part of the real number. The coefficients are determined by requiring Eqs.(11a) and (11b) to be continuous throughout the interval $[x_<, x_>]$. Since higher order derivatives are accessible within the Chebyshev series representation, higher order interpolatory schemes can be utilized if needed. Eqs.(11) are efficient computationally, since they do not require either square roots or an interval search. (Note that R^3 in Eq.(11b) need not be evaluated since it is included in the R^4 factor in the expression for the total force on any atom as shown

in Eq.(14).) Additionally, they provide a smooth function and its first derivative. A similar interpolation scheme has been presented previously without the Chebyshev smoothing [32].

The third, and final, step concerns extrapolation outside the interval $[x_<,x_>]$. For $x < x_<$, (i.e., $R > R_{max}$), it is best to ensure continuity of the functions representing $V_c(i,j)$ and $S(i,j)$ and their derivatives. Hence, the extrapolation scheme should require both the function and its derivative to be zero at some cutoff point, $x_0=R_0^{-2}$, and to be continuous with the interpolation scheme at $x=x_<$. These conditions can be satisfied using the form of Eqs.(11):

$$V_c(i,j;R>R_{max}) = V_c(i,j;R_0) + d \{ C_1(i,j;0) + d [C_2(i,j;0) + d\, C_3(i,j;0)] \} \quad (12a)$$

where the coefficients are defined as:

$$V_c(i,j;R_0) = 0 \quad (12b)$$

$$C_1(i,j;0) = 0 \quad (12c)$$

$$C_2(i,j;0) = -f_1'/(x_1-x_0) + 3\, f_1/(x_1-x_0)^2 \quad (12d)$$

$$C_3(i,j;0) = f_1'/(x_1-x_0)^2 - 2\, f_1/(x_1-x_0)^3 . \quad (12e)$$

For $x > x_>$, (i.e., $R < R_{min}$), extrapolation is done linearly since f_K and f_K' are the only information that is consistent with the remainder of the procedure. However, we always try to ensure that R_{min} is smaller than any separation in the collision.

Up to this point x_0 has only to be less than $x_<$. In order to ensure a monotonic approach of the function representing $V_c(i,j)$ and its derivative to zero, however, it is necessary that its second derivative with respect to x be less than or equal to zero at x_0 and the third derivative with respect to x be less than or equal to zero for all $x \in [x_0,x_1]$. These additional conditions limit x_0 to be in the interval $[x_1 - 3\, f_1/f_1',\ x_1 - 2\, f_1/f_1']$. Similar conditions for the function representing S(i,j) lead to an analogous limitation on x_0, with f_1 and f_1' referring to S(i,j) and its derivative, of course. Thus, there are two possibly distinct intervals for the location of x_0 determined by the two different functions. In all of our work, these intervals have overlapped since their respective ratios, f_1/f_1', have been very similar. As a result $V_c(i,j)$ and S(i,j) can be placed conveniently on the same grid.

The above procedure ensures continuity of the function and its derivative, and forces them to vanish at the point $R_0=x_0^{-2}$. For convenience each pair of atom types uses the same values of R_{min}, R_{max}, K and R_0 for both $V_c(i,j)$ and S(i,j). In order to minimize the number of operations necessary for the evaluation of these functions and their derivatives, both the coefficients in Eqs.(11a) and (11b) multiplied by constant factors are stored. The storage (in words) required per pair of atom types is 15 times the number of cubic polynomial knots, K. The particular value of K depends upon the energy range of interest. This range determines R_{min} and R_{max}. For the applications in this paper, R_{min} is chosen so that Eq.(6) yields

an interaction energy of approximately +100 eV for each pair of atom types when isolated. R_{max} is chosen so that the coulomb energy is approximately -0.001 eV. In such applications a value of K=400 has been found to yield interpolation inaccuracies well within the uncertainty of the Chebyshev expansions for all systems including atoms up to Au. Thus, for an extremely wide range of energies, there is a modest storage requirement of 6000 words per pair of atom types. Hence, a system with 5 different kinds of atoms would require only 90,000 words of storage, a trivial amount by today's computing standards.

This procedure provides a complete solution to the representation of essentially any well-behaved (one-dimensional) function and its derivatives. It depends critically upon the properties of Chebyshev series in providing a near minimax fit, and in the ability to generate the function at the relevant Gauss-Chebyshev points for evaluation of the coefficients in the series. This would be available for any analytic function, no matter how complex, and only needs to be done once to set up the Chebyshev coefficients.

In Eq.(6) each $\Delta F_J(A_i;n_i)$ poses an additional problem since it is known only at a small (<20) set of points as shown in Figure 2 for Pd. In addition, a large gap between the diatomic and bulk regions occurs for each ΔF_C. This precludes the use of an expansion such as Eq.(10a). In such cases, the functions cannot be calculated with arbitrary accuracy at the required Gauss-Chebyshev points. The common way to circumvent this problem involves fitting a quasi-Hermite spline [33] to the values of ΔF_J. These splines can be treated as analytic functions and the procedure leading to Eqs.(11) can be followed with $x=n_i$. An example is shown in Figure 3 for ΔF_C(Pd).

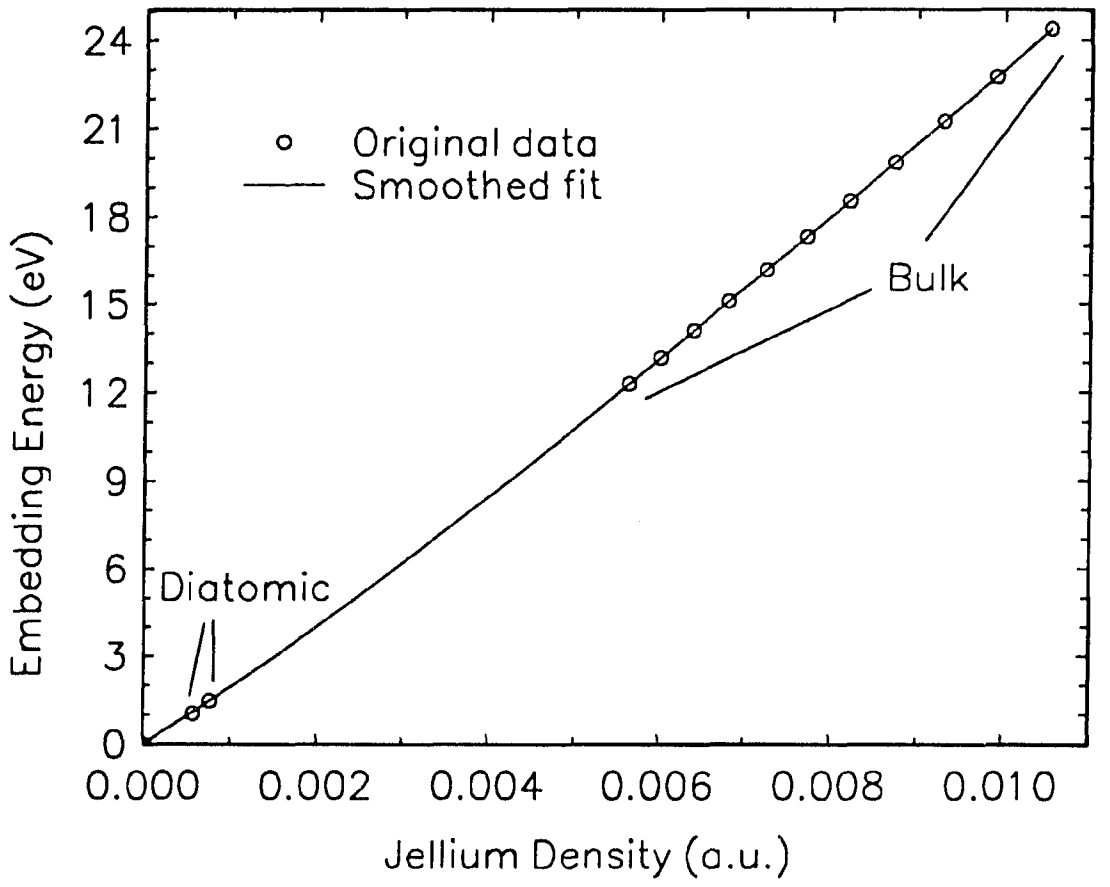

Figure 2. The covalent embedding function, ΔF_C, for MD/MC-CEM for the Pd system

The open circles correspond to the original unsmoothed data. The values labeled diatomic are calculated as the bond length varies, with only the $1.00R_e$ and $1.05R_e$ results shown for clarity. The values labeled bulk are calculated from the monatomic metal as the lattice constant varies. The solid curve is the result of the weighted least-squares Chebyshev smoothing procedure described in the text. A quasi-Hermite spline fit to the data is indistinguishable from the Chebyshev representation on the scale of this plot.

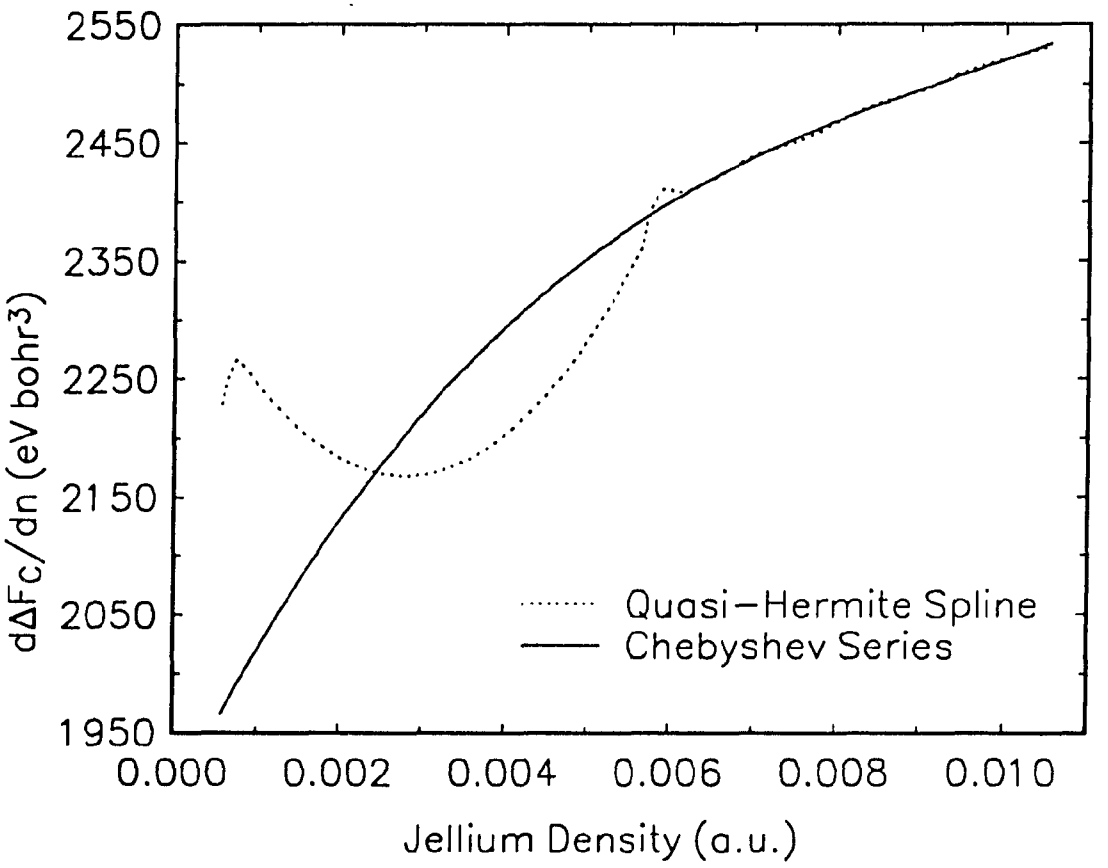

Figure 3. Derivative of the covalent embedding function in Figure 2 with respect to jellium density for MD/MC-CEM for the Pd system

The solid and dashed curves correspond to the Chebyshev series smoothing described in the text and the direct quasi-Hermite spline interpolation, respectively.

Note however the unreasonable nature of the derivatives of these splines. Clearly, this purely interpolative approach is unsatisfactory even though the original functions appear quite smooth.

Alternatively, and independently of the SCT89 program, the original data set can be fit to a Chebyshev series using a weighted linear least squares procedure. An estimate of the uncertainty of each point in the data set is used to determine its weight. This procedure allows the embedding energy values to adjust slightly to ensure smooth derivatives. In Figure 2 the smoothed function for Pd is shown with the corresponding derivative shown in Figure 3. Clearly, the functions are nearly unchanged while the derivatives are smooth. The original data set is then replaced by a set of points distributed uniformly along the fitting interval as evaluated from this Chebyshev expansion. (This enables use of flexible input data sets for SCT89 without being fixed to a particular smoothing procedure.) A quasi-Hermite spline fit of this adjusted data set can be treated as an analytic function and the procedure leading to Eq.(11) followed with $x=n_i$.

The density range is chosen such that the first non-zero density value is n_{min} and the last density point is n_{max}. The region from n=0 to $n=n_{min}$ is evaluated by the quadratic form,

$$\Delta F_J(A_i;n_i) = \Delta F_J(A_i;0) + d\,[\, C_1(i,j;0) + d\, C_2(i,j;0)\,]\,. \qquad (13)$$

In this case the coefficients are determined by requiring both the function and its derivative to be continuous at n_{min} and the function to have the appropriate zero density value.

To conclude this section, we provide the explicit force on any atom based upon Eq.(6):

$$\vec{f}_i = \Sigma_{j \neq i} \{ 1/2 [Z_i^{-1}(\partial \Delta F_J/\partial n_i) + Z_j^{-1}(\partial \Delta F_J/\partial n_j)] [\partial S(i,j)/\partial x] + [\partial V_c(i,j)/\partial x] \} (2/R^4) (\vec{R}_i - \vec{R}_j) . \quad (14)$$

In order to evaluate Eq.(14) all the n_i must be known. Consequently, it is impossible to evaluate $\vec{f}_i$ by one loop over all pairs formed by atom A_i with every other atom. On a Silicon Graphics SGI 4D/380S the above techniques require 867 seconds to propagate 442 Cu atoms through 1000 time steps. For comparison, the identical calculation using a LJ(12,6) PES requires 401 seconds.

GENERAL OVERVIEW OF THE PROGRAM

SCT89 consists of a main driver of about 2500 lines along with about 90 subroutines for a total length of 13000 lines. With the exception of Cray Assembler Language (CAL) routines to replace non-vectorizable conditional loops, all code is written in ANSI standard Fortran 77. The Fortran equivalent of these routines is used when running on non-Cray machines. All input parameters are read by the main driver. The program can be run in a special interactive mode that prompts the user for input parameters and saves the entered responses in a file. This file can then be used as an input file. The MD/MC-CEM force and potential energy evaluators provide performance in the range 50 to 60 million floating-point operations per second (MFLOPS) on a single processor of a Cray Y-MP. For comparison the single processor LINPACK rating for the Y-MP is 84 MFLOPS [34].

Setting up a System

SCT89 automates much of the effort necessary in setting up the system to be studied. In the simplest case a particular face of a metal can be setup by specifying only the symbol of the metal in standard chemical notation and the three Miller indices of the face. Internal databases are queried to determine values for quantities such atomic mass, Debye temperature, crystal type and lattice constant, as well as parameters used in setting up the interaction potentials. All of these default values can be overridden by the user. Given the Miller indices and the crystal type SCT89 determines the three-dimensional lattice vectors for the desired

face. Currently any face of a FCC, BCC, HCP or diamond crystal can be setup. The lattice vectors are used to create a slab of user-specified dimension. The number of layers in the slab and a set of min/max distances for each layer are specified by the user. The maximum distance determines the total width of each layer, while the minimum distance determines the width of each layer inside of which the atoms are allowed to move (i.e., are active). There are generally atoms in each layer which are fixed (i.e., inactive). One or more layers of adsorbates can be added by specifying the fractional coverage, the adsorption site and the adlayer structure via Wood's notation. For more complicated adlayer structures the initial position of each adsorbate atom can be specified by the user. The initial height of the gas above the surface and its initial azimuthal and polar angles are specified by the user. In most cases the initial (x,y) coordinates of the gas are picked randomly for each new trajectory so that the entire surface unit cell is sampled. The user can override this and specify the (x,y) coordinates directly.

Neighbor Lists

To make the calculation of the potential energy and interatomic forces more efficient for large systems, only the interactions between an atom and a set of its closest neighbors are evaluated. A list of all atoms within a sphere of a specified radius is compiled for each atom and used in the force and potential energy evaluators. The neighbor lists are constructed so that each pair of atoms is listed only once, i.e., if atom 2 appears in the neighbor list of atom 1, then atom 1 does not appear in the neighbor list of atom 2. If MD/MC-CEM is used for an interaction, all

associated neighbor list radii are setup automatically. For non MD/MC-CEM interactions a potential energy cutoff value for each interaction is specified by the user. The program then determines the distance at which the absolute value of the interaction energy between two atoms falls below the cutoff. That distance is then used as the neighbor list radius. When using MD/MC-CEM interactions each surface atom has ca. 60 surface atom neighbors.

Since the atoms are in motion it is necessary to update the neighbor lists periodically. At present all neighbor lists associated with the gas and/or adsorbates are updated after every integration step, while the surface-surface neighbor list is updated at user specified time intervals. Only the parts of the neighbor lists that change are updated; in particular, neighbor lists for fixed atoms interacting with other fixed atoms are never updated. (It is worthwhile to note that such interactions cannot be neglected in the MD/MC-CEM PES because of the many-body nature of the embedding energy.)

The reason for such a system is as follows. The gas and adsorbates are typically more mobile than the surface atoms and tend to move into the range of new neighbors quickly. If the surface temperature is far from the melting point and if the gas and/or adsorbates do not transfer large amounts of energy to the surface, the surface atoms will not move far from their equilibrium positions and the surface-surface neighbor lists will not need to be updated as often as for the more mobile components. In typical applications, there may be ten times as many surface atoms as adsorbate atoms, therefore the cost of evaluating the surface-surface neighbor list would dominate that of the adsorbate neighbor lists.

Outline of Execution

Initialization of gas atom(s)

For a single gas atom or the center of mass of a diatomic molecule the initial velocity vector is determined from user specified values for the initial gas kinetic energy, angle from the surface normal, and azimuthal angle. The initial height (z) above the surface is specified by the user while the initial (x,y) position is randomly sampled over the substrate (adsorbate if they are present) unit cell. Optionally, the initial (x,y) value may be specified for each trajectory. For a diatomic molecule, in addition to initializing the center-of-mass variables the internal variables need to be specified. This is done by entering the quantum numbers that specify the initial rotational-vibrational state of the molecule and sampling the conjugate momenta either classically or quasi-classically [35].

Initialization of adsorbate/surface atoms

The initial velocities of the surface and adsorbate atoms are sampled from a Maxwell-Boltzmann distribution for the specified temperature. The positions of the adsorbate and surface atoms are initialized using a molecular dynamics (MD) routine. The first step is to relax the atoms from their ideal bulk positions to an approximately equilibrium configuration for the desired temperature.

The clean surface is equilibrated before the addition of any adsorbate atoms. This ensures that energy liberated by the relaxation does not cause the ejection of any light adsorbates (e.g., with respect to the surface atoms) or weakly

bound adsorbates. The classical equations of motion are integrated for all atoms in the active zone. During equilibration **all** active atoms have local Langevin coupling applied to them. For non-zero temperature this process is allowed to continue until the fluctuation of the temperature falls below the limit from statistical mechanics of $T/N^{1/2}$. Here the temperature is calculated as, $T=<mv^2>/3k$. For T=0, the atoms are propagated until the temperature falls below some small cutoff $O(10^{-6})$. By using such a criteria, we assure that the T=0 relaxed positions correspond to a "stress free" crystal. If there are adsorbates the next step in the equilibration process is to adjust the height of the adsorbates above the surface until the potential energy is minimized, keeping the surface atoms in their previously relaxed positions. The adsorbates are left at this height to begin the next step of the equilibration process. The final stage of equilibration for an adsorbate covered surface is to repeat step one, but this time allowing both the adsorbate and surface atoms to move simultaneously. These equilibrium positions are used as the initial positions for each trajectory.

Trajectory propagation and termination

The classical equations of motion are integrated with the standard Verlet algorithm [36]. Each trajectory runs for a specified minimum time, after which the program begins to check for end-of-trajectory conditions. Generally these conditions depend on the status of the gas atom(s), but there is an option to simply end the trajectory after the minimum time is exceeded. Gas conditions which will end a trajectory are: 1) the gas scatters and moves upward out of the interaction range of

the surface while the lateral coordinates stay within the surface active zone; 2) the gas moves laterally out of the surface active zone while still inside the interaction range of the surface; 3) the gas fails to move one unit cell in twice the time that would be required if it was thermally equilibrated (e.g., twice the nearest neighbor distance divided by the average thermal speed); and, 4) the bond length of a diatomic molecule exceeds the gas-gas neighbor list distance.

Types of Output

The fundamental quantities determined by a MD simulation are the positions and velocities of all the particles in the system at every time step. For a simulation with 1000 atoms propagated for 1000 time steps this would correspond to six million numbers. Thus, decisions must be made about what kind and how much data should be saved from a simulation. In SCT89 an effort has been made to make the type and quantity of output flexible. Most output is processed and written from subroutines. In this way the main driver is simplified and adding different types of output consists of merely plugging in new modules.

The equilibrated positions of the adsorbates and surface atoms that are used as initial positions can be written out. The positions and velocities of the gas atom(s), can be written out as a function of the simulation time. In addition "snapshots" of the entire system or small pieces of it can be printed out in separate files as a function of time. Optionally, other quantities such as the kinetic and potential energy of the system, the surface temperature, and the gas-surface interaction energy can also be printed as a function of time.

Another option is to map out static cuts of the PES for the gas atom or diatomic molecule interacting with the adsorbate/surface system. For the atom-surface PES, the interaction energy is calculated as a function of height above the surface for each point on a user specified (x,y) grid. For the diatomic-surface PES, the gas CM is held over the surface at an user specified (x,y) point with an orientation determined by the two polar angles. The interaction energy is then calculated as a function of bond length and height above the surface. Optionally, the surface may be allowed to respond adiabatically (via Langevin dynamics) to the gas.

A dummy subroutine, ANALYSIS, is called at every integration step and contains all current atomic positions and velocities. The user may add any analysis to this function.

DESCRIPTION OF INPUT PARAMETERS

This section contains a detailed description of all SCT89 input parameters. Parameters appear here in the order in which they would be read by the program, however because of the diverse options available in SCT89 not all of these parameters will be used during a given program run. The units are generally eV for energies, Kelvin for temperature, Å for distance, 10^{-14} second for time, 10^{14} Hz for frequency and amu for mass. The only exceptions are some distances which for convenience are specified in terms of the lattice constant or the surface basis vectors; these are noted for the particular input parameter(s). The space-fixed cartesian coordinate system has the z-axis pointing along the surface normal into the vacuum and the x-axis pointing along the shorter surface basis vector. The SCT89 input parameters are:

Title (character string)

The first line is an illustrative title. If it begins with the prefix "mk" then the program enters an interactive mode in which all further input is prompted by the program with explanations of options in clear, concise English. All user responses are written to a file which can be used afterwards as input to the program.

Random number seed (integer)

This value of at least 6 digits initializes the random number generator.

Potential range cutoff (real number)

The longest range of any interaction in the system is used as an initial guess for setting up neighbor lists. It is later refined by the program so only a rough estimate is needed. If MD/MC-CEM interactions are used, this value is ignored.

Surface atom name (character string)

The exact chemical symbol for the surface atoms is used by the program to search an internal database for the mass of the lattice atoms, lattice Debye frequency, a-lattice constant, c-lattice constant and the crystal structure type. If the surface atom name is not found then these values must be entered. (Allowed structural types are cubic, face centered cubic, body centered cubic, hexagonal close packed, and diamond.)

Miller indices (integers)

Three Miller indices specify the surface crystal face. The surface basis vectors are calculated, not read from tabulated values, allowing arbitrarily high index surface faces.

Number of surface layers (integer)

This controls the number of layers of surface atoms to be used in the simulation. There are two variations: (1) a positive integer denotes the total number of active and fixed layers; (2) a negative integer tells the

program to determine the number of layers that constitute a repeating unit and to set up this integer magnitude of active units plus three fixed units.

$R_<$ and $R_>$ (real numbers)

These are in units of the length of the longer surface basis vector and define the side lengths of the square regions in each layer. Atoms within $R_<$ of the origin move while atoms outside of $R_<$ and inside $R_>$ are fixed. To force a fixed layer, set $R_< = 0$. If the number of layers is positive, $R_<$ and $R_>$ are required for each layer. If the number of layers is negative, only one $R_<$ and $R_>$ are required.

Fraction of first layer vacancies (real number)

If positive, the specified fraction of the first layer atoms are removed randomly. If negative, only the atom at (0,0,0) is removed.

Main surface motion switch (character string)

This controls overall surface motion, allowing for either a rigid surface, which overrides the active and fixed zones established by $R_<$ and $R_>$, or a non-rigid surface, which enables atoms within $R_<$ to move.

Edge atom force switch (character string)

Any atom in the active zone with at least one nearest-neighbor in the fixed zone is labelled as an edge or boundary atom. This switch specifies

whether to treat these edge atoms with a local Langevin technique, i.e., frictional plus random forces as in Eq.(4).

Surface-surface cutoff energy (real number)

The cutoff energy is used to set the surface atom-surface atom neighbor list radius. The value of the radius is the distance at which the magnitude of the interaction energy between two surface atoms falls below the cutoff energy. For MD/MC-CEM interactions, the radius is determined automatically and this input value is ignored.

Temperature ramping switch (character string)

This controls whether ramping of the surface temperature is allowed.

Surface temperature (real number)

For no temperature ramping, this specifies the surface temperature.

Temperature program (real numbers)

For temperature ramping, these are a set of three temperatures (T_0, T_1, T_2) and four time values (t_0, t_1, t_2, t_3) specifying the ramping program. The surface temperature, T, as a function of the elapsed simulation time, t, changes as:

A) $T=T_0$ $0 < t < t_0$

B) $T=T_0+(t-t_0)(T_1-T_0)/(t_1-t_0)$ $t_0 < t < t_1$

C) $T=T_1$ $t_1 < t < t_2$

D) $T=T_1+(t-t_2)(T_2-T_1)/(t_3-t_2)$ $t_2 < t < t_3$

E) $T=T_2$ $t_3 < t <$ stopping time.

Initialized position write switch (character string)

This switch controls whether to write the positions of the surface and adsorbate atoms after they have been initialized from their ideal positions. If initialization of these atoms is disabled and this switch is on, the ideal terminated bulk positions are written.

Number of gas atoms (integer)

One or two gas atoms can be treated at present. Propagation of the gas atom(s) can be disabled by entering -1 or -2. In this case, all further gas atom input is still read but the gas is fixed. This is very useful for the study of overlayer dynamics.

Gas atom name(s) (character string)

The exact chemical symbol for the gas atom(s) is used by the program to search an internal database to find all necessary parameters. If a gas atom name is not found the mass is read from the input file.

Initial height of gas (real numbers)

This initial location of the gas atom or the center of mass (CM) of a diatomic should exceed the range of the gas-surface and gas-adsorbate interactions.

Initial direction of gas (real numbers)

Two angles (in degrees) specify the direction of the initial velocity vector of the gas atom or diatomic CM. These two angles are Θ, the polar angle from the surface normal, and ϕ, the azimuthal angle from the x-axis.

Gas-gas cutoff energy (real number)

The cutoff energy is used to set the gas-gas neighbor list radius. The value of the radius is the distance at which the magnitude of the interaction energy between two gas atoms falls below the cutoff energy. For MD/MC-CEM interactions, the radius is determined automatically and this input value is ignored.

Gas-surface cutoff energy (real number)

The cutoff energy is used to set the gas-surface neighbor list radius. The value of the radius is the distance at which the magnitude of the interaction energy between a gas and surface atom falls below the cutoff energy. For MD/MC-CEM interactions, the radius is determined automatically and this input value is ignored.

Main adsorbate control switch (character string)

This controls whether to enable the presence of adsorbates. If adsorbates are disabled no further adsorbate input is required.

Adsorbate atom name (character string)

The exact chemical symbol for the adsorbate atom is used by the program to search an internal database for all necessary parameters. If the adsorbate atom name is not found the mass is read from the input file.

Adsorption site position vector (real numbers)

Two values specify the components of a vector, in the substrate basis, pointing from (0,0) to the desired adsorption site.

Wood's notation parameters (real numbers)

Three values define the adlayer pattern in terms of the substrate basis vectors. The first two are the ratio of the length of the adsorbate basis to the length of the surface basis for each basis vector. The third is the rotation angle (in degrees) of the adsorbate vectors relative to the x-axis.

Fractional coverage (real number)

The filling of the adlayer can be specified three ways: (i) values in [0,1] cause random filling of a single adsorbate layer in the specified pattern up to the entered value for the fractional coverage. If the desired fractional

coverage is greater than the saturation coverage of the pattern, the program saturates the pattern but does not fill past saturation; (ii) values >1 create multiple layers in a (1x1) pattern. The integer portion of the entered value is the number of fully filled layers while the fractional portion is used, as in (i), to fill the specified pattern on top of the last (1x1) layer; (iii) negative values require input of the number and (x,y,z) coordinates of each adsorbate atom, with the latter in units of the surface lattice constant.

Adsorbate motion switch (character string)

This controls overall adsorbate motion, allowing for either a rigid adsorbate, which overrides the active and fixed zones established by $R_<$ and $R_>$, or a non-rigid surface, which enables atoms within $R_<$ to move.

Adsorbate position write switch (character string)

This switch controls whether to write the positions of all active adsorbates at user specified time intervals.

Adsorbate coverage write switch (character string)

This switch controls whether to write the fractional coverage of the active adsorbates at user specified intervals. For multiple trajectory runs, the coverage at each time is averaged over trajectories and this average curve is written out at the end of the run.

Adsorbate cutoff energies (real numbers)

These cutoff energies are used to set the adsorbate-adsorbate, adsorbate-surface, and adsorbate-gas neighbor list radii. The value of each radius is the distance at which the magnitude of the interaction energy between a pair of atoms falls below the cutoff energy. For MD/MC-CEM interactions, the radius is determined automatically and this input value is ignored.

System initialization switch (character string)

There are two options for initialization of the adsorbate/surface system: (1) MD method; and (2) No initialization (i.e., use a perfectly terminated solid).

Main CEM control switches (character strings)

A switch is read in for each component of the system (gas, surface, and adsorbate) to determine whether or not to use MD/MC-CEM. There is a hierarchy of interactions when CEM is enabled. At the lowest level CEM can be used only to treat surface-surface interactions. If CEM is enabled for adsorbate-adsorbate interactions, then it must also be used for adsorbate-surface and surface-surface interactions. If CEM is enabled for gas interactions then CEM must also be used for all adsorbate and surface interactions.

CEM embedding function types (character strings)

If MD/MC-CEM is enabled for a component, the PES is completely determined by specifying the embedding function for that component. There are two options: 1) Embedding function from LMTO calculations on the bulk solid, i.e., $\Delta F_J = \Delta F_{LMTO}$ in Eq.(6), which are included for the FCC metals Al, Ni, Cu, Rh, Pd, Ag, Pt, and Au; 2) Auxiliary user-supplied embedding function which is found in the file embed.aux. For an auxiliary embedding function, the name of the embedding function must be read (as it appears in the file embed.aux).

Non-MD/MC-CEM PES parameters

For non-MD/MC-CEM interactions, a variety of empirical forms are available. The following is a list of the switches and parameters which control these.

Surface atom density type (character string)

Some parts of V_{SG} and V_{SA} are functions of the electron density due to the surface atoms, e.g., Eq.(9). There are two options for specification of this electron density: (1) densities fit to Hartree-Fock outer shells; (2) full Hartree-Fock densities.

Valence occupation numbers (real numbers)

When using the density fit to Hartree-Fock outer shells these two values specify the occupation of the outermost S and D orbitals.

Surface-surface interaction form (character string)

There are three options for surface-surface interactions: (1) Morse potential fit to lattice constant, Debye temperature, and heat of formation [7],

$$V_{SS} = D_{SS}\{\exp[-2\alpha_{SS}(R-R_{SS})]-2C_{SS}\exp[-\alpha_{SS}(R-R_{SS})]\} ; \quad (15)$$

(2) Lennard-Jones potential fit to lattice constant and heat of formation [5],

$$V_{SS} = D_{SS}\{(R_{SS}/R)^{12}-2C_{SS}(R_{SS}/R)^{6}\} ; \quad (16)$$

(3) Lennard-Jones potential fit to lattice constant and Debye temperature with the same form as above [26d].

Surface-surface potential parameters (real numbers)

If tabulated values for the parameters of the above forms are not found the program reads the parameters (D_{SS}, α_{SS}, R_{SS}, C_{SS}) for the Morse or (D_{SS}, R_{SS}, C_{SS}) for the LJ form.

Gas-surface embedding energy fit (character string)

Part of the surface-gas PES is the homogeneous embedding energy which is fit to the Morse potential-like form [29]:

$$\Delta E_J(\rho) = D_H\{\exp[-2\alpha_H(R_s-R_H)]-2C_H\exp[-\alpha_H(R_s-R_H)]\} \qquad (16a)$$

where

$$R_s = (4\pi\rho/3)^{-1/3} . \qquad (16b)$$

Four options to supply (D_H, α_H, R_H, C_H) are: (1) direct read; (2) values from internal database; (3) fit to ΔE_C from MD/MC-CEM; (4) fit to ΔE_P.

Gas-surface embedding parameters (real numbers)

(D_H, α_H, R_H, C_H) are read if this is selected or if tabulated values cannot be found. These are stored for each type of gas atom.

Atom-surface two-body interaction form (character string)

There are four options for a single gas atom interacting with a surface: (1) Morse potential fit to lattice constant, Debye temperature, and heat of formation [7], Eq.(15); (2) Lennard-Jones potential fit to lattice constant and heat of formation [5], Eq.(16); (3) Lennard-Jones potential fit to lattice constant and Debye temperature [26d], Eq.(16); (4) User-defined atom-surface interaction potential which assumes that the user supplied function is a completely self-contained module. Selecting option (4) causes the program to ignore the previously

specified embedding energy term. Options "1-3" are useful in the study of homogeneous epitaxial growth processes.

Atom-surface two-body interaction parameters (real numbers)

Tabulated values for the parameters of the above forms are found for metallic atoms colliding with metallic substrates of the same chemical type. When tabulated values are not found, the program reads the parameters (D_{SG}, α_{SG}, R_{SG}, C_{SG}) for the Morse or (D_{SG}, R_{SG}, C_{SG}) for the LJ form.

Diatomic-surface interaction form (character string)

There are two options for the diatomic-surface interaction: (1) LEPS 4-body potential [29]; (2) user-defined diatomic-surface interaction potential which assumes that the user supplied function is a completely self-contained module. Selecting this option causes the program to ignore the previously specified embedding energy term.

Diatom-surface two-body interaction parameters (real numbers)

Values of (D_{SG}, α_{SG}, R_{SG}, C_{SG}) for the Morse form are specified for each gas atom.

Sato parameters (real numbers)

Three parameters on the range [-1,1] determine the relative strengths of the bonding and anti-bonding curves within the LEPS formalism. This controls the size and location of the barriers to reaction. The parameters are $\Delta_{G,G}$, $\Delta_{S,G(1)}$ and $\Delta_{S,G(2)}$ which are the Sato parameters for the relevant interactions.

Gas-gas two-body interaction parameters (real numbers)

Values of (D_{GG}, α_{GG}, R_{GG}, C_{GG}) for the Morse form are specified for the interaction between the two gas atoms.

Initial state of the diatomic (integers)

The first two parameters specify the initial vibrational and rotational state of the diatomic molecule. The third is a switch to indicate whether to use classical or quasi-classical (i.e., including zero point energy) vibrational energy.

Adsorbate-adsorbate two-body interaction parameters (real numbers)

Values of (D_{AA}, α_{AA}, R_{AA}, C_{AA}) are specified for the adsorbate-adsorbate Morse potential.

Adsorbate-surface embedding energy fit (character string)

Part of the surface-adsorbate PES is the homogeneous embedding energy which is fit to the Morse potential-like form in Eq.(16). Four options to supply (D_H, α_H, R_H, C_H) are: (1) direct read; (2) values from internal database; (3) fit to ΔE_C from MD/MC-CEM; (4) fit to ΔE_P.

Adsorbate-surface embedding parameters (real numbers)

(D_H, α_H, R_H, C_H) are read if this is selected or if tabulated values cannot be found. These are stored for each type of atom.

Adsorbate-surface two-body interaction parameters (real numbers)

Values for the parameters (D_{SA}, α_{SA}, R_{SA}, C_{SA}) for the Morse form are read.

Gas-adsorbate two-body interaction parameters (real numbers)

Values for the parameters (D_{AG}, α_{AG}, R_{AG}, C_{AG}) for the Morse form are read.

THIS IS THE END OF THE NON-CEM PES PARAMETERS.

Surface-surface neighbor list update time (real number)

The neighbor list for active surface atoms is updated every time interval of T_{LSSS}. Evaluation is a time consuming process so care should be used to

specify as large a value as acceptable. This number should be set to >1000 for low energy collisions, and only if surface damage (i.e., ejection or vacancies) is expected should a small number be used. The program chooses a reasonable value if a negative number is entered.

Trajectory control parameters (real numbers)

Three parameters control the trajectory propagation: (1) estimated height of closest approach which is used to shift the starting (x,y) coordinates of the gas CM to ensure a "hit" in the center of the cell; (2) elapsed time to start checking for the end of a trajectory which is also the minimum time a trajectory will run; (3) integration time step.

Trajectory end switch (character string)

There are two options to end a trajectory: (1) run-time only, in which a trajectory ends when the run-time exceeds the specified limit; (2) run-time and gas conditions, in which after the run-time exceeds the specified limit, the program begins checking the condition of the gas atom(s) to see if an ending condition has been fulfilled.

Gas kinetic energy ramp parameters (two real numbers and one integer)

Three values specify the minimum and maximum translational energies and the number of steps between these. This allows performance of calculations at multiple energies in the same run.

Number of trajectories (integer)

This is the number of trajectories to run for each gas kinetic energy. If negative, the absolute value of the entered number is used and the (X,Y) aiming point of each trajectory (in units of the substrate basis) must be specified.

Standard output type switch (character string)

At user-specified time intervals the program writes out information about the status of the current trajectory. This switch controls what quantities are to be written, with three options: (1) full output consists of the elapsed trajectory time, position and velocity of the gas atom(s), kinetic and potential energy of the gas, temperature of the surface and adsorbates, and total kinetic and potential energy of the system; (2) compact output consists of the elapsed trajectory time, position and velocity of the gas atom(s), and kinetic and potential energy of the gas; (3) very compact output consists of the position and velocity of the gas CM. Full and compact trajectory output automatically print out the initial and final conditions as well as the conditions at the turning point of the gas. Very compact output will not print out initial and turning point conditions, but will print the final conditions as well as any times enabled by the print out interval specified below.

Print out time interval (real number)

This specifies how often to write out the trajectory status as well as all other quantities which are written as a function of time. A very small value will yield a great amount of output, while a large value will print rarely. To investigate the behavior around the turning point, you must use a small number and then throw away the vast majority of output describing the initial and final uninteresting trajectory data.

PES print out switch (character string)

This controls whether to map out the gas-adsorbate/surface PES instead of doing the dynamics. If enabled, the program calculates the interaction between the gas and the adsorbate/surface system as a function of (x,y,z) (z is the surface normal) over a user specified (x,y) grid. As an option, the surface can be allowed to respond via damped MD to the approaching gas. There are three choices: (1) the atom-surface PES is written as a function of the location in the unit cell and the height with the zero of energy being the separated atom and surface; (2) the diatom-surface PES is written as a function of the height above the surface and the bond length with the zero of energy being the isolated diatomic at its equilibrium bond length and surface; (3) the surface-mediated diatomic interaction is written as a function of the height above the surface and the bond length. The zero of energy, which is recalculated at each different value of the height above the surface, is the separated atoms of the diatomic interacting with the solid.

PES surface response switch (character string)

This determines whether to allow the surface to respond adiabatically to the approaching gas.

Atom-surface PES options (real numbers)

Three parameters control the (x,y) grid and the surface response, if enabled: (1) grid size in units of the lattice constant; (2) fraction of the side to map; (3) maximum surface relaxation time at every step.

Diatomic-surface PES options (real numbers)

Five parameters control: (1) the (x,y) position of the gas CM in units of the surface basis vectors; (2) the angles (in degrees) between the diatomic axis and the z-axis and the projection of the diatomic axis onto the surface and the x-axis; (3) the maximum surface relaxation time at every step.

Surface mediated diatomic PES options (real numbers)

Five parameters control: (1) the (x,y) position of the first gas atom in units of the surface basis vectors; (2) the angles (in degrees) between the diatomic axis and the z-axis and the projection of the diatomic axis onto the surface and the x-axis; (3) the maximum surface relaxation time at every step.

Visualization output switch (character string)

This controls whether to write out atomic positions in a form suitable for input to visualization software. The format of this output is one line per atom listing the chemical symbol of the atom and the components of its position vector. In addition, any two atoms which are less than a user specified distance apart are considered to bonded. This bonding information is saved along with the atomic positions. If enabled, the number of trajectories is forced to be one and several additional parameters are necessary.

File name prefix (character string)

The visualization output is written to a series of external files with the extension "mol". The file names consist of this prefix with the value of the simulation time appended.

Molecular modelling parameters (two real numbers and one integer)

There two ways to initialize the trajectory used for visualization:
(1) specify the aiming point of either the gas atom or gas molecule CM;
(2) specify the random number seed for a previously run trajectory. A single line of input containing two real numbers and one integer is read by the program. If the value of the integer parameter is greater than zero the program uses it as the random number seed to start the trajectory. In this case the two real parameters are ignored. If the integer parameter is

negative the two real parameters are assumed to be the (x,y) aiming point of the gas in units of the substrate basis.

Origin of plot region (real numbers)

These specify the origin of the simulation cell which is to be used in the modelling, in units of the substrate basis vectors.

Depth of plot region (real number)

This specifies the depth of the region of the simulation cell which is to be used in the modelling, in units of the ideal interlayer spacing.

Surface cutoff distance (real number)

This specifies the maximum distance from the origin of the region of the simulation cell which is to be used in the modelling, in units of nearest-neighbor distance .

Bond length scale factor (real number)

This specifies the fraction of the nearest-neighbor distance, inside of which two atoms should be considered bonded, and have bonds drawn.

SAMPLE INPUT FILES

To demonstrate the versatility and the ease of use of SCT89, three sample input files are reproduced in Tables 1-3. These files result directly from the special interactive mode mentioned in the beginning of the previous section under titles. This is extremely useful since each input file varies greatly due to the wide variety of available options in SCT89. The brief documentation on the right-hand-side of the tables helps in making small changes to any one type of input file.

Table 1 contains an input file for the scattering of Ar from a H covered Pd(111) surface. The surface is modelled by three active layers and three fixed layers, with the former having a shell of fixed atoms with a width of three nearest-neighbor distances. The adsorbates are located in 3-fold sites in a p(1x1) layer. The temperature of the adsorbate/surface system is maintained at 100 K by local Langevin coupling. The Ar is incident with 1 eV of initial kinetic energy at 45^0 from the normal along an azimuth of 30^0 from the x-axis. Since MD/MC-CEM is used for all interactions, the cutoff energies are ignored. The embedding functions are specified as the LMTO embedding function, $\Delta F_{LMTO}(Pd)$; the function, $\Delta F_P(H)$, in the auxiliary embedding file and which duplicates full CEM calculations of the H adsorption onto Pd(111); and the function, $\Delta F_C(Ar)$, in the auxiliary embedding file which duplicates the bulk and diatomic potential data with the latter from work of Aziz and Salamon [37]. The surface-surface reset time is large because the gas-surface collision is not expected to cause significant distortion of the substrate atoms. The specified type of output gives only the final kinetic energy and velocity

Table 1. Sample input file #1
Ar scattering from (1x1)H/Pd(111).

Ar/H/Pd(111) T=100K	
4223421	Random Number Seed
0.100000E+02	Longest PES Range
Pd	
1 1 1	Miller Indices
6	Num. Surface Layers
0.500000E+01 0.800000E+01	R< and R>
0.500000E+01 0.800000E+01	R< and R>
0.500000E+01 0.800000E+01	R< and R>
0.000000E+00 0.800000E+01	R< and R>
0.000000E+00 0.800000E+01	R< and R>
0.000000E+00 0.800000E+01	R< and R>
0.000000E+00	Frac. 1st L Vacancy
Non-Rigid surface	
Langevin Dynamics for secondary atoms	
0.100000E-01	Cutoff E For S-S PES
No-Ramping of the temperature.	
0.100000E+03	Surface Temperature
No-Write initial positions of surface atoms	
1	Num. of Gas Atoms

Table 1. (continued)

Ar	
0.100000E+02	Init. Height of Gas
0.450000E+02 0.300000E+02	Init. Gas Theta, Phi
0.100000E-02	Cutoff E for G-S PES
Adsorbates are present	
H	
0.666667E+00 0.666667E+00	Origin of Adlayer
0.100000E+01 0.100000E+01 0.000000E+00	Woods Notation Vals
0.100000E+01	Fract Cov of Adlayer
Non-Rigid adsorbates	
No-Write positions of adsorbates	
No-Write adsorbate coverage	
0.100000E-01 0.100000E-01	cutoff E for A-A,A-S
0.100000E-02	cutoff E for G-A PES
D=Mol. Dyn. initialization of S+A	
CEM as MD/MC-CEM for surface atoms	
CEM as MD/MC-CEM for adsorbate atoms	
CEM as MD/MC-CEM for gas atoms	
LMTO Double Embedding Ehom for Surface	
Auxiliary embedding Ehom for Adsorbate	
HPd bulk+puska Ecorr0	

Table 1. (continued)

Auxiliary embedding Ehom for Gas			
Ar bulk+AS Ecorr0			
0.100000E+03			reset time for S-S
0.250000E+01	0.100000E+02	0.400000E+00	Est. T.P., Tmax, DT
Gas condition and timer trajectory stop			
0.100000E+01	0.100000E+01	1	Eg<, Eg>,#ofK.E.stp
1000			num. of trajectories
Very compact output for trajectory			
0.100000E+04			trajectory write int
No PES mapping Enabled			
No graphics output written			

vector of the Ar atom. This file is typical of a large scale production run with 1000 trajectories.

Note that it is a trivial matter to change the initial angles and kinetic energy of the gas as well as properties of the adsorbate/surface system such as crystal face, number of layers, temperature, and adlayer coverage and pattern. For example, a convenient way to run on an adsorbate free surface is to specify the fractional coverage as zero. Integration controls such as neighbor list resetting time, time step, and maximum run time can also be changed easily. For all these changes, one could simply edit the input file without reverting to the special interactive mode.

In Table 2, input for the collision of an Ar atom with the Pt(557) surface is shown. This file demonstrates the use of SCT89 to generate a potential energy map. It also shows the combination of MD/MC-CEM and non MD/MC-CEM interactions. Here only the surface-surface interactions are treated via MD/MC-CEM theory and the Ar-surface embedding interaction is treated with a Morse-like potential, Eq.(16), with parameters read from an internal database (D_H = 60 meV, α_H = 0.80 $Å^{-1}$, R_H = 6.2 Å, and C_H = 1.0). The Ar-surface two-body interaction is turned off by setting D_{SG} = 0. The Ar-surface PES is mapped out by specifying what fraction of the unit cell to map, the grid size, and whether to relax the surface before each potential calculation. In this case, the grid size is 0.1 lattice constant; one full unit cell is mapped out; and the surface is allowed to respond for $10x10^{-14}$ second before each potential energy evaluation. At each grid point (x,y) the gas is moved towards the surface in 0.2 Å increments. The program stops after the full PES is calculated and

Table 2. Sample input file #2
Mapping the PES for Ar on Pt(557).

Ar/Pt(557) T=500K	
634345	Random Number Seed
0.100000E+02	Longest PES Range
Pt	
5 5 7	Miller Indices
-2	Num. Surface Layers
0.100000E+01 0.150000E+01	R< and R>
0.000000E+00	Frac. 1st L Vacancy
Non-Rigid surface	
Langevin Dynamics for secondary atoms	
0.100000E-01	Cutoff E For S-S PES
No-Ramping of the temperature.	
0.500000E+03	Surface Temperature
No-Write initial positions of surface atoms	
1	Num. of Gas Atoms
Ar	
0.100000E+02	Init. Height of Gas
0.600000E+02 0.900000E+02	Init. Gas Theta, Phi
0.100000E-02	Cutoff E for G-S PES
No-Adsorbates are present	

Table 2. (continued)

D=Mol. Dyn. initialization of S+A	
CEM as MD/MC-CEM for surface atoms	
No-CEM for gas atoms	
HF surface atom densities used	
Fitted Ehom parameters for gas	
Morse potential for G-S	
0.000E+00 0.000E+00 0.000E+00 0.100E+01	Dgs,Algs,Rgs,CgsLR
LMTO Double Embedding Ehom for Surface	
0.500000E+01	reset time for S-S
0.250000E+01 0.100000E+02 0.200000E+00	Est. T.P., Tmax, DT
Gas condition and timer trajectory stop	
0.150000E+01 0.150000E+01 1	Eg<, Eg>,#ofK.E.stp
10	num. of trajectories
Full output for trajectory	
0.500000E+01	trajectory write int
Atom-Surface PES mapping Enabled	
Relaxed surface in PES	
0.100000E+00 0.100000E+01 0.100000E+02	GrdSz,Fracmap,reltim
No graphics output written	

before any trajectories are run. The Pt(557) surface consists of close-packed (111) terraces separated by single atom high steps. SCT89 always constructs surfaces with the z-axis parallel to the true surface normal **not** the normal of a terrace plane. In this coordinate system the interlayer spacing (along the z-axis) becomes smaller as the Miller indices increase. For this reason it takes several layers of atoms to form a complete surface. Specifying "-2" layers tells the program to estimate how many layers are necessary to form a surface and then create a slab with 2 times that many active layers plus 3 times that many layers of fixed atoms. For the Pt(557) surface the program estimates that it takes 8 layers to form a repeating unit. Therefore the "-2" option causes the creation of 16 active layers and 24 fixed layers.

Table 3 shows the input for N_2 scattering on a clean W(110) surface. This example demonstrates the use of SCT89 with non MD/MC-CEM potential energy forms. The surface-surface potential is specified to be a Lennard-Jones (12,6) with parameters chosen to reproduce the lattice constant and heat of formation [5] of W (D_{SS} = 1.07 eV, R_{SS} = 2.56 Å). The gas-surface potential is of the LEPS form with the parameters corresponding to those of DePristo and Kara. The N_2 molecule is started in its rotational-vibrational ground state with zero point vibrational energy added. The initial molecule CM kinetic energy is ramped from 0.1 to 1.0 eV in steps of 0.1 eV. A run such as this would be used to determine dissociation probabilities as a function of initial kinetic energy.

Table 3. Sample input file #3
Scattering of N_2 from W(110).

N2/W(110) T=800K	
8353451	Random Number Seed
0.100000E+02	Longest PES Range
W	
1 1 0	Miller Indices
6	Num. Surface Layers
0.300000E+01 0.600000E+01	R< and R>
0.300000E+01 0.600000E+01	R< and R>
0.300000E+01 0.600000E+01	R< and R>
0.000000E+00 0.600000E+01	R< and R>
0.000000E+00 0.600000E+01	R< and R>
0.000000E+00 0.600000E+01	R< and R>
0.000000E+00	Frac. 1st L Vacancy
Non-Rigid surface	
Langevin Dynamics for secondary atoms	
0.100000E-01	Cutoff E For S-S PES
No-Ramping of the temperature.	
0.800000E+03	Surface Temperature
No-Write initial positions of surface atoms	

Table 3. (continued)

2	Num. of Gas Atoms
N	
N	
0.100000E+02	Init. Height of Gas
0.000000E+00 0.000000E+00	Init. Gas Theta, Phi
0.100000E-02	Cutoff E for G-G PES
0.100000E-02	Cutoff E for G-S PES
No-Adsorbates are present	
D=Mol. Dyn. initialization of S+A	
No-CEM for surface atoms	
No-CEM for gas atoms	
HF surface atom densities used	
H(form) and lat. const. fit for LJ(12,6)	
Read of Deff, Aeff, Reff for gas	
0.14E+01 0.149171E+01 0.198838E+01 1.0	deff,aeff,reff,ceflr
Read of Deff, Aeff, Reff for gas	
0.14E+01 0.149171E+01 0.198838E+01 1.0	deff,aeff,reff,ceflr
LEPS 4-body PES for molecule-surface	
0.678E+01 0.2059E+01 0.1245E+01 0.1E+01	Dgs,Algs,Rgs,CgsLR
0.678E+01 0.2059E+01 0.1245E+01 0.1E+01	Dgs,Algs,Rgs,CgsLR
-0.369E+00 0.241E+00 0.241E+00	Satos GG, G1S, G2S

Table 3. (continued)

0.990000E+01	0.268400E+01	0.109000E+01	Dgg,Algg,Rgg
0	0	0	Nin,Jin,Icls
0.100000E+02			reset time for S-S
0.200000E+01	0.200000E+02	0.200000E-01	Est. T.P., Tmax, DT
Gas condition and timer trajectory stop			
0.100000E-01	0.100000E+00	10	Eg<, Eg>,#ofK.E.stp
500			num. of trajectories
Compact output for trajectory			
0.100000E+02			trajectory write int
No PES mapping Enabled			
No graphics output written			

SAMPLE CODE AND TIMINGS

Reproduced in Tables 4 and 5 are two loops from the MD/MC-CEM interatomic force evaluator which, along with the routine to evaluate neighbor lists, Table 6, account for upwards of 95 % of the time required for trajectory propagation. In these applications, **nyfc**, the number of active surface atoms, is ca. 300 and **nnsss(i)**, the number of surface atom neighbors of surface atom "i", is ca. 60 and is always less than 128. This ensures that each loop can be completed in at most two vector cycles. The matrix element **dsqinvss(n,i)** which appears in all three loops is the inverse of the square distance between atoms "i" and its "n^{th}" neighbor. This matrix needs to be updated after each propagation step. Evaluation can take place in one of three routines: 1) in the force evaluator; 2) in the potential energy evaluator; 3) in the neighbor list evaluator. A set of switches passed between these routines ensures that **dsqinvss** is evaluated only once per propagation step.

The code in Table 4 (referred to as loop 1) evaluates the overlap of atomic electron densities between atoms and their neighbors. Note the use of piece-wise cubic polynomials to evaluate the overlap integral, **sumij**, between each pair of atoms as a function of their separation. The total electron density overlap of atom "i" is accumulated in the vector **dhhf**. Owning to the sophistication of the cft77 compiler there is no need to perform the summation of **dhhf** explicitly outside the loop in order to achieve vectorization. It is however, necessary to use a compiler directive to force vectorization, since the compiler cannot determine whether the values of **ic** and **jc** are independent prior to program execution. The coefficient

Table 4. Computation of electron density overlaps between surface atoms using a piece-wise cubic polynomial
This is part of the MD/MC-CEM force evaluation with the Fortran code shown in upper case.

Loop over the number of active surface atoms, nyfc.

```
      DO 190 I=1,NYFC
```

The array element itype(i) specifies the chemical identity of atom "i". The atoms of the system are listed in itype in the order gas, adsorbate, surface. This ordering means that the first gas atom is also the first atom in itype, the index of the first adsorbate atom is the number of gas atoms, ngas, plus one, and the index of the first surface atom is the number of gas and adsorbate atoms, ngasnads, plus one.

```
      IC=NGASNADS+I
      ITI=ITYPE(IC)
```

CDIR$ specifies a command for the Cray Fortran compiler (cft77); In this case telling it to ignore any vector dependencies (IVDEP) within the 180 loop.

```
CDIR$ IVDEP
```

Loop over the neighbors of atom "i" as specified by a neighbor list. The array element nnsss(i) is the number of surface atom neighbors (both active and fixed) of surface atom "i".

```
      DO 180 N=1,NNSSS(I)
```

Table 4. (continued)

Determine the identity of the "n^{th}" neighbor atom. The matrix element nnss(n,i) is the index of the "n^{th}" surface atom neighbor of surface atom "i".

```
      JC=NGASNADS+NNSS(N,I)
      ITJ=ITYPE(JC)
```

Determine the appropriate interaction to use. Given the chemical identity of both interacting atoms (the values of iti and itj) the matrix element ipair(iti,itj) specifies the set of cubic polynomial coefficients that describe the electron density overlaps of the two atoms.

```
      ITIITJ=IPAIR(ITI,ITJ)
```

Determine the index for the appropriate radial interval. The knots of the line are evenly spaced in 1/R**2 (where R is the distance between the two atoms). Therefore, given the value of 1/R**2, rijsqinv, the index of the appropriate radial interval can be determined analytically. Since the value of 1/R**2 is used several times during the evaluation of the forces and potential it is calculated once and stored in the matrix element dsqinvss(n,i).

```
      RIJSQINV=DSQINVSS(N,I)
```

This expression calculates the index and makes sure that it is in the proper range, [0,nsp]. Here nsp is the number of radial intervals; xs(m,itiitj) is the "x-value" of the m^{th} interval of coefficient set itiitj; and sincinv(itiitj) is the "x-spacing" of coefficient set itiitj.

```
      K=MIN( MAX1(ONE + (RIJSQINV - XS(1,ITIITJ)) *
     &    SINCINV(ITIITJ) ,ZERO ), NSP)
```

Table 4. (continued)

Since this index is used again later it is stored in the matrix element kndexss(n,i).

```
            KNDEXSS(N,I)=K
```

Calculate the local "x-variable". The Fortran intrinsic function dim(arg1,arg2) returns the difference arg1-arg2 if arg1>arg2 and zero if arg1<arg2. This ensures that if the separation of two atoms exceeds the range of the polynomial there will be no anomalous behavior.

```
            D=DIM(RIJSQINV,XS(K,ITIITJ))
```

Calculate the density overlap, sumij, between the two atoms using a cubic polynomial. The 3-dimensional array cmats stores all of the overlap coefficients while the knots are stored in the matrix yss.

```
            SUMIJ=( ( CMATS(K,3,ITIITJ)*D + CMATS(K,2,ITIITJ) )*D
     &      + CMATS(K,1,ITIITJ) )*D + YSS(K,ITIITJ)
```

Accumulate the total overlap for each atom in the array dhhf. Since the overlap is only a function of radial distance it is possible to add the contributions to both atoms simultaneously. Note: the neighbor list is defined so that there will be no double counting and the value of "ic" can never equal the value of "jc".

```
            DHHF(IC)=DHHF(IC)+SUMIJ
            DHHF(JC)=DHHF(JC)+SUMIJ
        180 CONTINUE
        190 CONTINUE
```

Table 5. Computation of interatomic forces between surface atoms using a piece-wise cubic polynomial
This is part of the MD/MC-CEM force evaluation with the Fortran code shown in upper case.

```
      DO 290 I=1,NYFC
      IC=NGASNADS+I
      ITI=ITYPE(IC)
CDIR$ IVDEP
      DO 280 N=1,NNSSS(I)
      J=NNSS(N,I)
      JC=NGASNADS+J
      ITJ=ITYPE(JC)
      ITIITJ=IPAIR(ITI,ITJ)
      RIJSQINV=DSQINVSS(N,I)
```

Retrieve the interval index which is stored in the matrix element kndexss(n,i).

```
      K=KNDEXSS(N,I)
      D=DIM(RIJSQINV,XS(K,ITIITJ))
```

Calculate the magnitude of the force, fcij, between the two atoms using a cubic polynomial. The 3-dimensional array dcmats stores all of the overlap coefficients while the 3-dimensional array dcmatc stores all of the Coulomb coefficients. Note: the matrix element dcmatc(_,M,_) is -M*cmatc(_,M,_) and the matrix element dcmats(_,M,_) is -M*cmats(_,M,_). The array dehomdn contains the derivative of the homogeneous embedding energy with respect to the electron density.

Table 5. (continued)

```
      FCIJ=( ( ( DCMATC(K,3,ITIITJ)*D + DCMATC(K,2,ITIITJ) )*D
     &   + DCMATC(K,1,ITIITJ) )
     &   + ( ( DCMATS(K,3,ITIITJ)*D + DCMATS(K,2,ITIITJ) )*D
     &   + DCMATS(K,1,ITIITJ) )*(DEHOMDN(IC)+DEHOMDN(JC))
     &   )*RIJSQINV**2
```

Calculate the vector components of the force on atom "i" due to atom "j". The matrix element ynow(p,q) contains the p^{th} component (p=1,3) of the q^{th} surface atom.

```
      F1IJ=(YNOW(1,I)-YNOW(1,J))*FCIJ
      F2IJ=(YNOW(2,I)-YNOW(2,J))*FCIJ
      F3IJ=(YNOW(3,I)-YNOW(3,J))*FCIJ
```

Accumulate the total force on each atom in the matrix frcs. Since the magnitude of the force is only a function of radial distance it is possible to add the contributions to both atoms simultaneously. Note: the neighbor list is defined so that there will be no double counting and the value of "i" can never equal the value of "j".

```
      FRCS(1,I)= F1IJ + FRCS(1,I)
      FRCS(2,I)= F2IJ + FRCS(2,I)
      FRCS(3,I)= F3IJ + FRCS(3,I)
      FRCS(1,J)=-F1IJ + FRCS(1,J)
      FRCS(2,J)=-F2IJ + FRCS(2,J)
      FRCS(3,J)=-F3IJ + FRCS(3,J)
  280 CONTINUE
  290 CONTINUE
```

Table 6. Evaluation of the neighbor lists for active surface atoms with all (active and fixed) surface atoms
The actual Fortran code is shown in upper case.

Set switch to tell force and/or potential that the dsqinvss matrix has been updated. Since the square distance between all pairs of atoms must be evaluated to determine the neighbor lists some work can be saved in the force and potential evaluators by loading the dsqinvss matrix in this module. The switch inlstss is used to tell the force and/or potential evaluators whether or not they need to calculate dsqinvss. A value of 1 for inlstss instructes the force and/or potential evaluators that dsqinvss has been updated. When the atoms are propagated, inlstss is set to 0 and unless this module is called before the next trip into the force and/or potential evaluators they will update dsqinvss themselves.

```
      INLSTSS=1
```

Loop over the number of active surface atoms, nyfc.

```
      DO 100 I=1,NYFC
```

Calculate the square distance between all pairs of surface atoms. The 110 loop is only over atoms with index greater than "i", thereby ensuring that each pair of atoms is counted only once. The neighbor list for an active surface atom can include both active and fixed surface atoms, therefore the upper limit of the 110 loop is the total number of surface atoms, ntat. The matrix element ynow(p,q) contains the p^{th} component (p=1,3) of the q^{th} surface atom.

```
      DO 110 J=I+1,NTAT
      DIS2(J)=(YNOW(1,I)-YNOW(1,J))**2+
     &  (YNOW(2,I)-YNOW(2,J))**2+
```

Table 6. (continued)

```
     &    (YNOW(3,I)-YNOW(3,J))**2
     110  CONTINUE
```

The neighbors of atom "i" can now be determined by finding which elements of the array dis2 are less than or equal to the square of the neighbor list cutoff distance, dis2mx. There is Cray library module, whenfle, that will perform this operation [38].

```
     CALL WHENFLE(NTAT-I,DIS2(I+1),1,DIS2MX,NNB,NNSSS(I))
```

The output from whenfle consists of the number of elements less than or equal to dis2mx, nnsss(i) (the number of neighbors of atom "i"), and the indices of these elements, the vector nnb. When running on machines other than the Cray, a Fortran subroutine which mimics whenfle is added to SCT89.

All that remains to be done is to transfer the elements of nnb to the neighbor index matrix, nnss. The matrix element nnss(p,q) is the index of the p^{th} neighbor of atom "q". Also, the dsqinvss matrix is loaded using the values in dis2.

```
          DO 120 N=1,NNSSS(I)
          NNSS(N,I)=NNB(N)+I
          DSQINVSS(N,I)=ONE/DIS2(NNSS(N,I))
     120  CONTINUE
     100  CONTINUE
          RETURN
          END
```

Table 6. (continued)

The following is the Fortran equivalent of whenfle used on non-Cray computers. Note: the 100 loop is not vectorizable on the Cray due to the "if" conditional statement.

```
      SUBROUTINE WHENFLE(N,ARRAY,INC,TARGET,INDEX,NVAL)
      IMPLICIT DOUBLE PRECISION (A-H,O-Z)
      DIMENSION ARRAY(1),INDEX(1)
      INA=1
      NVAL=0
      IF(INC.LT.0)INA=1-(N-1)*INC
      DO 100 I=1,N
      IF(ARRAY(INA).LE.TARGET)THEN
          NVAL=NVAL+1
          INDEX(NVAL)=I
      ENDIF
      INA=INA+INC
100   CONTINUE
      RETURN
      END
```

pointer, **k**, is evaluated in this loop and stored for future use. The code in Table 5 (loop 2) totals the force on each surface atom due to all neighboring surface atoms. Its structure is very similar to that of loop 1 with regards to the use of cubic polynomials and implicit summation. As in loop 1, a compiler directive must be used to force vectorization. The magnitude of the force is computed by directly evaluating the first derivatives of the piece-wise cubic polynomials for the Coulomb and embedding energies, Eq.(14). To save operations the first derivative coefficient matrices **dcmatc** and **dcmats** are multiplied by the appropriate constant factors during the initial setup. In this loop the coefficient pointer, **k**, is retrieved from the matrix **kndexss** instead of being recalculated. The heart of the neighbor list evaluator, Table 6, is the routine **WHENFLE** that returns the indices of those elements of a real vector which are less than or equal to a specified value. When running on a Cray **WHENFLE** calls a CAL library module. For machines other than a Cray, **WHENFLE** is replaced by the Fortran code shown at the end of Table 6.

We have timed the above loops for a single processor on Cray YMP, and Silicon Graphics (SGI) 4D/25 and 4D/380S Iris computers. These values appear in Tables 7 and 8. The two Silicon Graphics machines use a MIPS R2000 at 20 MHz and MIPS R3000 at 33 MHz, respectively.

Table 7. MFLOPS (millions of floating point operations per second) rate for MD/MC-CEM potential energy and force evaluators

All values are for execution on a single processor.

Machine	Loop	MFLOPS	Speed (relative to Cray)
Cray YMP	1	45.9	1
	2	63.7	1
SGI 4D/380S	1	2.33	1/20
	2	2.68	1/24
SGI 4D/25	1	1.40	1/33
	2	1.67	1/38

Table 8. Surface-surface neighbor list evaluation time
All values are for execution on a single processor.

Machine	Time (seconds per active atom)	Time (relative to Cray)
Cray YMP	5.0×10^{-5}	1
SGI 4D/380S	1.6×10^{-3}	32
SGI 4D/25	3.0×10^{-3}	60

CONCLUSIONS

Several factors contribute to make SCT89 a powerful tool for studying processes on metal surfaces. The MD/MC-CEM potential energy surface provides the ability to consistently treat multi-component systems. This leaves the user free to "experiment" with many different systems without having to construct explicitly a new PES for each one. SCT89 is intended to be used as part of a number of present and future research projects and it is therefore important that it be easy to use by individuals other than the original authors. The ability to create its own input files makes SCT89 easier for new users to run. Concise input files that use character string input wherever possible make changing program options simple. SCT89 was also designed to be adaptable towards treating new problems. Users can easily introduce special gas-surface potential energy functions while still utilizing the MD/MC-CEM description of the surface. The user written analysis module allows for modification of the output to suit any new application. Finally, SCT89 provides reasonable performance on a range of computing platforms. Care was taken to ensure that SCT89 would exploit the vector capabilities of Cray supercomputers. In addition, we have found that much can be done on the new generation of mini-supercomputers and workstations.

ACKNOWLEDGEMENT

Ames Laboratory is operated for the U.S. Department of Energy by Iowa State University under contract No. W-7405-Eng-82. The research on energies and forces of metallic systems was supported by the Division of Chemical Sciences, Office of Basic Energy Sciences. The code development and research on surface scattering was supported by NSF grants CHE-8609832 and CHE-8921099. Calculations on the CRAY YMP were performed at the Pittsburgh Supercomputer Center and those on the Silicon Graphics 4D/380S were performed locally on a machine purchased by an NSF instrumentation grant. The authors wish to thank Leslie S. Perkins for her work in preparing the release version of the SCT89 code.

REFERENCES

1. A. E. DePristo and H. Metiu, *J. Chem. Phys.* **90** (1989) 1229.

2. M. Berkowitz and J. A. McCammon, *Chem. Phys. Lett.* **90** (1982) 215.

3. C. L. Brooks III and M. Karplus, *J. Chem. Phys.* **79** (1983) 6312.

4.a. R. Lucchese and J. C. Tully, *Surf. Sci.* **137** (1983) 1570.
b. R. Lucchese and J. C. Tully, *J. Chem. Phys.* **80** (1984) 3451.

5. T. Halicioglu and G. M. Pound, *Phys. Stat. Solidi* **A30** (1975) 619.

6. H. Metiu and A. E. DePristo, *J. Chem. Phys.* **91** (1989) 2735.

7. L.A. Girifalco and V.G. Weizer, *Phys. Rev.* **114** (1959) 687.

8.a. R. Car and M. Parinello, *Phys. Rev. Lett.* **55** (1985) 2471.
b. D. Hohl, R.O. Jones, R. Car and M. Parinello, *Chem. Phys. Lett.* **139** (1987) 540.
c. D. Hohl, R.O. Jones, R. Car and M. Parinello, *J. Chem. Phys.* **89** (1988) 6823.
d. P. Ballone, W. Andreoni, R. Car and M. Parinello, *Phys. Rev. Lett.* **60** (1988) 271.
e. G. Galli, R. M. Martin, R. Car and M. Parrinello, *Phys. Rev. Lett.* **62** (1989) 555.

9. P. A. Bash, M. J. Field and M. Karplus, *J.A.C.S.* **109** (1987) 8092.

10.a. M. S. Daw and M. I. Baskes, *Phys. Rev. B* **29** (1984) 6443.
b. S. M. Foiles, M. I. Baskes and M. S. Daw, *Phys. Rev. B* **33** (1986) 7983.
c. N. Ting, Y. Qingliang, and Y. Yiying, *Surf. Sci.* **206** (1988) L857.
d. M. S. Daw, *Phys. Rev. B* **39** (1989) 7441.

11.a. M. W. Finnis and J. E. Sinclair, *Philos. Mag. A* **50** (1984) 45.
b. M. W. Finnis, A. T. Paxton, D. G. Pettifor, A. P. Sutton, and Y. Ohta, *Philos. Mag. A* **58** (1988) 143.

12.a. F. Ercolessi, M. Parrinello, and E. Tosatti, *Surf. Sci.* **177** (1986) 314.
b. F. Ercolessi, A. Bartolini, M. Garofalo, M. Parrinello, and E. Tosatti, *Surf. Sci.* **189-190** (1987) 636.
c. F. Ercolessi, A. Bartolini, M. Garofalo, M., Parrinello, and E. Tosatti, *Phys. Scr.* **T19B** (1987) 399.
d. F. Ercolessi, M. Parrinello, and E. Tosatti, *Philos. Mag. A* **58** (1988) 213.

13.a. B. J. Garrison, N. Winograd, D. M. Deaven, and C. T. Reimann, *Phys. Rev. B* **37** (1988) 7197.
b. M. Lundberg, *Phys. Rev. B* **36** (1987) 4692.
c. A. F. Voter, *Proc. SPIE-Int. Soc. Opt. Eng.* **821** (1988) 214.
d. M. I. Baskes, S. M. Foiles, and C. F. Melius, *J. Nucl. Mater.* **145** (1987) 339.

14.a. J. K. Norskov and N. D. Lang, *Phys. Rev. B* **21** (1980) 2136.
b. M. J. Stott and E. Zaremba, *Phys. Rev. B* **22** (1980) 1564.
c. K. N. Jacobsen, J. K. Norskov, and M. J. Puska, *Phys. Rev. B* **35** (1987) 7423, and references therein.
d. J. K. Norskov, *J. Chem. Phys.* **90** (1989) 7461.

15.a. K. W. Jacobsen, *Comments Condens. Matter Phys.* **14** (1988) 129.
b. T. McMullen, M. J. Stott, and E. Zaremba, *Philos. Mag. A* **59** (1989) 161.
c. P. Stoltze, J. K. Norskov, and U. Landman, *Phys. Rev. Lett.* **61** (1988) 440.

16. J. D. Kress and A. E. DePristo, *J. Chem. Phys.* **87** (1987) 4700.

17. J. D. Kress and A. E. DePristo, *J. Chem. Phys.* **88** (1988) 2596.

18. J. D. Kress, M. S. Stave and A. E. DePristo, *J. Phys. Chem.* **93** (1989) 1556.

19. T. J. Raeker and A. E. DePristo, *Phys. Rev. B* **39** (1989) 9967.

20. T. J. Raeker and A. E. DePristo, *Surf. Sci.* **235** (1990) 84.

21. T. J. Raeker and A.E. DePristo, *Int. Rev. Phys. Chem.* **10** (1991) 1.

22.a. M. J. Puska, R. M. Nieminen and M. Manninen, *Phys. Rev. B* **24** (1981) 3037.
b. M. J. Puska, (private communication).

23.a. M.S. Stave, D.E. Sanders, T.J. Raeker, and A.E. DePristo, *J. Chem. Phys.* **93** (1990) 4413.
b. S.B. Sinnott, T.J. Raeker, M.S. Stave, and A.E. DePristo, (to be submitted).

24. T. J. Raeker, D. E. Sanders and A. E. DePristo, *Journal of Vac. Sci. Tech. A* 8 (1990) 3531.

25.a. P. S. Bagus, T. L. Gilbert, and C. J. Roothan, *J. Chem. Phys.* **56** (1972) 5195.
b. E. Clementi, *IBM J. Res. Develop. Suppl.* **9** (1965).

26.a. S. A. Adelman and J. D. Doll, *Acc. Chem. Res.* **10** (1977) 378.
b. S. A. Adelman, *Adv. Chem. Phys.* **44** (1980) 143 and references therein.
c. J. C. Tully, *J. Chem. Phys.* **73** (1980) 1975.
d. A. E. DePristo, *Surf. Sci.* **141** (1984) 40.

27. M. Schmidt and K. Ruedenberg, *J. Chem. Phys.* **71** (1979) 3951.

28. S. Huzinaga, *Prog. Theor. Physics Suppl.* **40** (1967) 279.

29.a. C. Y. Lee and A. E. DePristo, *J. Chem. Phys.* **85** (1986) 4161.

b. A. E. DePristo in Interactions of Atoms and Molecules with Solid Surfaces, eds. A. Bortolani, N. March, and M. Tosi (Plenum Press, N.Y., USA, 1989).

c. A. Kara and A. E. DePristo, *Surf. Sci.* **193** (1988) 437; *J. Chem. Phys.* **88** (1988) 2033; *J. Chem. Phys.* **88** (1988) 5240; *J. Chem. Phys.* **92** (1990) 5653.

d. A. E. DePristo and A. Kara, *Adv. Chem. Phys.* **77** (1990) 163.

30.a. P. Siegbahn, M. Blomberg, I. Panas and U. Wahlgren, *Theor. Chim. Acta.* **75** (1989) 143.

b. I. Panas, P. Siegbahn and U. Wahlgren, *J. Chem. Phys.* **90** (1989) 6791.

31.a. M. Abramowitz and I. A. Stegun, Handbook of Mathematical Functions (Dover, New York, 1972).

b. W. H. Press, B. P. Flannery, S. A. Teukolsky, and W. T. Vetterling, Numerical Recipes (Cambridge University Press, New York, 1986).

32. T. A. Andrea, W. C. Swope, and H. C. Andersen, *J. Chem. Phys.* **79** (1983) 4576.

33.a. H. Akima, *J. Assoc. Comput. Mach.* **17** (1970) 589.

b. P. Lancaster and K. Salkauskas, Curve and Surface Fitting, (Academic Press, New York, 1986).

34. J. J. Dongarra, Performance of Various Computers Using Standard Linear Equations Software in a Fortran Environment, (Argonne National Laboratory, 1989).

35. R. N. Porter, L. M. Raff and W. H. Miller, *J. Chem. Phys.* **63** (1975) 2214.

36.a. L. Verlet, *Phys. Rev.* **159** (1967) 98.

b. M. P. Allen and D. J. Tildesley, Computer Simulation of Liquids, (Claredon Press, Oxford, 1987).

37.a. R. A. Aziz and M. J. Slaman, *Mol. Phys.* **57** (1986) 825.

b. R. A. Aziz and M. J. Slaman, *Mol. Phys.* **58** (1986) 679.

38. Programmer's Library Reference Manual, (Cray Research, Inc., 1987).

CONCLUSIONS

In this dissertation, the dynamics of epitaxial film growth in FCC(001) metal systems was investigated. Two processes which dominate the early stages film growth - atom deposition and diffusion - have been studied in microscopic detail using computer simulations.

Single atom deposition on a clean (001) surface has been simulated via molecular dynamics for the homonuclear Ni, Cu, Rh, Pd, Ag, Pt, and Au systems. It was found that none of these systems exhibit significant transient or ballistic motion of the adsorbing atom. Rather, most adatoms tend to remain in the first unit cell impacted upon during deposition. The explanation for this is the efficient transfer of over 80 % of the adatom's energy to the metallic substrate during the first instant of collision. The transferred energy is then quickly dissipated among the substrate atoms.

The Cu/Cu(001) system was explored further to determine the effect of changing simulation parameters. It was found that the amount of adatom mobility was generally insensitive to the choice of potential energy function. However, the dimensions of the simulation cell were found to play an important role. An insufficient number of active substrate layers lead to anomalous results which supported the concept of transient or ballistic motion of the adsorbate. The number of layers needed in the simulation can be reduced using Langevin coupling to simulate frictional dissipation.

The diffusion of a single metal atom adsorbed on the surface of a FCC(001) metal was also examined. Direct MD simulations of the long-time motion of the adsorbate were performed in the Ag on Ag(001) and Rh on Rh(001) systems. The results of these simulations indicate that a kinetic model of diffusion is valid for diffusion on FCC(001) surfaces.

A combination of TST and the MD/MC-CEM PES was then used to predict diffusion rate constants for all 49 adsorbate/substrate combinations of the metals Ni, Cu, Rh, Pd, Ag, Pt, and Au. Comparisons to the available experimental data indicated that the results were of good accuracy. Even for the atomically smooth Ag on Ag(001) system, which has an unusually small barrier, TST was found to be accurate by comparison to full MD simulations of diffusion. Thus, these results represent the beginning of a reliable database for the modelling of diffusion.

Methods of simulating epitaxial growth may be developed which would incorporate the best features of molecular dynamics and kinetic models. As pointed out in this work, the early stages of epitaxial growth are dominated by atom deposition and diffusion. In future codes, MD simulations would still be used to deposit atoms (and small clusters) on the surface. Once the newly deposited atoms were equilibrated the simulation would switch to a kinetic model. These would propagate the adatoms during the relatively long times between deposits. Such an approach, unfortunately, becomes difficult when significant clustering of the adatoms occur. For isolated atoms we have seen that it is possible to extract diffusion rate constants with TST, however in more complex configurations identifying the transition state becomes more demanding.

The two applications of computer simulation presented in this dissertation only begin to answer the questions about epitaxial growth. There are a number of directions in which future work may proceed. Direct MD simulation of film growth is only limited by computational constraints. The advent of parallel computers may help overcome this bottleneck, but the next generation of MD codes such as SCT89 will require much reworking to take advantage of the parallel architecture.

REFERENCES

1. M. El-Batanouny, M. Strongin, G.P. Williams, and J. Colbert, *Phys. Rev. Lett.* **46** (1981) 1723.

2. A. Zangwill, Physics at Surfaces, (Cambridge University Press, 1988), ch. 16.

3. N. Eustathopoulos and J.-C. Joud, Current Topics in Material Science, (North-Holland, Amsterdam, 1980), vol. 4, p. 281.

4. S.B. Sinnott, T.J. Raeker, M.S. Stave, and A.E. DePristo, (manuscript to be submitted).

5. L.S. Perkins and A.E. DePristo, "Phonon Frequency Distributions in Metal Surfaces", (manuscript in preparation).

6. P.J. Schmitz, W.-Y. Leung, G.W. Graham, and P.A. Thiel, *Phys. Rev. B* **40** (1989) 1.

7. T.J. Raeker and A.E. DePristo, "Theoretical Studies of Dynamical Phenomena in Epitaxial Surface Systems", *Surf. Sci.* (accepted 12/90).

8.a. M. Schneider, A. Rahman, and I.K. Schuller, *Phys. Rev. Lett.* **55** (1987) 604.
b. K.-H. Müller, *J. Vac. Sci. Technol. A* **6** (1988) 1690.
c. E.T. Gawlinski and J.D. Gunton, *Phys. Rev. B* **36** (1987) 4774.
d. D.W. Brenner and B.J. Garrison, *Surf. Sci.* **198** (1987) 151.

9. T. Halicioglu and G.M. Pound, *Phys. Stat. Solidi A* **30** (1975) 619.

10. W.F. Egelhoff and I. Jacob, *Phys. Rev. Lett.* **62** (1989) 921.

11. D.K. Flynn, J.W. Evans, and P.A. Thiel, *J. Vac. Sci. Technol. A* **7** (1989) 2162.

12.a. J.W. Evans, *Vacuum* **41** (1990) 479.

b. J.W. Evans, D.E. Sanders, P.A. Thiel, and A.E. DePristo, *Phys. Rev. B* **41** (1990) 5410.

c. D.E. Sanders and J.W. Evans, "Downward Funneling Model of Low-Temperature Epitaxial Growth: A Hybrid Molecular (MD) - Monte-Carlo (MC) Study", submitted for *Proceedings of the ICSOS-III Conference*, Milwaukee, WI (1990), to appear in The Structure of Surfaces III, Editors: M.A. Van Hove, S.Y. Tong, and X. Xide, Springer Verlag, Berlin.

13. N. Shamir, J.C. Lin, and R. Gomer, *J. Chem. Phys.* **90** (1989) 5135.

14.a. G. Ayrault and G. Ehrlich, *J. Chem. Phys.* **60** (1974) 281.

b. W.R. Graham and G. Ehrlich, *Thin Solid Films*, **25** (1975) 85.

c. D.W. Bassett, *Surf. Sci.*, **53** (1975) 74.

d. D.W. Bassett and P.R. Webber, *Surf. Sci.* **70** (1978) 520.

e. T. Tung and W.R. Graham, *Surf. Sci.* **97** (1980) 73.

f. J.D. Wrigley and G. Ehrlich, *Phys. Rev. Lett.* **44** (1980) 661.

g. G.L. Kellogg and P.J. Feibelman, *Phys. Rev. Lett.* **64** (1990) 3143.

h. C. Chen and T.T. Tsong, *Phys. Rev. Lett.* **64** (1990) 3147.

15.a. K. Binder and D.P. Landau, *Adv. Chem. Phys.* (1989) 91.

b. W.H. Weinberg, *Ann. Rev. Phys. Chem.* **34** (1983) 217.

16.a. A.E. DePristo and H. Metiu, *J. Chem. Phys.* **90** (1989) 1229.

b. M. Berkowitz and J.A. McCammon, *Chem. Phys. Lett.* **90** (1982) 215.

c. C.L. Brooks III and M. Karplus, *J. Chem. Phys.* **79** (1983) 6312.

d. R. Lucchese and J.C. Tully, *Surf. Sci.* **137** (1983) 1570.

e. R. Lucchese and J.C. Tully, *J. Chem. Phys.* **80** (1984) 3451.

17. D.D. Chambliss and R.J. Wilson, "Relaxed Diffusion Limited Aggregation of Ag on Au(111) Observed by Scanning Tunneling Microscopy", *J. Vac. Sci. Technol.*, (to appear March/April 1991).

18. A.F. Voter, *Phys. Rev. B* **34** (1986) 6819.

19. L.A. Girifalco and V.G. Weizer, *Phys. Rev.* **114** (1959) 687.

20.a. R. Car and M. Parinello, *Phys. Rev. Lett.* **55** (1985) 2471.

b. D. Hohl, R.O. Jones, R. Car and M. Parinello, *Chem. Phys. Lett.* **139** (1987) 540.

c. D. Hohl, R.O. Jones, R. Car and M. Parinello, *J. Chem. Phys.* **89** (1988) 6823.

d. P. Ballone, W. Andreoni, R. Car and M. Parinello, *Phys. Rev. Lett.* **60** (1988) 271.

e. G. Galli, R. M. Martin, R. Car and M. Parinello, *Phys. Rev. Lett.* **62** (1989) 555.

21.a. J.D. Kress and A.E. DePristo, *J. Chem. Phys.* **88** (1988) 2596.

b. J.D. Kress, M.S. Stave, and A.E. DePristo, *J. Phys. Chem.* **93** (1989) 1556.

c. T.J. Raeker and A.E. DePristo, *Phys. Rev. B* **39** (1989) 9967.

d. T.J. Raeker and A.E. DePristo, *Surf. Sci.* **235** (1990) 84.

e. T.J. Raeker and A.E. DePristo, *Int. Rev. Phys. Chem.* **10** (1991) 1.

22. M.S. Stave, D.E. Sanders, T.J. Raeker, and A.E. DePristo, *J. Chem. Phys.* **93** (1990) 4413.

ACKNOWLEDGEMENT

I thank my major professor, Andrew DePristo, for his guidance during this work. He always gave me the freedom to pursue my own interests, but was there to provide direction and an occasional push. Professor DePristo's frank and honest criticism of my work has helped immeasurably in the development of my research skills. I also thank fellow group members Mark Stave and Dr. Todd Raeker for providing helpful discussions during the development of SCT89.

I thank professors Pat Thiel and James Evans whose work and ideas provided much of the motivation for the applications in this thesis. Scientific research cannot go forward in a vacuum; it is therefore gratifying to work with people who share their thoughts so openly and freely.

I thank my wife, Dr. Diane Sanders, for her love and support during my graduate work. Her confidence in me and words of encouragement gave me the energy sometimes necessary to continue. Next, I mention some of those whose friendship has made our time in Ames cherished. I thank Dan and Dr. Mary Walczak for all those wonderful meals and evenings around the VCR. A special thanks goes to Leslie Perkins for her help with SCT89 as well as her quick wit which always kept the office interesting. Finally, I thank my hunting buddies, Drs. Jeff Crain, Steve Johnson, and Bill Pfeffer, for the good times had stalking the wilds of Iowa.

Funding for this work came from several sources. First, I thank IBM for the support provided by their Graduate Fellowship. This award allowed me to freely

pursue my own interests. Second, the Silicon Graphics computers used for these calculations were purchased with a NSF instrumentation grant. Finally, this work was performed at Ames Laboratory under contract no. W-7405-eng-82 with the U.S. Department of Energy. The United States government has assigned the DOE Report number IS-T 1530 to this thesis.